Experimental identification of the equation of motion in vibroacoustics

Michal Ruzek

THÈSE

IDENTIFICATION EXPÉRIMENTALE DE L'ÉQUATION DU MOUVEMENT DE MILIEUX VIBROACOUSTIQUES

présentée devant

l'Institut National des Sciences Appliquées de Lyon

par

Michal RUZEK

Ingénieur diplomé de l'Université technique tchèque à Prague

pour obtenir

le GRADE DE DOCTEUR

Ecole doctorale :

Mécanique, Energetique, Genie Civil, Acoustique

Spécialité : **Acoustique**

Thèse preparée au Laboratoire Vibrations Acoustique,

soutenue le 17/12/2013 devant la Commission d'examen

jury

JEAN-LOUIS GUYADER (Professeur)	INSA de Lyon	Directeur de thèse
CHARLES PÉZERAT (Professeur)	INSA de Lyon	Co-Directeur
ROBIN LANGLEY (Professeur)	Cambridge University	Rapporteur
EMMANUEL FOLTÊTE (Professeur)	ENSMM, Besançon	Rapporteur
ALAIN BERRY (Professeur)	Université Sherbrooke	Rapporteur
JERÔME ANTONI (Professeur)	INSA de Lyon	Examinateur
GILLES CHARDON (Researcher)	Acoustic research institute à Vienne	Examinateur

N° d'ordre Année 2013

A tous les doctorants, passés, présénts ou à venir

Remerciements

Je remercie dans un premier temps Jean-Louis Guyader ainsi que Charles Pézerat, mes directeurs de thèse, pour l'encadrement de mes recherches. Ils m'aidaient tout au long de ma these et ils me guidaient avec sagesse et patience. Leurs remarques étaient toujours intéressants et ils ont fructifiés mon travail. Je sentais qu'on partageait ensemble un esprit de curiosité scientifique pour retrouver les secrets de la nature.

Je dois aussi remercier tous mes collègues du labo qui ont vécu les hauts et les bas de la thèse. Je voudrais nommer particuli'erement Antonio, Dorian, Julie, Jéremy, Mickael, Kerem, Thibault, Carmen, Yu-liang, Liangfen, Ha, Roch, Efren, Rainer, Fulbert, Mathieu, Anders, Kostis, Bin Dong, Loic et tous les autres étudiants qui sont passés par labo. Je dois aussi mentionner la plus importante (bien que la moins payee) personne du labo, Daniel, qui m'a donné des précieux conseils.

Finalement, je voudrais remercier mes amis qui me soutenaient chez moi et en France. Je voudrais particulièrement remercier ma famille pour toutes ces années de soutien patient tout au long de mes longues études. Leur encouragement, tendresse et perséverance m'ont aidé a traverser les difficultés et arriver jusqu'au bout.

Mai 2013
Michal Ruzek

Acknowledgements

At first, I would like thank my two supervisors, Jean-Louis Guyader and Charles Pézerat. They helped me all along my thesis and guided me with wisdom and patience. Their remarks were always interesting and fruitful for the development of my work. I felt that we shared a common interest in scientific approach to unravel the puzzles of nature.

I must also thank all by lab mates with whom we shared the downs and ups through the years of thesis. Particularly, I would like to thank the fellow PhD students Antonio, Julie, Dorian, Jéremy, Mickael, Thibault, Carmen, Yu-liang, Liangfen, Ha, Roch, Efren, Rainer, Fulbert, Mathieu, Anders, Kostis, Bin Dong, Loic and all the other students who passed by. I must mention also the most important (although the least paid) person of the lab Daniel who gave me good advice.

Finally, I would like to thank my friends who supported me at home and in France. And especially to my family for all those years of patient support during my long studies. Their encouragement, tenderness and persistence made me cross over the difficult times and lead me safely until the end.

May 2013
Michal Ruzek

Résumé

Ce travail répond à la question de l'identifiquation de l'équation du mouvement à partir des mesures expérimentales. Les structures considérées ont soit une soit deux dimensions. La méthode presentée utilise les méthodes inverses locales qui se basent sur les mesures du champs vibratoire stationaire. Ces méthodes sont indépendentes des conditions aux limites qui sont inconnues pour l'observateur. Deux méthodes de sélection des modeles sont utilisées pour choisir l'équation du mouvement la plus adaptée parmi un ensemble des modeles a priori. La méthode est appliquée a des nombreux cas expérimentaux. Trois problématiques sont traités: identification de la force axiale dans les poutres et membranes, identification de l'orthotropie de la plaque et identification d'un panel sandwich épais.

Mots clés : mèthodes inverses vibratoires, inverse wave correlation, inverse wave decomposition, séléction des modèles, Akaike information criterion, Baysian information criterion.

Abstract

This works deals with a question of identification of the equation of motion based on experimental measurements. The considered structures are either one or two-dimensional plane structures. The developed methodology employs local inverse methods based on local steady-state vibration field and it is therefore independent of boundary conditions. Two different model selection techniques are used to select the most adapted equation of motion from a set of apriori candidate models. The method is applied to various experimental case studies as identification of axial force in beams and membranes, identification of plate orthotropy and identification of thick sandwich panel model.

Keywords: inverse vibration methods, Inverse wave correlation, Inverse wave decomposition, Model selection, Akaike information criterion, Bayesian information criterion.

Contents

1

General introduction

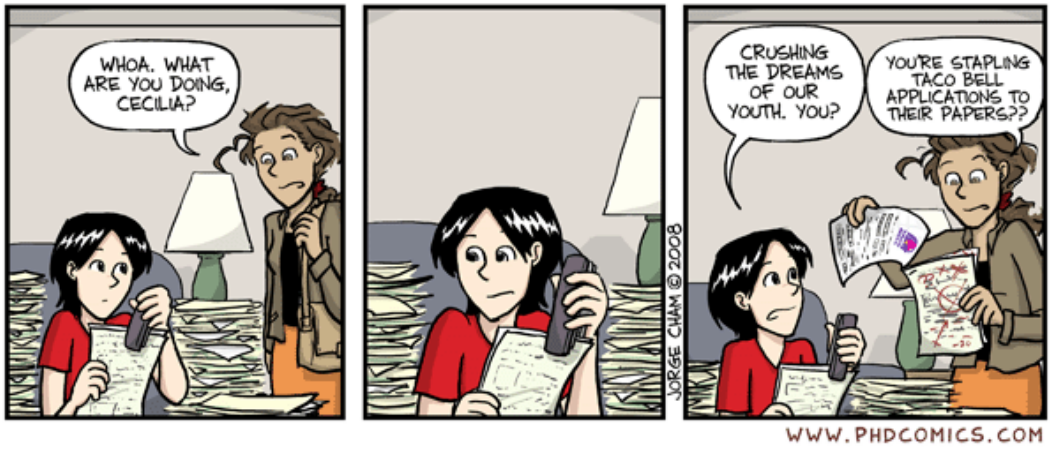

1.1 Scientific context

1.1.1 Local and global description of vibration problems

Vibration problems were among the first mathematical problems which were treated analytically in classical mechanics.

Historically, the first approach was based on solving the *differential equation of motion*. This equation puts in relation the kinematic variables and forces. It shows how a physical body moves under the application of external forces. The most famous example of an equation of motion is the Newton's second law $m\ddot{x} = F$ [1], which describes the translational motion of a rigid body. The equation of motion was first introduced for a discrete rigid-body motion. But later, similar equations of motion were developed for deformable continuous structures which are important for engineering applications like strings[2], beams[3] and plates[4]. In the continuous equation of motion, the displacement is described by a continuous and derivable function $u(x,t)$. This function is the solution of the vibration problem if it satisfies the partial differential equation of motion described by an operator $\mathcal{L}$

$$\mathcal{L}(u) = f \tag{1.1}$$

where f is the function of external forces. Eq.1.1 cannot be solved uniquely in most cases, its solution becomes unique if we applied the boundary and initial conditions requirements to our solution.

Advances in mathematics in 18^{th} century lead to so-called *variational methods* of solution of mechanical problems. These methods are represented by Lagrangian and Hamiltonian mechanics [5] While the first approach relies on the local behaviour of the structure and the solution is obtained by the integration of differential equation, variational methods consist in using the integral properties of the solution. In the case of Lagrange mechanics, the solution of the vibration problem must be a stationary point[6] of the following functional

$$\mathcal{J}(u) = T(u) - V(u) \tag{1.2}$$

where T is the total kinetic energy and V is the total potential energy. The boundary (and eventually initial) conditions must also be added to the Lagrangian. If the boundary conditions

[1] This law was first published by Isaac Newton in *Principia mathematica* in 1687.

[2] Vibration of strings was first described by equation of motion by d'Alembert in *Éléments de musique* in 1752.

[3] Euler-Bernouilli beam theory was introduced around 1750.

[4] Kirchhoff-Love plate model was introduced in *On the small free vibrations and deformations of elastic shells* published in 1888.

[5] Lagrangian mechanics were introduced in 1788 and Hamiltonian mechanics in 1833. Both formulations are equivalent.

[6] In this language a *point* means a *function* because the arguments of the functional are functions.

can be described by an integral relation $\mathcal{B}(u) = 0$ where $\mathcal{B}$ is a known functional, then the Lagrangian formalism if modified using the Lagrangian multipliers as follows

$$\mathcal{J}(u) = T(u) - V(u) + \lambda\mathcal{B}(u) \tag{1.3}$$

It should be noted that both approaches given by Eq.1.1 and Eq.1.3 lead to identical results. One formulation can also be developed from another. For example, the equation of motion (and boundary conditions) can be obtained from the Lagrangian by so-called Euler-Lagrange equations (for details see [67]). None the less the great advantage of the integral Lagrange formulation lies in the mathematical ease in which the stationary points of Eq.1.3 can be found. While it is sometimes very difficult to find the general solution of the differential equation of motion, it is simpler to find the stationary point of the functional (at least approximately)[7].

As it was mentioned in the preceding paragraph, the solution $u(x,t)$ is obtained either by integrating the equation of motion or by finding the stationary points of the Lagrangian. In both cases, the knowledge of the boundary conditions is essential for unique determination of $u(x,t)$. However, in this work we are interested in **inverse problems**. These problems consist mostly of determining the parameters of the model (either equation of motion $\mathcal{L}$ or the functional $\mathcal{J}$) from the observed solution $u(x,t)$. Traditionally, global methods like modal methods are employed for inverse technique. In such a case, the unknown operator is found by fitting the simulated eigenmodes to the eigenmodes of the studied structure. Such an approach works if we know fairly well the geometry of the problem, especially we should be sure about the boundary conditions. Moreover, a slight lack of knowledge of the boundary conditions tends to increase the prediction error with increasing frequency.

This can be demonstrated on the example shown in Fig.1.1. In this case the measurement was done on the wing part of a small experimental rocket. We can see that the response function in Fig.1.1B exhibits modal behaviour of two types. In the *low-frequency* range, the modes are well separated and modelling error due to lack of knowledge is not drastic. However, in the *mid-frequency range*, the modes of all the structure superpose each other, we see an important modal overlap. The inverse methods based on the modal response are therefore impossible for the mid-frequency range because the determination of modes is unstable with a lack of boundary conditions knowledge.

As the matter of fact, the boundary conditions are partially unknown and therefore the use of the global computational methods for either direct and/or inverse techniques is impossible. Two such examples treated in this work in Section 4 are shown in Fig.1.2. In the Example 1 the vibrational response of the structure A depends on the whole structure through unknown boundary conditions. The same hold for the membrane stretched by a number of strings to the cylinder as shown in Example 2. In both cases the object of interest (beam, membrane) is very simple but it is coupled to complicated structure and therefore its vibration response cannot be

[7]The Lagrangian formulation is also basis for numerical methods like Finite Elements Method.

simply predicted by some global model. Consequently, the inverse of the global model cannot be employed easily here.

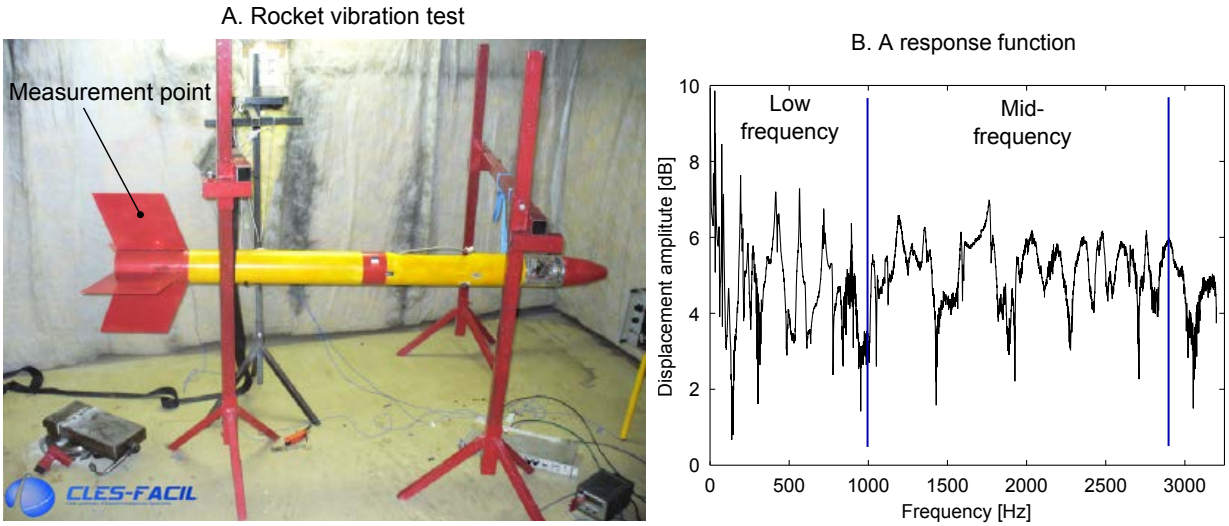

Figure 1.1: An experimental example of a measured displacement spectrum on an wing of a small experimental rocket (Courtesy of CLES-FACIL team).

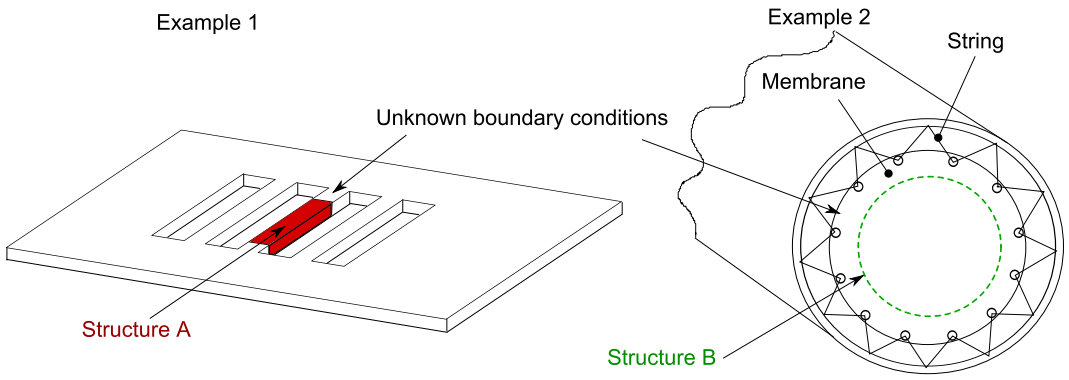

Figure 1.2: Two examples where the lack of knowledge of boundary conditions restrains the use of global methods.

The reasons mentioned above lead us to the conclusion that global models are not adapted for neither direct nor inverse problems in the mid-frequency range. In this thesis the emphasis is on the use of *local models*. Equation of motion is such a local model (Eq.1.1). Without the knowledge of boundary conditions, it cannot predict deterministically the response. None the less, the knowledge of the equation of motion in the mid-frequency range is still a benefit. It can be used to predict dispersion curves and radiation problems. By identifying the equation of motion we obtain indirectly the information about the structural properties which can be interesting from the engineering point of view. For example in Section 4.2 the presence and magnitude of axial force is determined in beams and membranes.

1.2 General strategy of identification of motion equation

The general strategy to identify the equation of motion can be decomposed into three parts as shown in Fig.1.3. *First*, there are some experimental observations of the structure whose equation of motion we want to identify. In our case these observations consist in a steady-state vibration field measured at a number of neighbouring points. *Second*, there are multiple candidate models (set of assumed equations of motion). An inverse method is used to fit these models to the observation. *Third*, a model selection technique is used to choose the most appropriate model which describes the best the measurement taking into account that these measurements cannot give exact data and perfect fit fit is not the best solution.

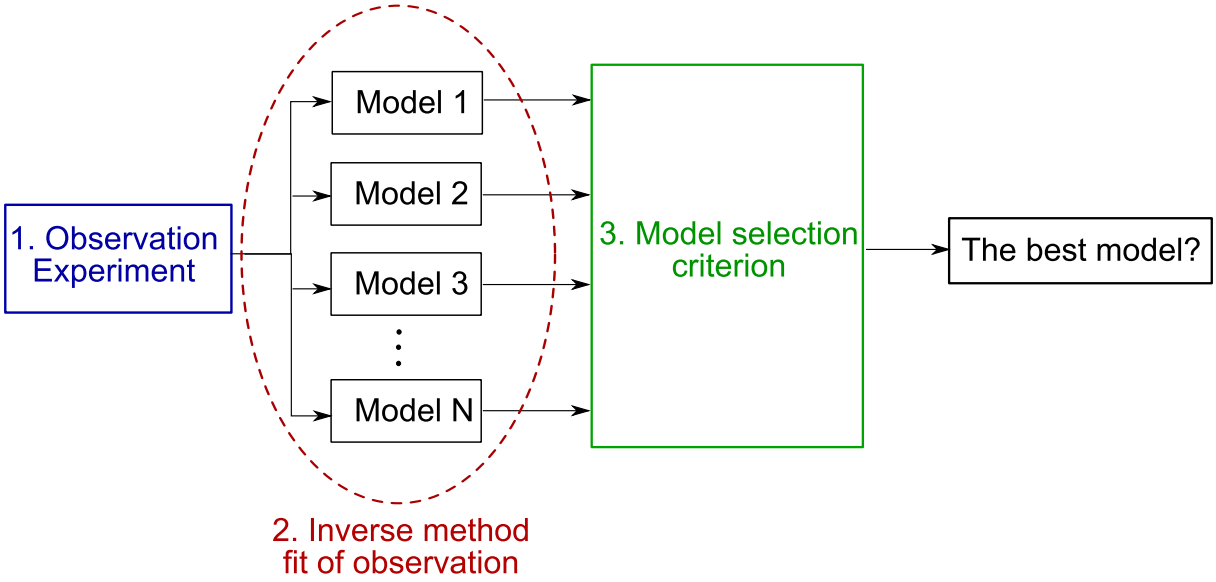

Figure 1.3: General strategy of the employed for identification of the motion equation.

It is important to notice the sequential nature of this identification. We cannot consider, for example, model selection technique without thinking of the nature of the inverse problem and the observation. It is shown that the choice of the observed quantities and subsequent inverse problem determines (or restricts) in some way the model selection criterion used.

The plan of this thesis follows this strategy. In this general introduction there is a bibliographical overview of existing inverse methods (Section 1.3) followed by an introduction to the model selection techniques (Section 1.4). These topics are developed further in Chapters 2 and 3. Chapter 2 describes in detail two inverse methods used in this thesis: Inverse wave correlation and Inverse wave decomposition. Both methods are adapted in order to be used for a model selection problem. Although these methods are not new, some new aspects and applications are presented. Chapter 3 describes in detail how the model selection techniques are applied as a post-process of the inverse methods, where it is shown the importance of respecting the hypothesis used by these techniques. It is particularly shown that the different nature of the

two inverse methods leads inevitably to use different model selection techniques. It is shown that non-respecting of the preliminary hypothesis leads to largely erroneous results.

Chapter 4 presents some highlight case studies where the equation of motion was identified. There are three distinct cases. The first is the study of the importance to include the preload for the description of vibration behaviour. The second deals with the question of mechanical orthotropy of wood and composite plates. The third case deals with the description of an complicated composite plate.

1.3 Identification of equation of motion

1.3.1 Direct and inverse problems

Before starting the description of different direct and inverse problems, we can define what we mean by the terms of *direct* and *inverse* problems. Whatever the nature of our research there are always some *models*. By model it is meant an abstract mathematical description of phenomena which can predict a *simulation* (Fig.1.4). Often simulated values can be observed experimentally. If it is possible we can construct the inverse problem which determines the model from the observed quantities. Mathematically, both problems are equal in nature, they are represented by a function mapping the variables from the model space into the data (observation/simulation) space and vice versa. But in most cases the direct problems are much easier, because they are are well-conditioned, while the inverse problems suffer from ill-conditioning.

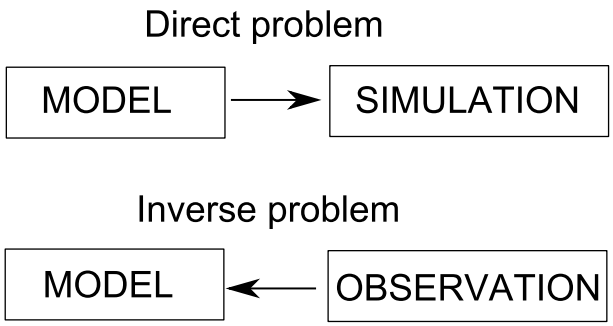

Figure 1.4: Direct and inverse problem.

In the following sections there is a bibliographic survey of a number of inverse problems which have been used in the past to identify parameters of equations of motion. While all these problems are **inverse problems**, they can be separated into two larger groups depending on the used methods to solve them:

- Inverse problems solved by an indirect method: These methods use some *solution* of the equation of motion (solution of the direct problem) and compares this solution to the observation. Generally, this solution is some *non-linear* function of the parameters of the equation of motion. By least-square optimization, an optimal value of these parameters can be found in order to match the solution to the observation.

- Inverse problems solved by a direct method[8]: These approaches use transformation of the partial differential equation of motion into a an algebraic equation. Coefficients of this equation are obtained directly from measured data. Unknown parameters of the equation of motion appear then linearly in these algebraic equations.

[8] Attention, not to be confounded with the direct problem.

1.3.2 Inverse problems solved by an indirect method

1.3.2.1 Modal methods

Modal methods consist in comparing some modal characteristics determined by the model to the measurement. The model is then updated until the modelled quantities fit optimally the measured data. The important feature of all modal methods is that the geometry and boundary conditions must be known because they make part of the model.

A typical example of an inverse method used for identification of a composite beam parameters can be found in Saito [35]. He used a Timoshenko beam theory to a beam with free boundary conditions. He compared the theoretical natural frequencies obtained by the model to the measured natural frequencies. Similar studies have been done by Barkanov [10] (cantilever sandwich beam) or Shi [38] (numerous literature examples of sandwich beams). In recent years, some authors used other measurements than the natural frequencies. For example, Cunha [18] used both natural frequencies and mode shapes in the objective function.

The modal methods are not employed in this thesis. Their main drawback is the necessity to know the boundary conditions and complete geometry of the structure. Approach in this work is based on local identification.

1.3.2.2 Inverse wave correlation method (IWC)

The principle of this inverse method was first mentioned in works of Ferguson [25] and later developed by Berthaut in his doctoral thesis [3] [9]. Its aim is to investigate the correlation of the local vibration field (as shown in Fig.1.5a) with a plane wave propagating in some direction (Fig.1.5b). This value of this correlation depends on the wave number k associated with the propagating wave. Berthaut postulated that the dominant (natural) wave number in the field can be found by maximizing the inverse wave correlation coefficient IWC with respect to k and γ [10]

$$\mathrm{IWC}(w,k,\gamma,\theta) = \frac{\mid \int_\Omega w.\psi(k,\gamma,\theta)\mathrm{d}\Omega \mid}{\sqrt{\int_\Omega |w|^2\mathrm{d}\Omega \int_\Omega |\psi(k,\gamma,\theta)|^2\mathrm{d}\Omega}} \tag{1.4}$$

where the function w represents the vibration field, θ is the angle of propagation and ψ is the propagating plane wave

$$\psi(k,\theta) = \exp\left(\mathrm{i}k(1+\mathrm{i}\gamma)(x\cos\theta + y\sin\theta)\right) \tag{1.5}$$

with k being the wave number and γ is the loss factor of the wave number.

We can see the evolution of IWC as function of k applied to the vibration field in Fig.1.5a

[9] This method is also closely related to so-called *Continuous Fourier transform (CFT)* described in the same work.

[10] This is only true for infinite wave fields, more details and discussion of this subject are in Section 2.20.

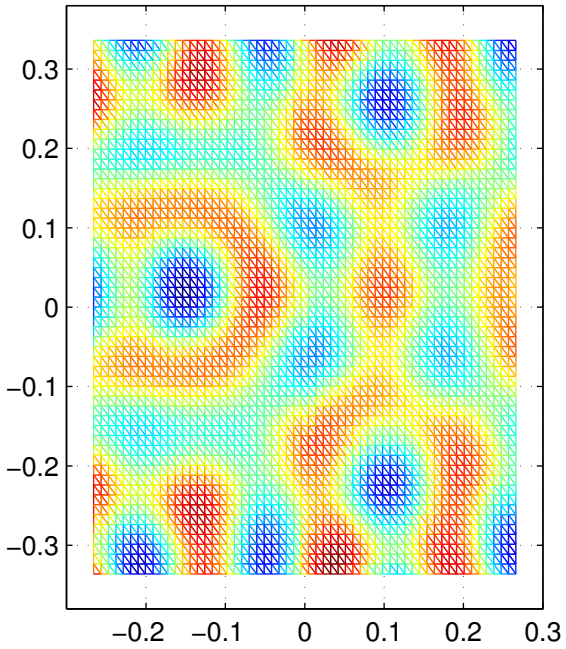

(a) Considered vibration field.

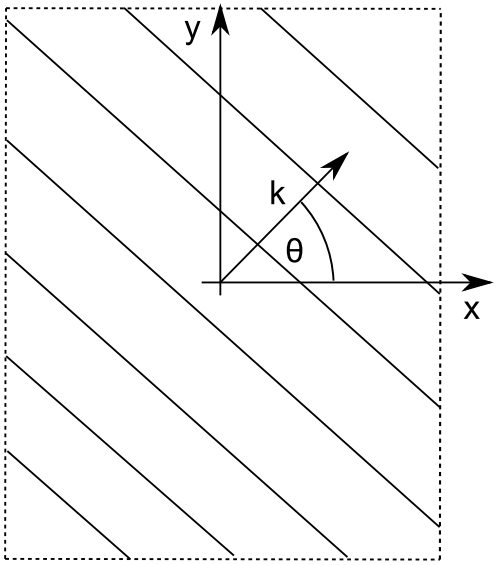

(b) Plane wave which is correlated with the field.

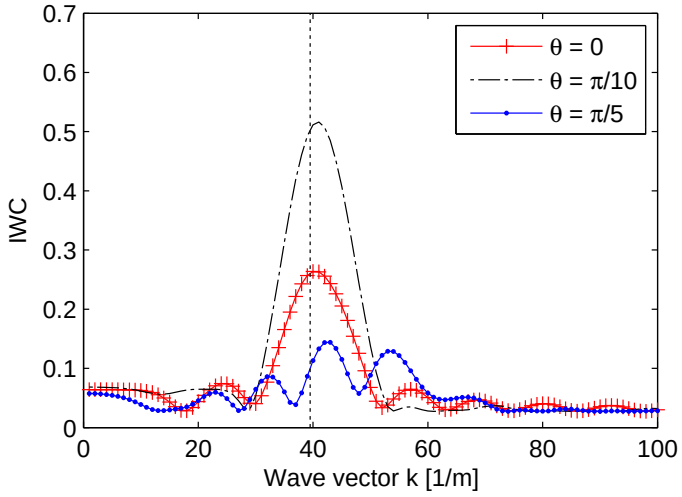

(c) Evolution of IWC with wave vector k.

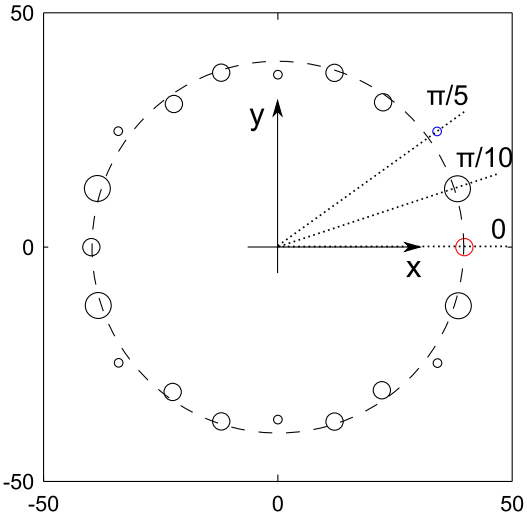

(d) Optimal value of k for different angles of travelling plane waves.

Figure 1.5: Principle of the method IWC used by Berthaut.

in Fig.1.5c for different angles θ. We can see that the maximum of the curve is not clearly distinguished for all the directions. This can be explained by the fact that some plane waves are badly correlated with vibration field. Their pattern is not "present" in the vibration field. Berthaut systematically eliminated these waves from the final analysis in order to keep only the dominant information from the field. The optimal values of k in different directions are shown

in the Fig.1.5d by circles. The size of the circle shows the level of correlation in the maximal point in the Fig.1.5c. We can see that the small circles are rather badly placed with respect to the big ones.

Once the optimal ("dominant") wavenumber k is determined, the corresponding parameters of the equation of motion can also be found to give the natural wavenumber equal to the one that has been found by the inverse technique. It should be noted that the wavenumber "loss factor" γ is often badly determined unless there are strongly damped waves. For most of the time in this work, it is considered that the damping is negligible and therefore $\gamma \approx 0$.

1.3.2.3 Inverse methods based on wave decomposition

Decomposition of the vibration field Let us imagine that we measure a field function $u(x, y)$ in the set of discrete points (x_i, y_i). This function can be either represented in the spatial $u(x_i, y_i)$ or in the Fourier domain as $\hat{u}(k_x^{(i)}, k_y^{(i)})$, where $\hat{}$ denotes the Fourier transform. Both representations are complete and there is no loss of information, since the Fourier transform is a bijection. As we can see in the Fig.1.6, if we deal with special functions like solutions of some vibrational problems ("displacement field") the information in the Fourier space is condensed in a very small number of unknowns. This idea lead many researchers to look for a decomposition of some vibration field into some kind of waves. The motivation was to simplify the numerical problem because the number of waves explaining the vibration field might be small (as it can be seen in the example in Fig.1.6).

The hypothesis made here on the vibration field is that it satisfies some *known* differential equation in the zone of interest Ω

$$\mathcal{L}u = 0 \qquad \text{in} \quad \Omega \tag{1.6}$$

where $\mathcal{L}$ is the differential operator and Ω is some bounded convex zone in 2D cartesian space.

In this thesis we will be dealing with two different approaches to decompose the vibration field $u(x, y)$ which is supposed to be a particular solution to Eq.1.6 (this approach was first used by Fox, Henrici and Moller in a so-called MPS - method of particular solutions [21],reviewed by Betcke [34]). The first decomposition is based on the *fundamental solutions* of the operator $\mathcal{L}$ and the second is based on the *plane-waves* satisfying the Eq.1.6. The comparison of the two approaches is shown in the Fig.1.7. Both method belong to the so-called Trefftz methods.

- **Method of fundamental solutions**: this is a numerical method developed from the 1970's. A good overview of this method was written by Fairweather [15]. Recent application in plate vibration analysis include Reutskiy [33] who used it for detemination of natural frequencies of a clamped plate, Alves [7] proposed a method for determination of eigensolutions of an arbitrarily-shapes plate, and a similar work done by Kang [32].

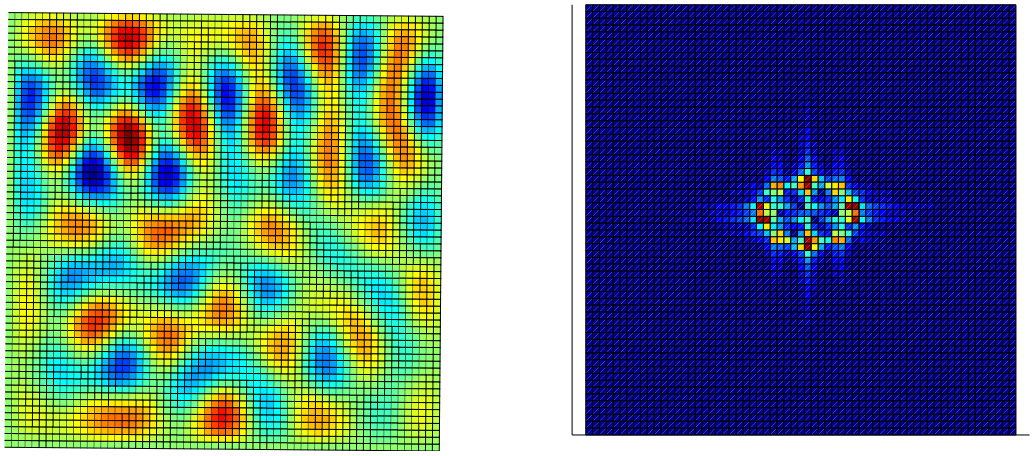

Figure 1.6: Displacement field on left and its FFT image on right.

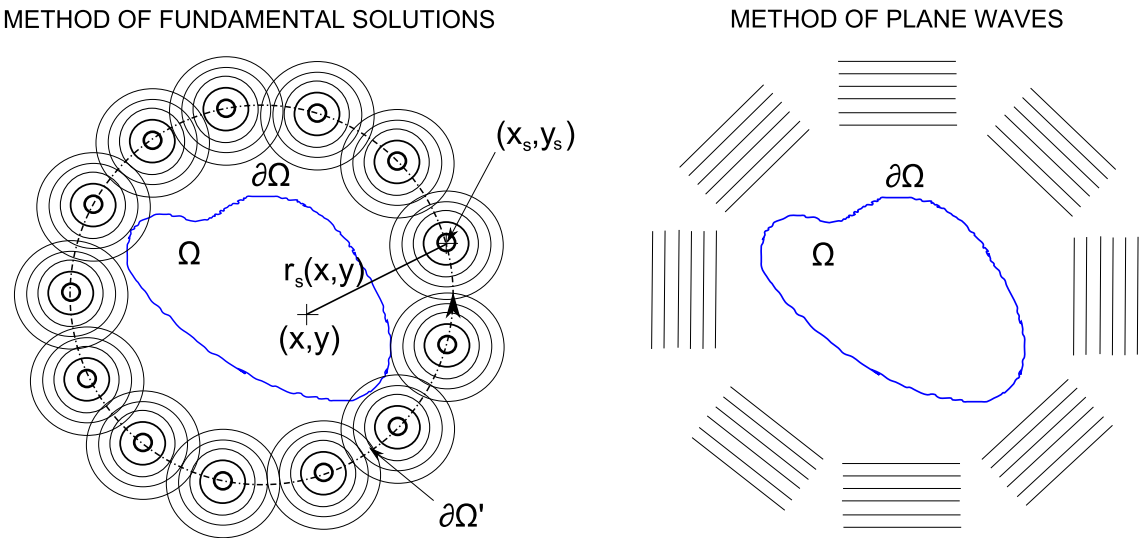

Figure 1.7: Comparison of decomposition in fundamental solutions and the in the plane-waves.

The method of fundamental solutions is based on approximation of the field $u(x, y)$ in the zone Ω by a set of fundamental solutions of the operator $\mathcal{L}$

$$u(x, y) = \sum_s \alpha_s \Phi_s(r_s(x, y)) \tag{1.7}$$

where Φ_s is the solution of $\mathcal{L}\Phi_s = \delta(x - x_s, y - y_s)$, $r_s = \sqrt{(x - x_s)^2 + (y - y_s)^2}$ and (x_s, y_s) are the points situated on some closed curve encircling the zone Ω (see Fig.1.7 on left). The number of fundamental solution functions and their origins (x_s, y_s) must be determined by numerical simulations in every independent case. There are some rare examples of geometry where the optimal distribution of the sources and the geometry of

the curve $\partial\Omega'$ are known (for example Katsurada [24] for a circular zones).

The limiting factor in the use of this method is that the fundamental solution of the operator $\mathcal{L}$ must be known. So far, the method has been used for Laplace, Helmholtz and biharmonic operators (see a review in [15]).

- **Method of plane-waves**: this is a simpler approach than the preceding decomposition. In this method the function $u(x, y)$ is decomposed into series of plane waves satisfying the equation of motion

$$\begin{aligned} u(x,y) &= \sum_{n=1}^{N} A_n \exp(-ixk\cos\phi_n - iyk\sin\phi_n) + \\ &+ \sum_{n=1}^{N} B_n \exp(-xk\cos\phi_n - yk\sin\phi_n) \end{aligned} \tag{1.8}$$

where $\phi_n = 2\pi(n-1)/N$ and k is the wavevector which is a solution of the dispersion equation associated with Eq.1.6.

The presented wave decomposition was used in many direct problems. Kovalevsky et al. [17] used this method for solution of vibration of composite plates and the same authors developed the method for the resolution of room acoustics problems in mid-frequency domain in [22]. Laghrouche [26] and Ortiz [27] investigated the diffraction of waves in two dimensions. Perray [13] studied the wave scattering in three dimensions. Pluymers et al. [4] discussed the use of plane waves Trefftz methods for interior and exterior acoustic problems. Vanmaele [9] studied the behaviour of the method in the presence of singularities in plates. Perray [12] showed the stability limits and precision of the wave decomposition with increasing N. Indeed, even if it was proven by Colton [8] that the decomposition given by Eq.1.9 is dense in the space of solutions of the Hemlholtz equation for convex zones Ω, the determination of coefficients A_n and B_n becomes ill-conditioned as N grows. Langley [30] demonstrated this phenomenon for Hemlholtz equation. A proof of denseness of the plane-wave solution in the case of the biharmonic operator using the propagating and evanescent waves was given by Chardon [5] based on the works of Moiola [1].

The denseness of the decomposed solution is particularly problematic in the inverse formulation and it will be demonstrated in this work. We are interested in keeping the value of N as low as possible without severely under fitting the measured field.

Method of Chardon (IWD): Chardon in [6] developed rather sophisticated method for interpolation of vibration field measured at few points based on the knowledge that the field is

solution of the Kirchhoff differential equation. He was interested mostly in diminishing the necessary number of measurement points for reliable identification of the vibration field. He showed that the a priori knowledge that the field is solution to the Kirchhoff equation enables to reconstruct the field from sparsely randomly distributed points with sampling in sub-Nyquist range.

Chardon considered that an observed field is a solution of the Kirchhoff-Love equation

$$D\Delta^2 u - \rho_S \omega^2 u = 0 \tag{1.9}$$

The coefficients of this equation are not necessarily known. But the approximative solution can be expressed by decomposition in the plane waves given by Eq.1.9. If the normal vectors for particular plane wave are $\nu_n = [\cos\theta_n, \sin\theta_n]^T$ and the observation points are $X = [(x_1, x_2, .., x_N)^T, (y_1, y_2, .., y_N)^T]$ then we can express the approximative solution in the matrix form

$$\mathbf{G}(k) = \quad [\exp(ik.\mathbf{X}\nu_1) \quad ... \quad \exp(ik.\mathbf{X}\nu_w) \quad \exp(k.\mathbf{X}\nu_1) \quad ... \quad \exp(k.\mathbf{X}\nu_w)] \tag{1.10}$$

The idea of Chardon was to find the optimal wave number k to obtain the best fit of the measured vector $\mathbf{u}_i$=$u(x_i, y_i)$ with the linear subspace given by Eq.1.10. The problem of fitting the measured vector $\mathbf{u}$ can be written in linear system of equations $\mathbf{G}\alpha = \mathbf{u}$. The projection (fit) of the vector $\mathbf{U}$ into the space spanned by $\mathbf{G}$ can be therefore written as $\mathbf{u}_F$=$\mathbf{G}\mathbf{G}^{-1}\mathbf{u}$=$\mathbf{P}\mathbf{u}$, where $\mathbf{P}$ is the projector. The estimation of optimal wave number $\hat{k}$ can be done by maximizing the projection of the measured vector $\mathbf{u}$ onto the space spanned by the plane waves

$$\hat{k} = \underset{k}{\operatorname{argmin}} \|\mathbf{u} - \mathbf{P}(k)\mathbf{u}\|^2 = \underset{k}{\operatorname{argmax}} \|\mathbf{P}(k)\mathbf{u}\|^2 \tag{1.11}$$

This equation is holds because the projection $\mathbf{P}$(k)$\mathbf{u}$ and residual $\mathbf{U}$-$\mathbf{P}$(k)$\mathbf{u}$ are related to each other by the Pythagorean triangle (see Fig.1.8). So we have $\|\mathbf{u}\|^2$=$\|\mathbf{u} - \mathbf{P}(k)\mathbf{u}\|^2$+$\|\mathbf{P}(k)\mathbf{u}\|^2$. So the norm of the projection $\mathbf{P}$(k)$\mathbf{u}$ is always smaller or equal to norm of measurement $\mathbf{u}$. The idea of the nonlinear inversion given by Eq.1.11 is to bring the projector space $\mathbf{P}$(k) as close to $\mathbf{U}$ as possible.

Method of McDaniel: McDaniel at al. in [23] who used an inverse technique based on wave decomposition for the measurement of the damping factor in steel box beam filled with granular polymer. But his method is actually a special mono dimensional case of the method of Chardon developed later. McDaniel considered that the equation of motion describing the box beam in the frequency domain is of the Euler type

$$EI\frac{\mathrm{d}^4 u}{\mathrm{d}x^4} - \omega^2 \rho_L u = 0 \tag{1.12}$$

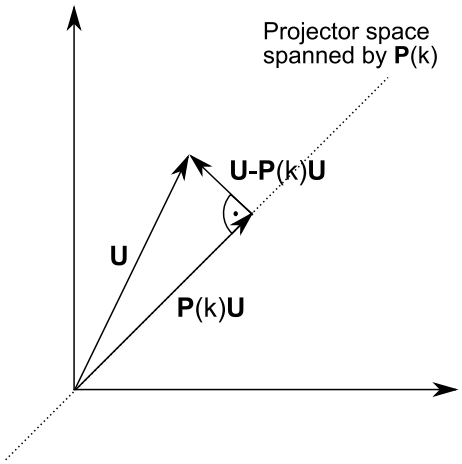

Figure 1.8: Scheme of the measured vector **u** and projected vector **Pu**.

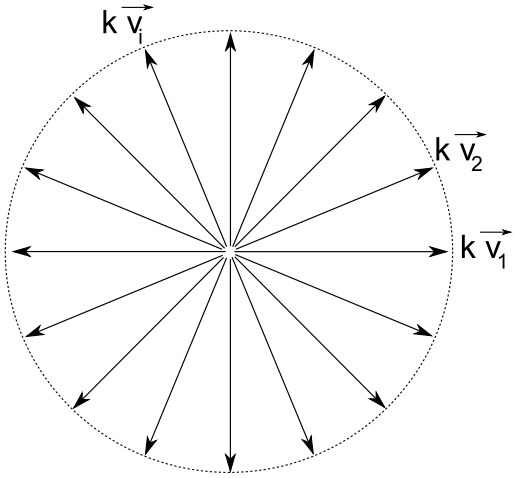

A. Plane wave approximation

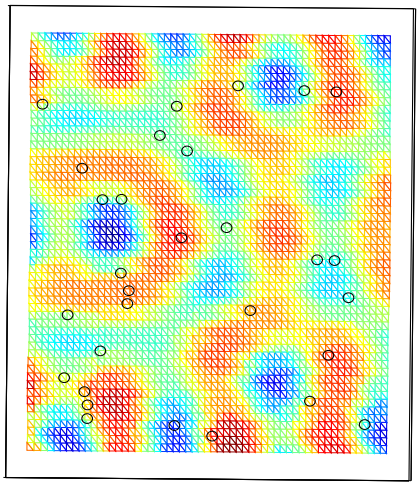

B. Vibration field and measurement points.

Figure 1.9: Method of Chardon. A. The plane wave approximation of the vibration field. B. Vibration field and randomly displaced measurement points.

in the zone without excitation. The goal of his inverse problem was to determine the complex value of EI as function of frequency. The advantage of one-dimensional differential equation of the type 1.12 is that the general equation exists and it is very simple in this case. Every solution of Eq.1.12 can be written in terms of four waves

$$u(x) = c_1 \sin kx + c_2 \cos kx + c_3 \mathrm{sh} kx + c_4 \mathrm{ch} kx \tag{1.13}$$

where the wave vector $k = \sqrt[4]{\omega^2 \rho_L / EI}$.

The measurement was taken at 13 points along the axis of the beam by accelerometers(Fig.1.10). For a given frequency, the vector of measured displacements can be approximated by $U^{(fit)}$

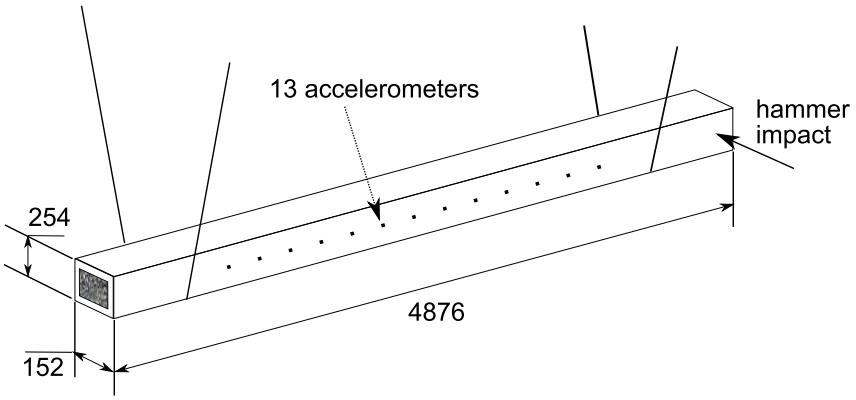

Figure 1.10: Scheme of the experiment undertaken by McDaniel.

$$\begin{bmatrix} U_1^{(fit)} \\ U_2^{(fit)} \\ .. \\ U_{13}^{(fit)} \end{bmatrix} = \begin{bmatrix} \sin kx_1 & \cos kx_1 & \mathrm{sh}kx_1 & \mathrm{ch}kx_1 \\ \sin kx_2 & \cos kx_2 & \mathrm{sh}kx_2 & \mathrm{ch}kx_2 \\ .. & .. & .. & .. \\ \sin kx_{13} & \cos kx_{13} & \mathrm{sh}kx_{13} & \mathrm{ch}kx_{13} \end{bmatrix} \times \begin{bmatrix} c_1 \\ c_2 \\ c_3 \\ c_4 \end{bmatrix} \tag{1.14}$$

The inverse problem can be formulated as finding the optimal value of k and c_i which minimize the error between measured vector $\mathbf{U}$ and $\mathbf{U}^{fit}$

$$k_{opt} = \underset{\mathbf{c},\mathbf{k}}{\operatorname{argmin}} \|U - U^{(fit)}\|^2 \tag{1.15}$$

Once the optimal value of k is known, the bending stiffness EI can easily be determined. We should note, that the mass properties of the beam must be known.

A very similar approach to McDaniel was chosen by Liao in [37]. The work of McDaniel marks the beginning of experimental methods which use the displacement field as experimental entry for the inverse problem. This work was based on the measurements done with accelerometers and was therefore limited to the one dimensional structures but the following researchers made use of scanning laser vibrometers which became available around the year 2000.

1.3.2.4 Asymptotic inverse methods

In this section the inverse method based on modal densities and mean value of mobility is presented. This method based on the works of Skudrzyk [14] and Xie [16] was proposed by Ege in his PhD thesis [19]. This method can be applied to Kirchhoff plate equation given by Eq.1.9. Plate stiffness parameter D and plate surface density ρ_S can both be determined.

The idea behind the method is the determination of two asymptotic quantities: *modal density* and *mean mobility*. Both quantities can be determined experimentally and theoretically. The inverse problem consists in fitting both theoretical values to the experimental values.

Modal density: the modal density is defined as follows: let $N(\omega)$ be a number of modes of the plate with modal frequency below ω. Then $n(\omega) = dN(\omega)/d\omega$ is the average modal density. According to Xie [16], the modal density of a finite plate can be expressed:

$$n(\omega) = p\beta + q\sqrt{\beta/f} \tag{1.16}$$

where $p = S/4\pi$, q is a constant depending on the boundary conditions [11] and $\beta = \sqrt{\rho_S/D}$ depends on the parameters of the equation of motion.

The modal density can also be calculated experimentally. As we are dealing with a multitude of modes at mid-frequency range with important overlap, traditional methods using local minima of the Fourier transform of the time signal are not adapted. Recently, the choice was made by Ege (for example Ege [20]) to use the method ESPRIT (Roy [29]) coupled with the method ESTER ([28]). This choice enables robust determination of the modal density from experimental measurements. Once the modal density n^{exp} was determined from the experiment, the optimal parameter β can be estimated:

$$\hat{\beta} = \underset{\beta}{\operatorname{argmin}} \sum_i \left(n_i^{exp} - p\beta - q\sqrt{\beta/f_i}\right)^2 \tag{1.17}$$

where f_i represent the frequencies where the modal density was determined.

Mean mobility: the mobility corresponds to the admittance of a structure V/F where V is velocity and F is input force. The so-called mean mobility is defined by Skudrzyk [14] as the mobility of the equivalent structure with infinite dimensions. Under the hypothesis described by Skudrzyk, the mean mobility can be asymptotically expressed:

$$G_C = \frac{1}{8\beta D} \tag{1.18}$$

Once the mean mobility is calculated from the time signals and the parameter β is determined by solving Eq.1.17, the parameter D can also be determined. The details of the inverse technique are presented by Elie in [11].

The interesting feature of this inverse method is that it is semi-local. Although the size of the plate must be known, the boundary conditions do not play a major role and the exact knowledge of the boundary geometry is not crucial. At higher frequencies, this method becomes local. Its advantage is also the simplicity of the measurement configuration. Theoretically, only one measurement sensor is sufficient and measurements are taken from impact hammer responses. Moreover, there is quite a large dispersion of modal density function n^{exp} obtained by the ESPRIT method. The determination of the modal density can be difficult because of high

[11] This dependence is rather simple, for example for a simply supported panel we have $q = -(L_x + L_y)/2$, for a free edges we have $q = L_x + L_y$. At higher frequencies this dependence on boundary conditions becomes negligible.

modal overlap in the mid-frequency range. To author's knowledge, this method was only use on isotropic and orthotropic Kirchhoff plates.

1.3.2.5 Galerkin inverse methods

The Galerkin method has been used for a very long time in its direct formulation for resolution of boundary problems. However, a very few researchers use the Galerkin method for inverse formulation. Shindar [2] used an inverse Galerkin method for the determination of unknown sources in the parabolic heat-conduction equation. Epstein [36] developed an inverse Galerkin method for the determination of optical properties of 1D medium. To author's knowledge these methods have not yet been applied to vibration problems. Both approaches are quite different, so it will be useful to look at them more closely.

Inverse Galerkin method applied to the parabolic differential equation: In his work [2] Shidfar considered the non-homogeneous parabolic equation of the type

$$\frac{\partial u}{\partial t} - \frac{\partial^2 u}{\partial x^2} = F(x,t) \tag{1.19}$$

where u can be for example temperature defined on the integral $< 0, 1 > x < 0, \infty >$ and F is the source term. The goal of his method was to determine F from some measurement of u in the space and time. If the initial and boundary conditions are known the unknown function u can be expressed by the integral formula with known kernel $g(\xi, \tau)$:

$$u(x,t) = \sum_{i=1}^{\infty} \left(\int_0^t \int_0^1 F(\xi,\tau) g(\xi, t-\tau) \mathrm{d}\xi \mathrm{d}\tau \right) \sin(i\pi x) \tag{1.20}$$

The principle of the Galerkin method lies in the approximation of the infinite-dimensional function $u(x,t)$ and $F(\xi,\tau)$ by a finite sum of basis functions. The sinc functions are used for the first function and the polynomials are used for the second. Then Eq.1.20 is approximated by the system of linear equations:

$$\mathbf{AX} = \mathbf{B}$$

where the vector $\mathbf{X}$ represents the distribution of sources F and $\mathbf{B}$ depends on the measurement of temperature u. This linear problem is generally ill-posed with matrix $\mathbf{A}$ close to singular. The author addresses the problem of optimal regularization of the inverse problem and obtains the inverse representation of F for several simulated data. The advantage of the parabolic equation with known boundary conditions is that we can express the solution in the closed integral form like Eq.1.20. In our case, this would not be possible because the boundary conditions are unknown.

Inverse Galerkin method applied optical tomography in 1D: Epshteyn developed in his work [36] an inverse Galerkin method for the determination of the coefficients of absorption and diffusion in the Diffusion approximation of the radiative transfer equation. This equation describes the photon transport in the optical medium. According to Arridge [31] the Diffusion approximation equation can be written:

$$-\nabla.D\nabla u + \mu u = f \qquad \text{in} \quad \Omega \tag{1.21}$$

where u is the optical density, f is the source term, D is the diffusion coefficient and μ is the absorption coefficient. Both coefficients can change in space with respect to the optical properties of the material. The boundary conditions are of the Robin type

$$u + 2D\frac{\partial u}{\partial \nu} = 0 \qquad \text{on} \quad \partial\Omega \tag{1.22}$$

Using the Galerkin approach and the integral identities, the boundary problem given by Eq.1.21 and Eq.1.22 can be expressed in its weak formulation:

$$\int_\Omega D\nabla u.\nabla v \mathrm{d}\Omega + \int_\Omega \mu u v \mathrm{d}\Omega + \int_{\partial\Omega} \frac{1}{2} u v \mathrm{d}s = \int_\Omega f v \mathrm{d}\Omega \tag{1.23}$$

where v is the test function from the Galerkin method. As the source term f is considered known, we can determine the unknown function u from the Eq.1.23. Epshteyn used a sum of cubic spline functions for approximation of the unknown u.

The inverse problem consist in finding the appropriate functions D and μ permit existence of the solution given by Eq.1.23 and which minimizes the error introduced in the boundary conditions given by Eq.1.22.

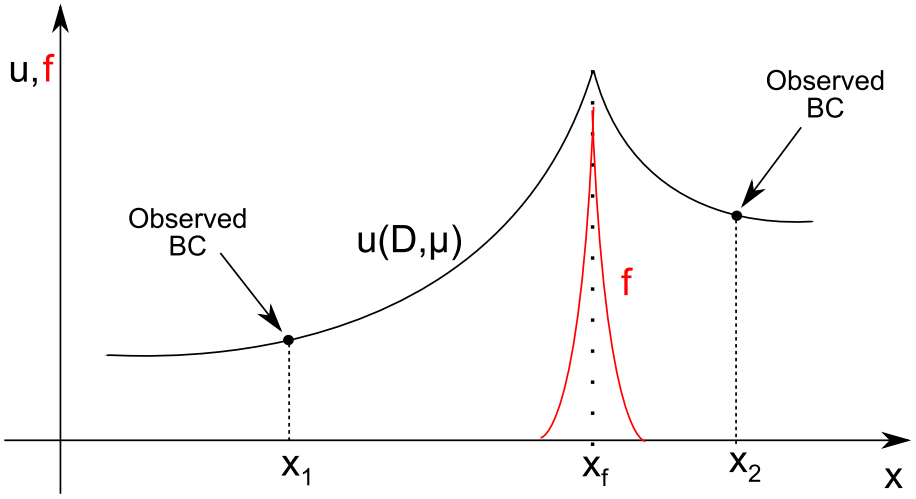

Figure 1.11: Principle of the inverse method used by Epshteyn. The source distribution f is considered known.

The inverse problem solved by Epshteyn can be seen on Fig.1.3.2.5. Let us consider that

the problem is defined between the points x_1 and x_2. The source distribution f is known (in this case it is approximated by a Dirac function). The boundary conditions can be experimentally determined at points x_1 and x_2. For every discrete approximation of functions D and μ, one can uniquely calculate the optical density $u(D, \mu)$ with integral formula Eq.1.23. The inverse problem lies in minimizing the error between the experimental boundary conditions and the boundary conditions corresponding to the parameters D and μ. In this way, the optimal D and μ can be determined.

The method proposed by Epshteyn is very similar to the one used in this thesis, but the difference is that the RHS of Eq.1.23 is zero in the case of this study. The absence of driving force f complicates the inversion problem because the excitation comes uniquely from outside of the zone Ω and it must be approximated by the (experimental) boundary conditions. The difference lies also in the dimension of the problem. The Galerkin inverse problem solved in this work is two-dimensional and hence more complicated.

1.3.3 Inverse problems solved by a direct method

1.3.3.1 Force analysis technique (FAT, RIFF)

The *Force analysis technique* (Or RIFF method[12]) was developed by Pézerat in his PhD thesis [41]. It was later developed for applications on plates ([42], [43]) and on thin cylinders ([48]). Its objective is to determine locally the external force applied to the structure from the vibration shape measurements. This method is an example of output-only inverse problem. No knowledge of boundary conditions or excitation are required.

The principle can be explained for the case of the Kirchhoff plate model. This model is described in its steady-state form by the differential equation

$$D\Delta^2 u(x, y) - \omega^2 \rho_S u(x, y) = F(x, y) \tag{1.24}$$

where u is the displacement, D is the bending stiffness, ρ_S is the surface density, ω is the angular frequency and F is the external excitation force. In the direct problem we suppose that we know the operator (represented by D, ρ_S), the excitation F and the boundary conditions. Then the solution u can be calculated by some numerical method. In the inverse logic of the FAT, the operator is known and the solution $u = u^{(exp)}$ is also known by measurements. Therefore, the *unknown* force F can be "directly" determined by:

$$F = D\Delta^2 u^{(exp)} - \omega^2 \rho_S u^{(exp)} \tag{1.25}$$

The problem with Eq.1.25 is that only the displacement $u^{(exp)}$ can be measured, the derivative $\Delta^2 u^{(exp)}$ cannot be measured. However, it can be approximated by finite differences from several

[12]The original French version is RIFF: Résolution inverse filtrée fenêtrée.

neighbouring points. So replacing the derivative operator Δ^2 by its finite difference estimator δ^4 we obtain:

$$F = D\delta^4 u^{(exp)} - \omega^2 \rho_S u^{(exp)} \tag{1.26}$$

The main difficulty of the FAT is the regularisation of the inverse problem. Although Eq.1.26 is theoretically correct, there is potentially a very important noise coming from the estimation of the fourth derivative (derivation "amplifies" noise). Therefore a lot of effort has been put in place in order to regularize the problem. Most methods rely on spatial low-pass filtering of the identified force F. For details see the works cited at the beginning of the section.

The principal goal of the FAT was the estimation of excitation force. However, as it was mentioned by Pézerat in [41] the same methodology can also be used for the determination of the operator of the structure. Let us suppose that we are measuring the zone which is not excited (i.e. $F = 0$), then we can write:

$$D\delta^4 u^{(exp)} - \omega^2 \rho_S u^{(exp)} = 0 \tag{1.27}$$

If the density of the structure ρ_S is known, then the parameter D can be determined *locally*. This is particularly interesting because this formulation permits to measure heterogeneous plates where D varies spatially. This method was investigated by F. Ablitzer (see [46]).

Another derivation of the FAT was investigated for localization of defects in beam structures by Xu [47]. He considered an similar beam equation like 1.27 with absence of external force (zero RHS). He showed that the presence of a damage was manifested by a non-zero values at the RHS of Eq.1.27. Another application of the FAT for detection of faults in plates was used by Renzi [44]. Therefore, from this point of view, looking for a damage is somewhat equivalent to a localisation of point force.

1.3.3.2 Continuous time identification

A method known as *Continuous time identification* is basically very close to FAT(RIFF) method described in the preceding section. The idea is to transform the partial differential equation describing the motion into a system of algebraic equations. Let us consider the method as it was employed by Chochol [40],[39]. She considered an equation of motion of an Euler beam without external excitation

$$EI\frac{\partial^4 u}{\partial x^4} + \rho S \frac{\partial^2 u}{\partial t^2} = 0 \tag{1.28}$$

The goal was to determine the ratio $EI/(\rho S)$ from measured displacement u. In order to do this, the measured displacement in space and time was put into a matrix $U_{ij} = u(x_i, t_j)$. This measurement was expanded to a linear combination of Chebychev polynomials $U_{i,\cdot} =$

$\sum_k \alpha_k \Psi_k(.)$. Similar expansion was done in the space coordinate. With these expansions coefficients α can be calculated by least-square fitting of measured data and then the partial derivatives in Eq.1.28 can be evaluated by derivation of the Chebychev polynomials.

Another application of this method was done by Rouby in [45]. He considered several methods for expansion of the measured displacements as well as application of wavelets. However, he only dealt with simulated data of discrete systems of a few-of-degrees of freedom.

Actually, the difference from FAT(RIFF) method is in the way how the derivatives of the partial differential equation are obtained. In the FAT method they are obtained via a finite difference scheme and spatial filtering. In the case of the Continuous time identification method these derivatives are found by interpolating the measured signal by suitable set of polynomial functions. Both methods face similar problems. The first relies strongly on suitable spatial filtering in order to avoid strong noise, the second is strongly dependent on the size of the functional basis used for expansion. If this basis is too small the expansion is not precise. If this basis is too large, then the expansion fits the noise and the inverse problem becomes ill-posed.

1.4 Model selection

1.4.1 Introduction

The model selection is a statistical discipline which deals with problems of finding the appropriate mathematical model for some physical phenomena. Let us consider that the *true model* is described by a function $y(x)$, where x is an independent variable. There are number of models which might describe the same phenomenon. They are designed as *candidate models* $\mathcal{M}_i$ and are put into a set $\mathcal{M} = [\mathcal{M}_1(\mathbf{p_1}), \mathcal{M}_2(\mathbf{p_2}), ...\mathcal{M}_n(\mathbf{p_n})]$. Vector of parameters $\mathbf{p_i}$ determines the i-th model. Function describing the i-th model is designed $y_i(x, \mathbf{p_i})$ (x is the independent variable). The real function (ground truth) which is usually unknown to observer is designed $y(x)$. How do we choose a optimal model M_{opt} from the set M? There are several way of tackling this problem.

- There are methods searching for a model which minimizes the *expectation of the residual* between the true model and the candidate model. The optimal model's index minimizes:

$$\text{opt} = \underset{i}{\text{argmin}}\, E_x(||y(x) - y_i(x, .)||^2) \tag{1.29}$$

  where E_x means the average value over all the admissible values of explanatory variable x. Methods searching the best model by minimizing the above quantity include Mallow's C_p, Subspace information criterion (SIC) and Cross-validation (details in Section 1.4.2).

- There are methods which look for a model *minimizing the Kullback-Leibler distance* (see Section 1.4.3 for details) between the true model and candidate models. In this case the optimal model is obtained as

$$\text{opt} = \underset{i}{\text{argmin}}\, KL(y, y_i) \tag{1.30}$$

  These methods include well-known Akaike information criterion (AIC) and its generalization Takeuchi information criterion (TIC).

- There in the *Bayesian information criterion* (BIC) (see Section 1.4.4 for details) which is based on looking for maximized posterior probability of the model if the truth (measurement) is given. Mathematically, we can write

$$\text{opt} = \underset{i}{\text{argmax}}\, P(y_i|y) \tag{1.31}$$

  where $P(y_i|y)$ is the conditional probability of model M_i (described by function y_i) given the measurement from the real function y.

- Finally, there is is the *Minimum description length principle* (MDL). This principle chooses a model which describes the measurement and has the least complexity. This method is not treated in this work. Readers are referred to the works of Hansen [59] and Barron [49] for further details.

1.4.2 Methods based on minimizing the expectation of residuals

The problem of minimizing Eq.1.29 is that we are always dealing with finite measurements with noise so we cannot do the average over all the values x. Instead we have a finite set of measurement points $\mathbf{X}=[x_1, x_2, ...x_{N_P}]$ and the corresponding measurement values are $y(x_i)$. Let us consider a model $\mathcal{M}_k$. Its optimal parameters are identified by minimizing the residual function as shown below:

$$\hat{\mathbf{p}}_k = \underset{\mathbf{p_k}}{\operatorname{argmin}} \sum_i ||y(x_i) - y_k(x_i, \mathbf{p_k})||^2 \tag{1.32}$$

Then, we can estimate the variance of residuals

$$\sigma_k^2(\text{estimated}) = \frac{1}{N_P - 1} \sum_i ||y(x_i) - y_k(x_i, \hat{\mathbf{p}}_\mathbf{k})||^2 \tag{1.33}$$

In this estimation, measurement points 1 to P are used. Generally, this variance always diminishes with growing complexity of model $\mathcal{M}_k$ (black line in Fig.1.12). However, if we have a look at the true variance (see Stone [60] for reference)

$$\sigma_k^2(\text{true}) = \text{Var}(y - y_k(., \hat{\mathbf{p}}_\mathbf{k})) \tag{1.34}$$

we can see that this variance reaches a minimum for a certain model complexity but it increases for a very complex models (red line in Fig.1.12).

The problem of variance estimation given by Eq.1.41 is that it can underestimate the true variance given by Eq.1.34. This happens when the model is either more complex then the reality (in such a case, the inversion becomes unstable, its parameters of the model $\mathcal{M}_k$ are badly determined) or there are not enough measurement points (in such a case, an excessively complex model fits more the noise instead of physics of the phenomenon measured).

There are several methods which try to find the minimum of $\sigma_k^2(true)$. Mallow's C_p and SIC methods use the estimated $\sigma_k^2(estim.)$ function with some penalty in order to take into account for the model complexity. The Cross-validation method tries to obtain estimate of $\sigma_k^2(true)$ directly.

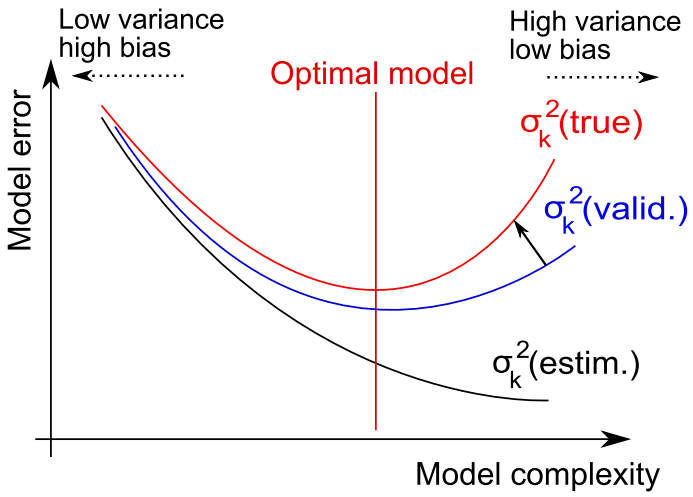

Figure 1.12: Typical curve of the modelling errors as function of model complexity.

1.4.2.1 Mallow's Cp

The method based on statistics C_p was developed by Mallows (see for example Mallows [51]). This method is adapted for problems where the models $\mathcal{M}$ form all nested *linear* models. Model $\mathcal{M}_k$ is defined as:

$$y_k(x) = \sum_{i=0}^{k} \beta_i(k)\eta_i(x) \tag{1.35}$$

where η_i is some known functions of x (for example Taylor Polynomials). Coefficients β represent the model parameters $\mathbf{p}$. Model $\mathcal{M}_k$ contains all the preceding models. In other words, $\mathcal{M}_1 \subset \mathcal{M}_2 \subset ... \subset \mathcal{M}_k$. Therefore we call these models *nested* models. The statistic C_p for the k-th model is defined as:

$$C_p(k) = \frac{\mathrm{RSS}_k}{\hat{\sigma}^2} - N_P + 2k \tag{1.36}$$

where $\hat{\sigma}^2$ is the estimation of variance of the measurement, N_P is the number of measurement points, k is the number of parameters. The residual sum of squares for the k-th model RSS_k is defined as:

$$\mathrm{RSS}_k = \sum_i ||y(x_i) - y_k(x_i, \hat{\mathbf{p}}_\mathbf{k})||^2 \tag{1.37}$$

The estimation of $\hat{\sigma}^2$ is crucial. It should be estimated from measurement conditions. However, it can be estimated also a posteriori from the fit of the models. Function C_p represents a statistics whose minimum with respect to the number of parameters k should yield an optimal model in terms of minimizing the variance of residuals (Eq.1.34). There are two important terms: the residual RSS_k diminishes with growing k as the model fits better the measurement.

However, the term $2k$ increases with model complexity and eventually its increase becomes larger than the decrease in the first term. Curve C_p as a function of k looks similar to the red curve in Fig.1.12.

The limitation of Mallow's method is that it can only be used for nested models and, more importantly, to linear models [13].

1.4.2.2 Subspace information criterion

The subspace information criterion (SIC) was first published by Sugiyama and Ogawa in [61]. The SIC criterion can be applied to any problem that can be expressed in terms of so-called *learning operator*. If we consider k-th model $\mathcal{M}_k$ its learning operator is $\mathbf{X}_k$ and the estimate of the model is:

$$y_k(x) = \mathbf{X}_k y(x) \tag{1.38}$$

Typical example where Eq.1.38 can be used is the linear fitting problems. If we consider a $\mathbf{y} = \mathbf{Ax}$ function, then the estimation of $\mathbf{y}$ using model A is $\hat{\mathbf{y}} = \mathbf{AA^{-1}y}$ and therefore, in this case, we obtain $\mathbf{X} = \mathbf{AA^{-1}}$.

Then, we suppose that there exists a model $\mathcal{M}_u$ which gives unbiased estimate of y, in other words $E(y_u) = y$, where $y_u = \mathbf{X}_u y$.[14] In these requirements are met, then the SIC criterion is defined for k-th model as:

$$\mathrm{SIC}_k = \|y_k - y_u\|^2 - \mathrm{tr}(\mathbf{X}_0\mathbf{Q}\mathbf{X}_0^T) + \mathrm{tr}(\mathbf{X}_k\mathbf{Q}\mathbf{X}_k^T) \tag{1.39}$$

where $\mathbf{X}_0 = \mathbf{X}_k - \mathbf{X}_u$ and $\mathbf{Q}$ is a matrix of noise covariance. The model with lowest value of SIC is chosen. It should minimize the variance of residuals given by Eq.1.34. There are two main limitations of the SIC method. The first is that the noise covariance matrix should be known with a fair precision. The second is that the matrices $\mathbf{X}_k$ must exist. This is not always the case. Especially, in the case of nonlinear fit, such a relation as Eq.1.38 does not exist. Unfortunately, the inverse problem as it is discussed in Section 3 is non-linear and the noise matrix is a priori unknown.

1.4.2.3 Cross-validation techniques

The cross-validation technique is very simple to use. Its theoretical basis was established by Stone [60]. The principle lies in the division of the measurement into two sets.[15] The *first* set is called *training set*. This set serves for the identification of the model parameters $\mathbf{p}$. The *second*

[13] This means that the value of function representing the model is a *linear* function of model parameters.

[14] In practice Sugiyama uses often the most complex model among the candidate models and supposes that the estimate would be unbiased (see Fig.1.12).

[15] The way, how this division should be done is somewhat arbitrary. None the less, there should be more measurement points in the validation set.

set is called the *validation set*. This set of measurements serves for the validation of the model. In other words, the predictive capacity of the identified model are tested. Using the notation employed in this section, we consider our measurement defined over P points $[x_1, x_2, ...x_{N_P}]$. Let us consider that all the measurement points with indices 1,2,..N_T belong to the training set and all the points with indices N_T+1,N_T+2,..N_P to the validation set.

Then, the k-th model is identified from the training set of measurements:

$$\hat{\mathbf{p}}_k = \underset{\mathbf{p_k}}{\operatorname{argmin}} \sum_{i=1}^{N_T} \|y(x_i) - y_k(x_i, \mathbf{p_k})\|^2 \tag{1.40}$$

The residual of different models in the training phase is not of importance. The important quantity is the residual of the identified model when applied to the validation set of measurements:

$$\sigma_k^2(\text{validation}) = \frac{1}{N_P - N_T - 2} \sum_{i=N_T+1}^{P} \|y(x_i) - y_k(x_i, \hat{\mathbf{p}}_\mathbf{k})\|^2 \tag{1.41}$$

If we have sufficiently independent measurements in the validation set then the validation variance should converge to the true variance defined by Eq.1.34 (see Fig.1.12):

$$\sigma_k^2(\text{validation}) \rightarrow \sigma_k^2(\text{true}) \tag{1.42}$$

The conditions of this convergence are, however, very difficult to asses. The advantage of the cross-validation method is its versatility. There are no a priori presumptions. The models can be linear or non-linear. Their complexity and number of parameters does not matter. If the model is too complex it would naturally get ill-posed and its prediction would become unstable and therefore increasing the validation error given by Eq.1.42. On the contrary, models which are too simple should be biased with respect to the validation set of measurements. The limitation of the cross-validation method is an absence of the theoretical framework. The open question is also the statistical importance of σ_k^2(validation). If, for example, σ_k^2(validation) is close to σ_{k+1}^2(validation), can we make a choice between these two models? This question is treated in Section 3.

1.4.3 Methods based on minimizing Kullback-Leibler distance

The Kullback-Leibler distance is a sort of information gain when we pass from function g to f.[16] It was defined by Kullback and Leibler in [58] as:

$$KL(f, g) = \int f(x) \ln\left(\frac{f(x)}{g(x|\theta)}\right) \mathrm{dx} \tag{1.43}$$

[16] Another equivalent formulation can be: How much information is lost when we use function g instead of f.

If $f = g$ then the $KL(f, g) = 0$. In the model selection problem treated by Akaike (AIC) and Takeuchi (TIC), the Kullback-Leibler distance given by Eq.1.43 is a quantity which is minimized, where f is considered as the truth and g represents different models. Even though the true function f is not known, Akaike and Takeuchi find ways to asymptotically estimate the lowest value of Kullback-Leibler distance of different models. The details of the Kullback-Leibler distance and AIC criterion are discussed in Section 3.2.1.

1.4.3.1 Akaike information criterion (AIC)

Akaike information criterion (AIC) was invented by Akaike [54]. He found that maximized the log-likelihood function is a asymptotically *biased* estimate of the Kullback-Leibler distance. The bias of this estimate is equal to the number of parameters of a model K. The AIC criterion is defined as:

$$\mathrm{AIC} = -2\ln(L(\mathcal{M}(\hat{\mathbf{p}})|\mathrm{data}) + 2K \tag{1.44}$$

where $L(\mathcal{M}(\hat{\mathbf{p}}))|\mathrm{data})$ is the maximized value of the likelihood function for the model $\mathcal{M}$. The optimal value corresponds to the lowest value of AIC. We can see that even though the goal of the AIC criterion are different from the methods based on the minimization of the expectation of residuals, the resulting form of the criterion looks similar to criteria such as Mallow's C_p and SIC. There is a first term decreasing with model complexity and the second increasing with model complexity.

1.4.3.2 Takeuchi information criterion (TIC)

Takeuchi derived a more advanced criterion (Takeuchi [57]) by omitting some a priori hypothesis made by Akaike. Notably, he dropped the assumption that the true model is among the candidate models. The criterion named TIC is defined as:

$$\mathrm{TIC} = -2\ln(L(\mathcal{M}(\hat{\mathbf{p}})|\mathrm{data}) + 2\mathrm{tr}\left\{\mathrm{J}(\hat{\mathbf{p}})[\mathrm{I}_F(\hat{\mathbf{p}})]^{-1}\right\} \tag{1.45}$$

where J is the expectation of the Hessian of the $\ln(L(\mathcal{M}(\hat{\mathbf{p}})|\mathrm{data}))$ and I_F is the expectation of the Fisher information. For details, see Burnham [56]. The optimal model has the lowest value of TIC. Although the TIC criterion is more general and it is based on fewer assumptions, due to the difficulty of evaluating the penalty term, it is rarely used in practice. In this work, this criterion is not used, either. The reason is that in the vibration problems, we can expect that at least one of the candidate models is rather close to the reality. For discussion on the subject of the selection of candidate models see Section 3.1.1.

1.4.4 Bayesian information criterion (BIC)

The Bayesian information criterion was developed by Schwarz [53]. Its principle is very different from the preceding two methods. The target model for BIC is the model M which has asymptotically the largest probability $P(M|\text{data})$. In other words, we are looking for a model which would be the most "likely" if the *data* is given. Some elements of derivation of BIC are presented in Section 3.2.2. Finally, the criterion BIC is defined as:

$$BIC = -2\ln L(\text{data}|\mathcal{M}(\hat{\mathbf{p}})) + K\ln N_P \tag{1.46}$$

where N_P is number of independent measurements and K is the number of parameters of the model $\mathcal{M}$. The optimal model has a lowest value of BIC. We can see that the resulting form of BIC 1.46 is very much similar to the AIC 1.45. This is quite surprising if we consider that different approaches were used at the beginning. We can see that if we have more than $e^2 = 7.4$ points N_P then the penalty of the BIC is more strict than the penalty of AIC. BIC is therefore considered more conservative than AIC. It tends to choose simpler models.

1.4.5 Comparison of different model selection methods

We have seen that there are multiple possible strategies of model selection. The choice of strategy depends strongly on the mathematical nature of the problem which is employed (inverse method). Some of the characteristics of the model selection methods are presented below in Tab.1.1.

Method	**Inverse problem**	**Meas. errors**	**True model among candidates**	**Other limits**
C_p	linear regr.	indep. known	no	only for nested models
SIC	linear regr.	any known	no	
Cross-valid.	any	indep. (unknown)	no	need for large independent samples
AIC	non-linear regr.	indep. (unknown)	yes	asymptotic
TIC	non-linera regr.	indep. (unknown)	no	asymptotic, difficult to use
BIC	non-linear regr.	indep. (unknown)	no	asymptotic

Table 1.1: Chosen characteristics of different model selection methods.

1.4.6 Examples of use of the model selection in mechanical problems

1.4.6.1 Identification of models from seismic measurements (BIC)

Beck et al.[55] used the BIC criterion for the selection of an adequate model in the seismic mechanical models. Two examples were considered.

The *first example* is a system with one DOF described by the equation of motion:

$$m\ddot{x} + c\dot{x} + f_s(x, k_1, k_2, x_y) = f(t) \tag{1.47}$$

where the seismic excitation $f(t)$ is known. Beck considers three possible forms of Eq.1.47 (see Fig.1.13A). The first model class is a linear damped model with $k_1 > 0$, $c_1 > 0$, and $x_y \to \infty$. The second model corresponds to a elastic-plastic model with $k_1 > 0$, $k_2 = 0$, $c = 0$ and $x_y > 0$. The third model is a bilinear hysteretic oscillator with $k_1 > 0$, $k_2 > 0$, $c = 0$ and $x_y > 0$. None of this models is the *true* model used for the simulated measurements. BIC criterion used by Beck uses the measurement output time signal and compares it with the signal simulated by different models.

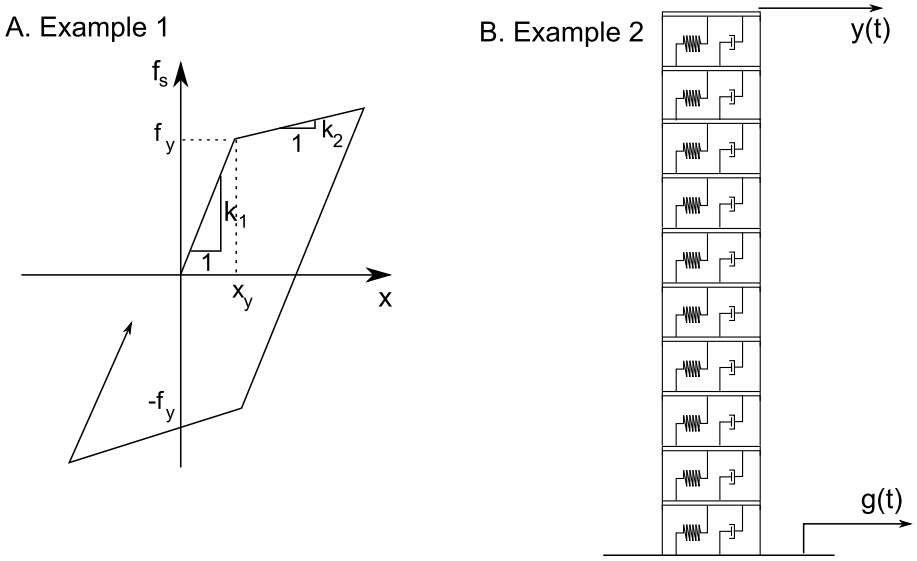

Figure 1.13: A. Hysteresis loop considered by Beck to describe the non-linear response to the seismic excitation. B. Ten-story building approximated by a model with springs and dampers. The excitation is forced by the ground motion g.

The *second example* consist in choosing the appropriate number of modes to describe a response of a ten-story building (see Fig.1.13B). This building is excited by a random stationary seismic ground motion. The spectrum obtained from the measurement y at the top of the building is used for comparison with a model of different modal size. The optimal number of modes is obtained by minimizing the BIC criterion.

1.4.6.2 Use of the cross-validation for the selection of the fatigue crack growth laws

Hombal et al. [62] used a modified cross-validation technique to select an optimal model to describe the law of propagation of fatigue cracks. As shown in Fig.1.14 there exist three distinct crack propagation behaviours shown by the zones I, II and III. Paris proposed a well-known *linear* law describing the part II ([78]). The nonlinear behaviour of the tail zone III was described by Lukas [76]. Hombal developed a cross-validation method which permits to split the space of ΔK into the regions where the Paris law is optimal and the regions where the Klesnil-Lukas law gives better predictions. It should be noted that both models (Paris and Klesnil-Lukas) are purely empirical, so none of them can be considered as the "true" model.

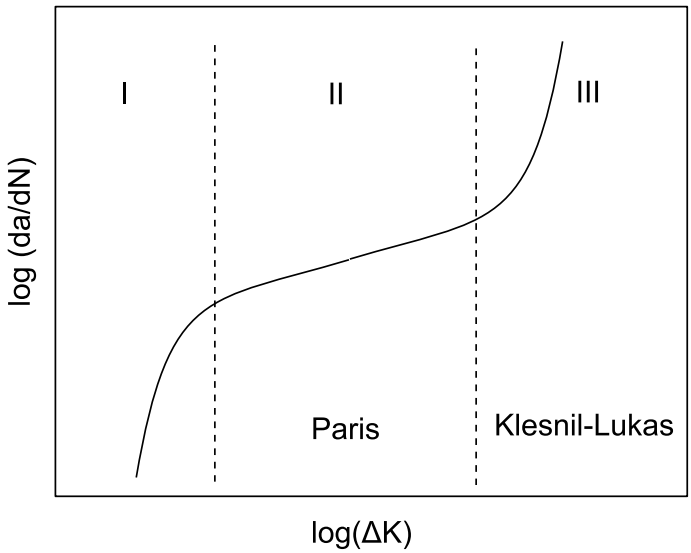

Figure 1.14: Typical curve of the propagation of the crack with three distinct zones. da/dN means the stands for the change of crack length per stress cycle, ΔK is the effective amplitude of the stress intensity factor.

1.5 Outline of the thesis

The outline of this thesis is as follows. After the introductory Chapter 1, the following chapters deploy the ideas of this work.

The Chapter 2 further develops two of the inverse methods discussed in Section 1.3: Inverse wave correlation (IWC) and Inverse wave decomposition (IWD). These methods belong to a class of inverse methods which use the local measurement of the vibration field and determine the parameters of the equation of motion. These two methods were chosen for their performance and relative robustness, because other methods are quite sensitive to the measurement noise.

The Chapter 3 presents the basic elements of the model selection developing the introduction part in Section 1.4. It is shown that each of the inverse problems must be treated with different model selection technique. The information theory criteria (AIC and BIC) are used for the IWC inverse problem and Cross-validation technique is used for the IWD inverse problem. A particular attention is given to show why the information criteria cannot be used generally. It is shown, that residuals of the inverse problem are rarely statistically independent.

In Chapter 4, three typical experimental cases are treated. The first case consists in determining the presence of axial force in beams and membranes, the second addresses the question of the orthotropy of unknown composites, the third case represents a problem of identification of unknown structures with complicated vibration behaviour.

Chapter 5 concludes the thesis and presents the perspectives of this work.

Appendix A describes the experimental details of the measured structures presented in the manuscript. Appendix B describes the modified version of the three-point static test employed on beams. Appendix C discusses the problem of coupling the vibration of plates with surrounding air. Appendix D describes the Dym-Lang sandwich model used in the identification of the equation of motion.

2

Inverse methods

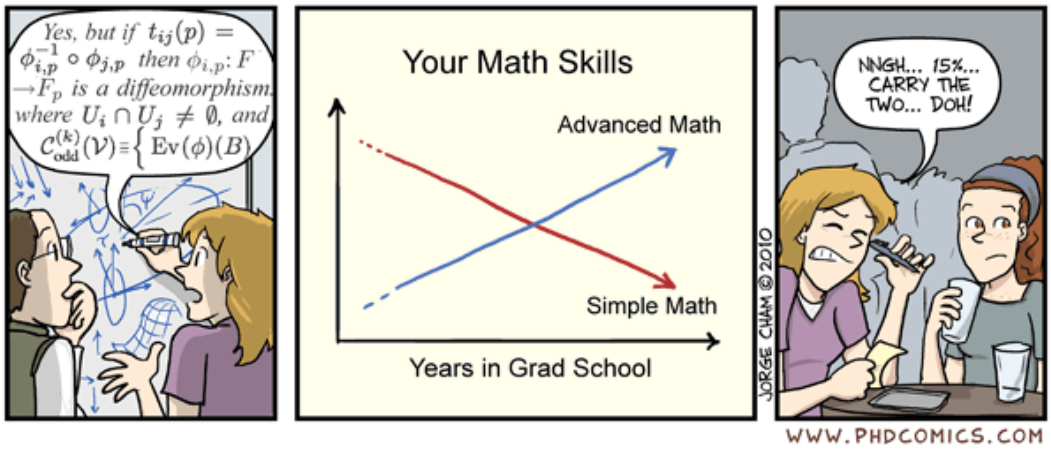

"Make things as simple as possible, but not simpler." (Albert Einstein)

2.1 Statement of the inverse problem

Traditionally, the problem of calculating vibration response can be separated in three parts (see Fig.2.1): input (excitation), system (model) and output(measurement, simulation). In the direct approach we calculate the response (output) from the known input (excitation) and from the known system. Typically, the inverse problems either seek to determine the excitation from the known system and output or the system from the known excitation and the known output and input.

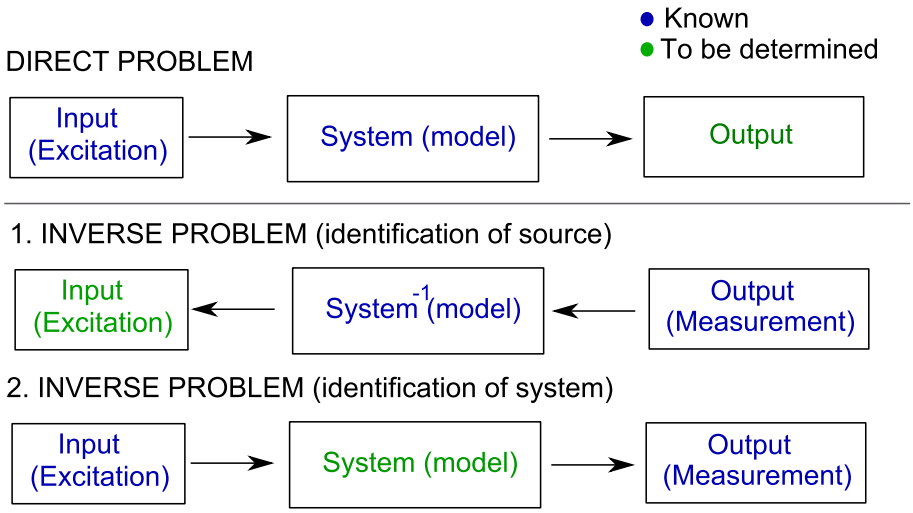

Figure 2.1: Typical direct and inverse problems in vibroacoustics.

There are three different inverse methods presented below in this section:

- Inverse wave correlation (IWC)
- Inverse wave decomposition (IWD)
- Inverse Galerkin method

They all belong to the second inversion scheme in Fig.2.1, their goal is to determine the system. However, the difference is that they do not determine the system completely but only partially as can be seen in Fig.2.2. They use only output as inversion data and their only goal is to determine the *equation of motion* of the system. The boundary conditions, geometry and initial conditions are not determined. This weakness is also a strength in some sense because the inverse methods are at the same time *independent* of boundary conditions and geometry of the structure.

Typical problems solved by the mentioned inverse methods can be seen in Fig.2.3. On the left, we can see a complicated engineering structure which can be nevertheless modelled as a structure composed of several linear elements joined together. Although we know neither the

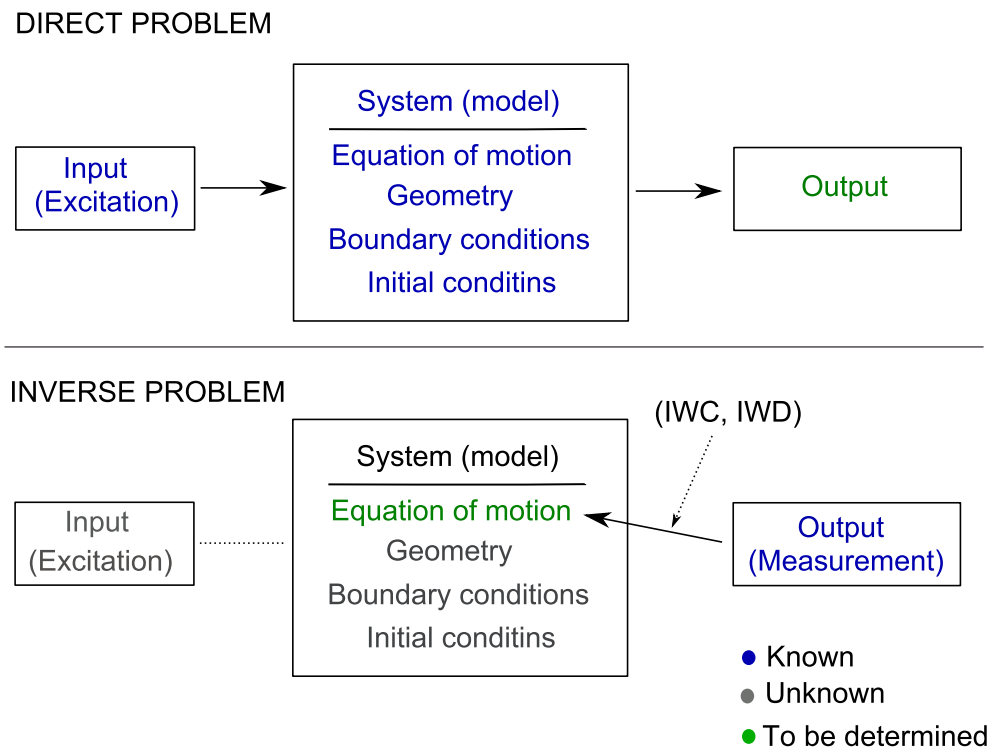

Figure 2.2: Schematics of the inverse methods used. The important feature of the inverse methods used in this work is that they enable only the estimation of the equation of motion.

excitation force represented by point force F nor the boundary conditions we can employ the inverse methods to determine the *local* equation of motion of the linear structure between the points A and B.

Another problem can be represented by the measurement effected on guitar backboard represented in Fig.2.3 on right. Although we know neither the excitation nor the boundary conditions and complicated geometry of the guitar as a *whole* object, we can still use the local inverse method on planar wooden plate part designed as Ω and determine local equation of motion adapted for the zone Ω.

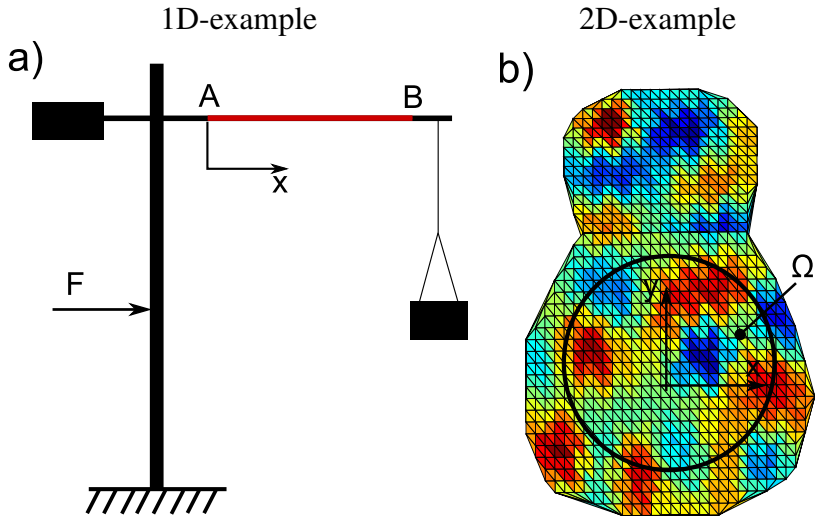

Figure 2.3: Two exemplary problems which could be solved by the presented inverse methods. a) A beam-like structure Ω between the points A and B. b) Backboard vibration field of the acoustic guitar.

2.2 Considered equations of motion

2.2.1 Equations of motion in one dimension

Let us suppose that we are dealing with a following self-adjoint linear operator $\mathcal{L}$ which has the form

$$\mathcal{L}(u) = c_0 u(x) + c_2 \frac{d^2u(x)}{dx^2} + c_4 \frac{d^4u(x)}{dx^4} + c_6 \frac{d^6u(x)}{dx^6} + ... = f(x) \tag{2.1}$$

where u is the transverse (flexural) displacement of the string or beam described by the x coordinate and f is the external generalized force. This force is considered zero in our zone of interest Ω (see Fig.2.3). Several 1D models will be studied in this thesis, their overview is in the Tab.2.1.

	Model	Coefficients
A_1	String	$c_0 = \rho_L \omega^2$ $c_2 = T$
A_2	Euler	$c_0 = -\rho_L \omega^2$ $c_4 = EI$
A_3	Euler+Force	$c_0 = -\rho_L \omega^2$ $c_2 = -T$ $c_4 = EI$
A_4	Timoshenko	$c_0 = -\rho_L \omega^2 + \frac{\rho_L^2 \omega^4 I}{\kappa A^2 G}$ $c_2 = \omega^2 \rho_L \frac{I}{A}(1 + \frac{E}{\kappa G})$ $c_4 = EI$
A_5	Nilsson	$c_0 = \omega^4 I_p \rho_L - \omega^2 G_e H \rho_L$ $c_2 = \omega^2 (D_1 \rho_L + 2D_2 \rho_L + I_p G_e H)$ $c_4 = G_e H D_1 - 2D_2 I_p \omega^2$ $c_6 = -2D_1 D_2$

Table 2.1: Overview of 1D models.

- The ***String*** model describes the thin string under an axial tension T and a linear density ρ_L. The bending stiffness of the string is neglected. Unlike the other operators, this operator is of second order. Its general solution is composed uniquely of propagation waves, while all the other operators have also evanescent waves as solution.

- The ***Euler*** model represents the most simple model for the flexural vibration of thin beams. The shear deformation effects are neglected and it is supposed that the sections of the beam remain plane during deformation. This model describes well the behaviour at low frequencies. The term EI represents the bending stiffness, with E the Young's modulus and I the moment of inertia of the beam section.

- The ***Euler+Force*** model is the mix of the preceding two models. It can either be a beam which is submitted to some external axial force (can be a traction or compression). Or it can be a string submitted to some traction axial force T where the bending stiffness is not negligible. The later case can typically be a steel cable used in suspended bridge constructions or a low E bass guitar string.

- The ***Timoshenko*** model is adapted for vibration of beams at higher frequencies where the *Euler* model is not precise enough. This model takes into account the shear effect of the initially plane sections of the beam. G is the shear modulus, A is the beam section and $\kappa = 5/6$ for rectangular sections.

- The ***Nilsson*** model was specially developed by Nilsson [77]. It is adapted to the flexural vibration of relatively thin sandwich beams with rigid thin faces and light and soft core (see Fig.2.2.1). There are three unknowns related to stiffness of the beam D_1, D_2 and G_e. G_e is the shear modulus of the core. Coefficients D depend on Young modulus of the core and the laminated layers

$$D_1 = E_1 H^3/12 + E_2(H^2 h/2 + Hh^2 + 2h^3/3) \tag{2.2}$$
$$D_2 = E_2 h^3/12 \tag{2.3}$$

where h is the thickness of the layer and H is the thickness of the core. Generally, $H \gg h$ and $D_1 \gg D_2$. The mass moment of inertia per unit width I_p is defined as

$$I_p = \rho_c H^3/12 + \rho_l(H^2 h/2 + Hh^2 + 2h^3/3) \tag{2.4}$$

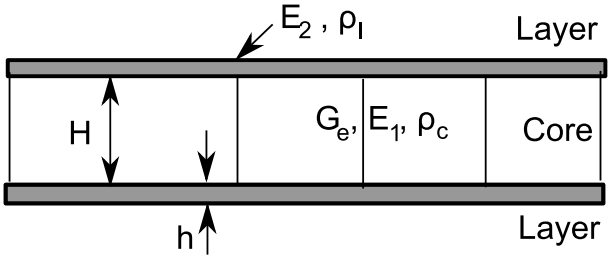

Figure 2.4: Geometry of the Nilsson sandwich beam.

The sixth-order equation of the Nilsson model can be approximated by equivalent fourth-order equation $c_4^{app} u^{(IV)} + c_0 u = 0$ where $c_0 = -\rho_L \omega^2$ and $c_4^{(app)}$ is the solution of the following equation :

$$\left(\frac{G_e H}{\rho_L^{1/2}\omega}\right)\left[\frac{(c_4^{\text{app}})^{3/2}}{D_1} - D_1^{1/2}\right] + c_4^{\text{app}} - 2D_2 = 0 \tag{2.5}$$

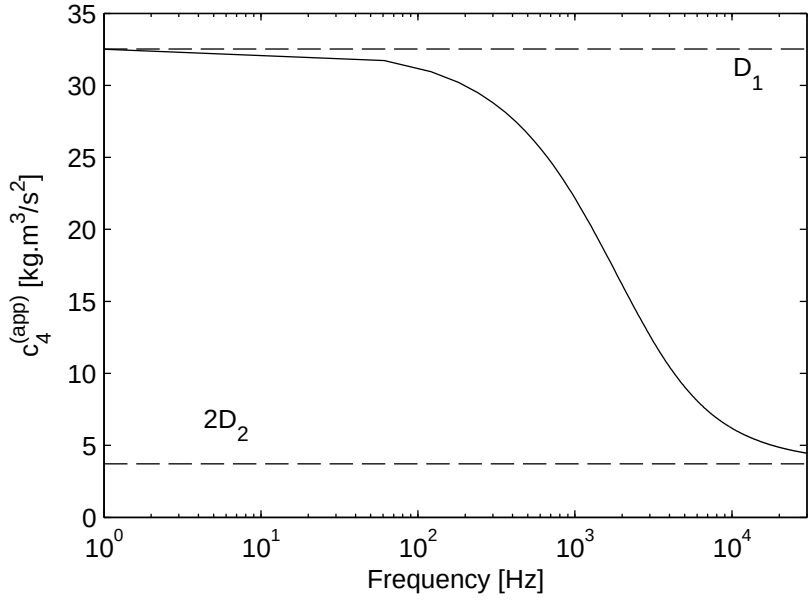

Figure 2.5: Typical evolution of apparent (equivalent) bending stiffness $c_4^{(app)}$ with frequency of the Nilsson sandwich beam.

This approximation can be seen as an equivalent *Euler* beam with changing stiffness $EI = c_4^{(app)}(\omega)$. A typical example is shown in the Fig.2.5. We can see the relevance of the parameters D. The parameter D_1 represents the *static* or low-frequency stiffness while the high-frequency stiffness is represented by double the stiffness of the layers $2D_2$. This can be a disadvantage of sandwich beams which might be very stiff in static conditions but they soften rapidly at higher frequencies. It should be noted that it is difficult to use the Nilsson model at high frequencies because the vibration field becomes two and three-dimensional and the simplifying hypothesis of beams are no longer true.

2.2.2 Equations of motion in two dimensions

2.2.2.1 Isotropic models

The *isotropical* models (in the plane (x,y) can be described by the following equation of motion:

$$\mathcal{L}(u) = c_0 u + c_2 \Delta u + c_4 \Delta^2 u = f \tag{2.6}$$

where the coefficients c are described in Tab.2.2. The external force is considered $f(x, y) = 0$ in the zone of observation Ω.

Model		Coefficients
B_1	Membrane	$c_0 = \rho_S \omega^2$ $c_2 = T$
B_2	Kirchhoff	$c_0 = -\rho_S \omega^2$ $c_4 = D$
B_3	Kirchhoff/memb.	$c_0 = -\rho_S \omega^2$ $c_2 = -T$ $c_4 = D$
B_4	Mindlin	$c_0 = \frac{\rho^2 \omega^4}{G^2}\left(1 - \frac{12\kappa^2 G}{\omega^2 h^2 \rho}\right)$ $c_2 = -\frac{\rho\omega^2}{G}\left(\frac{12D}{Gh^3} + \kappa^2\right)$ $c_4 = \kappa^2 \frac{12D}{Gh^3}$
B_5	Dym (sandwich)	in the text

Table 2.2: Overview of 2D isotropic models.

- ***Membrane*** model describes thin membrane with surface density ρ_S and uniform tension T. The flexural stiffness of the membrane is neglected. Due to the lightness of membrane structures, the condition $f = 0$ is not always respected due to the coupling with air. This question is treated in appendix.

- ***Kirchhoff*** model describes the vibration of thin plate. It is equivalent to Euler-Bernoulli model for thin beams. The shearing effect is neglected and plane section remain plane during the deformation. The model is generally considered valid for lower frequencies until the wavelength gets below ten times the thickness of the plate. Parameter D is the plate stiffness. For homogeneous isotropic materials it can be calculated from the elastic parameters

$$D = \frac{Eh^3}{12(1-\mu^2)} \tag{2.7}$$

  where h is the thickness of the plate, E is the Young's modulus, μ is the Poisson ratio.

- ***Kirchhoff/membrane*** model is the mix between the two preceding models. It can be either seen as a thick membrane with non-negligible bending stiffness D or as a thin plate pre-stressed by isotropic tension T.

- ***Mindlin*** model is plate equivalent of the Timoshenko model for beams. It is adapted to vibration of thick plates (or thin plates at higher frequencies). In the domain of low frequencies it is equivalent to Kirchhoff model. In Tab.2.2 G stands for the shear modulus, μ is the Poisson ratio, h is thickness of the plate, $\kappa \approx \pi/\sqrt{12}$.

- ***Dym*** sandwich model was proposed by Dym and Lang in [68]. This model considers a composite sandwich with two identical thin faces and a thick core (see Fig.D.1A). Core

and skins are supposed made from isotropic material. The somewhat lengthy mathematical description of the model can be found in Appendix D.

2.2.2.2 Orthotropic models

From the family of anisotropic models only the *orthotropic* models are considered due to their technical importance. Orthotropic models can be applied to most wooden plates as well as a majority of reinforced composites. The equation of motion takes the following form (later referred to as model B_6):

$$\mathcal{L}(u) = -\rho_S \omega^2 u + D_1 \frac{\partial^4 u}{\partial x^4} + D_3 \frac{\partial^4 u}{\partial y^4} + (D_2 + D_4) \frac{\partial^4 u}{\partial x^2 \partial y^2} = 0 \tag{2.8}$$

This equation corresponds to the Kirchhoff model applied to the orthotropic symmetry of the plate. Orthotropic model becomes isotropic when $D_1 = D_3 = D$ and $D_2 + D_4 = 2D$. In the orthotropic model there are four stiffness parameters but the equation of motion depends only on three (D_1, D_3 and the sum $D_2 + D_4$). For brevity, we will establish a new parameter $D_{24} = D_2 + D_4$.

There are many more models developed for vibration problems of plates (mostly the composite plates). However, their description is complicated and they cannot be expressed in single equation of like Eq.2.6 or 2.8. The problem from the inverse point of view is that they often necessitate a multitude of parameters which cannot be determined with confidence with the methods proposed in this thesis. The maximum of parameters determined from vibration field measurement in this thesis is three (orthotropic model).

2.3 Inverse wave correlation method (IWC)

The Inverse wave correlation method is described in introduction section 1.3.2.2. In this work the original method of Berthaut is used with small changes.

We assume that a particular equation of motion is given by the operator:

$$\mathcal{L}(u) = 0 \tag{2.9}$$

The differential operator $\mathcal{L}$ depends on an unknown vector of parameters $\mathbf{p}$. The goal of the inverse problem is to determine these parameters, to estimate $\hat{\mathbf{p}}$. The inverse method used in this work consists of two parts.

First, the IWC method is used to determine the optimal wavenumber from the vibration fields. We assume the vibration field is measured for N_{freq} frequencies and each field is investigated in N_{dir} directions (see 1.3.2.2). For a particular direction i and vibration field w_j corresponding to the j-th frequency, the (experimental) wave number is:

$$[\hat{k}_{ij}^{(exp)}] = \underset{k,\gamma}{\operatorname{argmax}}\, IWC(w_j, k, \gamma, \theta_i) \tag{2.10}$$

where the IWC value is given by Eq.1.4 and $\hat{k}^{(exp)}$ stands for the complex wave number $k(1+\gamma)$. In this work a modified method of Berthaut is used. The plane wave "correlation" function defined by Berthaut is given by Eq.1.5

$$\psi(k,\theta) = \exp\left(\mathrm{i}k(1+\mathrm{i}\gamma)(x\cos\theta + y\sin\theta)\right) \tag{2.11}$$

has zero phase at the coordinate origin, which does not always correlates well with the vibration field where the origin is arbitrary. In this work the plane wave correlating with the measured field is enlarged by a free *phase* term β:

$$\psi(k,\theta,\beta) = \exp\left(\mathrm{i}k(1+\mathrm{i}\gamma)(x\cos\theta + y\sin\theta + \beta)\right) \tag{2.12}$$

the modified IWC value is then obtained by finding optimal phase β which maximizes the correlation between w and $\psi(k,\theta,\beta)$:

$$\mathrm{IWC}_m(w,k,\gamma,\theta) = \max_\beta \frac{\left|\int_\Omega w.\psi(k,\gamma,\theta,\beta)\mathrm{d}\Omega\right|}{\sqrt{\int_\Omega |w|^2\mathrm{d}\Omega \int_\Omega |\psi(k,\gamma,\theta,\beta)|^2\mathrm{d}\Omega}} \tag{2.13}$$

The advantage of using Eq.2.13 instead of Eq.1.4 will be shown in Section 2.3.2.2.

Second, optimal parameter $\hat{\mathbf{p}}$ of the equation of motion (Eq.2.9) is found by minimizing the distance between the modelled wave numbers k_{ij}^{mod} and the experimental ones:

$$\hat{\mathbf{p}} = \underset{p}{\operatorname{argmin}} \sum_{i,j} (\hat{k}_{ij}^{exp} - k_{ij}^{mod}(\mathbf{p}))^2 = \underset{p}{\operatorname{argmin}} \sum_{i,j} (r_{ij}(\mathbf{p}))^2 \tag{2.14}$$

where $k_{ij}^{mod}(\mathbf{p})$ is the wave number corresponding to the propagating wavenumber[1] given by the dispersion equation associated to the operator Eq.2.9. The residual sum of squares RSS is defined as:

$$\mathrm{RSS} = \sum_{i,j} (r_{ij}(\hat{\mathbf{p}}))^2 \tag{2.15}$$

Another way of finding the estimate $\hat{\mathbf{p}}$ instead of minimizing the residual function is to maximize the likelihood function. If we suppose that the residuals $r_{ij} = k_{ij}^{(exp)} - k_{ij}^{mod}(\hat{\mathbf{p}})$ are identically independently[2] normally distributed with zero mean and variance σ^2, then the likelihood function can be written as (for example ([56], page 11))

$$L(\mathbf{p}) = \prod_{i=1}^{N_{freq}} \prod_{j=1}^{N_{dir}} \frac{1}{\sqrt{2\pi}\sigma} \exp\left(-\frac{r_{ij}^2(\mathbf{p})}{2\sigma^2}\right) = \left(\frac{1}{2\pi\sigma^2}\right)^{N/2} \exp\left(-\frac{\sum_{ij} r_{ij}^2(\mathbf{p})}{2\sigma^2}\right) \tag{2.16}$$

where $N = N_{freq}N_{dir}$ is the total number of identified wave numbers. The variance can be estimated as

$$\sigma^2 = \frac{\mathrm{RSS}}{N} \tag{2.17}$$

For the statistical purposes, the natural logarithm of Eq.2.16 is rather used. It is equal to:

$$\ln L(\mathbf{p}) = -\frac{N}{2}\ln(2\pi) - \frac{N}{2}\ln\sigma^2 - \frac{1}{2}\sum_{ij}\left(\frac{r_{ij}^2(\mathbf{p})}{\sigma^2}\right) \tag{2.18}$$

The maximum of the log-likelihood function determines the solution of the inverse problem.

2.3.1 Estimation of errors

2.3.1.1 Using the log-likelihood function

Log-likelihood function is not only used for estimation of the optimal parameter of a model but it can also serve for estimation of interval of confidence of this parameter. One technique is to see how fast the log-likelihood function drops down from its maximum. For a normal distribution the confidence interval of 67% is the union of the points satisfying the following

[1] This wavenumber can be complex if the damping is present. In the original method of Berthaut, complex values of wavenumber were considered, but author of this work discourages the use of the complex wavenumbers unless we deal with a highly-damped structures. The reason is that the inverse problem given by Eq.2.10 becomes much more unstable

[2] For a independence consideration see Section 2.3.2.5

inequality $\ln L(\mathbf{p}) > (\ln L(\hat{\mathbf{p}}) - 1)$ ([56], page 11). This can be demonstrated on the maximum likelihood estimation using IWC on the real data of the measurement of aluminium plate of 2mm thickness. The log-likelihood function corresponding to the Eq.2.18 is shown in Fig.2.6. Here we consider a Kirchhoff plate equation and the unknown parameter $\mathbf{p}$ is the plate thickness D.

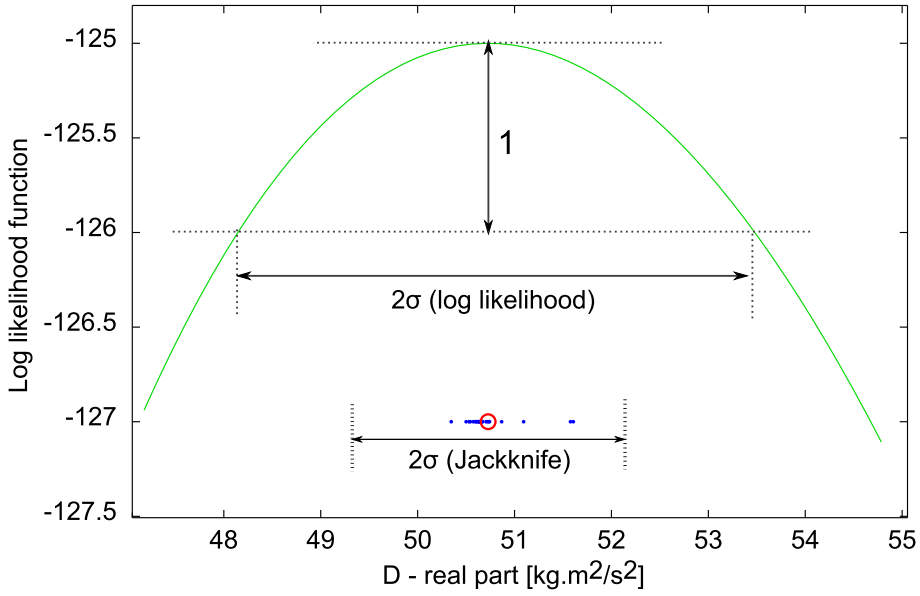

Figure 2.6: Comparison of two way to estimate the confidence interval of the IWC method. The green line represents the log-likelihood function. The blue dots represent the re-sampled solutions using the jackknife method. This example was taken from the analysis of the measurement done on 2mm thick aluminium plate.

2.3.1.2 Jackknife method

The *jackknife* method is based on re-sampling the initial set of measurements. Let us suppose we measured a vector $\mathbf{W} = [w_1, w_2, ...w_N]$ (w can be seen as the displacement field for one frequency in our case). This vector of measurements can serve to determine a model (represented by $\hat{\mathbf{p}}$) by some inverse technique as IWC. Schematically, we can write

$$[w_1, w_2, ...w_N] \xrightarrow{IWC} \hat{\mathbf{p}}$$

But if we omit the i-th component [3] from the vector $\mathbf{W}$ we would get different result $\hat{\mathbf{p}}^{(\mathbf{i})}$:

$$[w_1, w_2, ..., w_{i-1}, w_{i+1}, ...w_N] \xrightarrow{IWC} \hat{\mathbf{p}}^{(\mathbf{i})}$$

In this way we can obtain N slightly different values $[\hat{\mathbf{p}}^{(\mathbf{1})}, \hat{\mathbf{p}}^{(\mathbf{2})}, ...\hat{\mathbf{p}}^{(\mathbf{N})}]$. These so-called

[3] This procedure is called *leave-one out* technique. There exist also different schemes of jackknife where multiple entries in the vector $\mathbf{W}$ are omitted at the same time.

jackknife estimates can be used to estimate some statistical properties of the $\hat{\mathbf{p}}$. For our purposes, we will use the estimate of the covariance of the identified vector $\hat{\mathbf{p}}$. From Bontempi [70], the jackknife estimate of the covariance matrix of $\hat{\mathbf{p}}$ is:

$$\mathrm{Cov}(\hat{\mathbf{p}})_{ij} = \frac{N-1}{N} \sum_{k=1}^{N} (\hat{p}_i^{(k)} - \hat{p}_i^{(.)})(\hat{p}_j^{(k)} - \hat{p}_j^{(.)}) \tag{2.19}$$

where $\hat{\mathbf{p}}^{(.)} = 1/N \sum_k \hat{\mathbf{p}}^{(k)}$. The scheme of the described method can be seen in Fig.2.3.1.2. It should be noted that the estimate $\hat{\mathbf{p}}$ based on the complete set of measurements $\mathbf{W}$ is not necessarily the same as the mean of particular jackknife estimates $\hat{\mathbf{p}}^{(.)}$. [4]

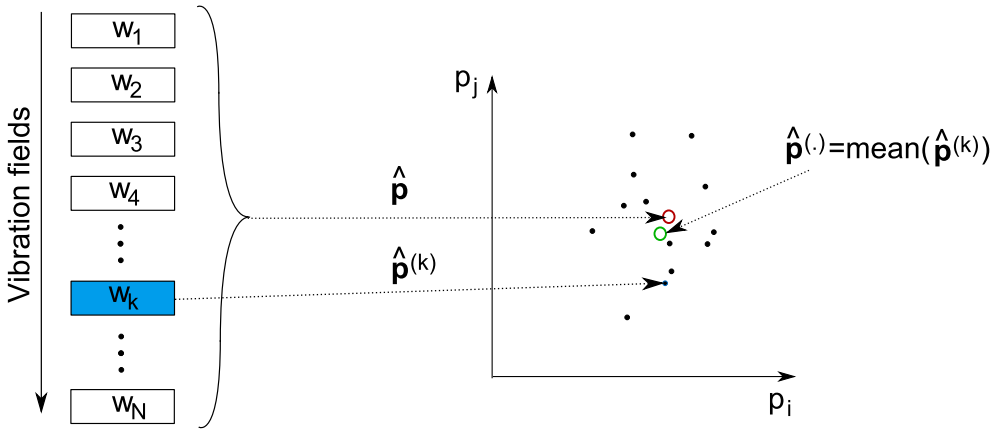

Figure 2.7: Scheme of the jackknife method. On left we have a set of independent displacement fields. When all displacement fields are used in the inverse problem (IWC) we obtain the parameter vector $\hat{\mathbf{p}}$. If the k-th vibration field is omitted we get the solution $\hat{\mathbf{p}}^{(k)}$.

The advantage of the jackknife method is that it does not necessitate any hypothesis about the distribution of $\mathbf{p}$ or $\mathbf{W}$. Neither the problem does necessitate to be linear. Otherwise, the estimated covariance seems to be too optimistic with respect to the preceding method. In case of the two estimates, the better choice is to take the estimate with the larger value.

2.3.2 Some remarks about the IWC method

As it was discussed in Section 1.3.2.2 the IWC function is maximized for the natural wave number which describes the vibration field. This is true, however, only for infinite wave fields. Two remarks are presented below to show how IWC function behaves on finite wave fields.

2.3.2.1 Asymptotic properties of the IWC function

As it was mentioned in Section 1.3.2.2, the estimate $\hat{k}$ (Eq.2.10) approaches asymptotically to the natural wavenumber of the equation of motion which defines the displacement function w.

[4] Actually the difference $(N-1)(\hat{\mathbf{p}}^{(.)} - \hat{\mathbf{p}})$ is an estimate of the bias of the jackknife estimator. Its large value can show that the estimation is biased (the distribution is not symmetric).

This behaviour can be shown easily in one dimensional space. Let us consider a sine function w =sin(kx). This function is correlated with a "correlation" wave ψ =sin($k_p x$). Both functions are defined on the finite interval <0,L>. The IWC value for the two functions is:

$$\mathrm{IWC} = \left| \frac{\int_0^L \sin(kx)\sin(k_p x)\mathrm{d}x}{\sqrt{\int_0^L \sin^2(kx)\mathrm{d}x \int_0^L \sin^2(k_p x)\mathrm{d}x}} \right| \tag{2.20}$$

It can be shown that the integral 2.20 can be evaluated as follows [5]

$$\mathrm{IWC} = \frac{N(k, k_p, L)}{\sqrt{2kL - \sin 2kL}\sqrt{2k_p L - \sin 2k_p L}} \tag{2.23}$$

where the nominator N is independent of the length L and can be bounded by $|N| < 4\sqrt{k_p k}/|k - k_p|$. However, the denominator of Eq.2.23 is unbounded and asymptotically behaves as $\propto 2kk_p L$. Consequently, if the wave numbers k and k_p are not the same the IWC function vanishes to zero with growing interval L. However, if the wave numbers are the same $k = k_p$ than the IWC value is always equal to 1 regardless to the interval length L.

2.3.2.2 Question of correlation wave phase

In the original works of Berthaut the non-zero phase shift β was not included in the plane wave formulation Eq.2.12. It can be shown that this omission can bias the maximum of the IWC function. It is reasonable to use this phase shift because the origin of the coordinate system (x,y) is freely chosen so we should not prefer a plane wave which has zero phase at the origin.

Example of the influence of free phase parameter β is shown in the case of an one-dimensional wave $w = \sin(20x + \pi/3)$ defined over the interval $[0, 1]$. This wave is correlated with the wave having a zero phase shift given by Eq.2.11 and with the wave having the free phase given by Eq.2.12. In Fig.2.8 we can see the comparison of the IWC function as defined by Eq.1.4 and its modification given by Eq.2.13 applied to the function w. We can see that the maximum of the IWC function is then biased if the phase shift β is not taken into account. However, it should be noted that the inclusion of the free phase β enlarges the width of the IWC peak and consequently leads to bigger standard deviance estimators of the wavenumber estimate.

[5] We use the following identities:

$$\int_0^L \sin(ax)\sin(bx)\mathrm{d}x = \frac{b}{a^2 - b^2}\sin(aL)\cos(bL) + \frac{a}{b^2 - a^2}\cos(aL)\sin(bL) \tag{2.21}$$

$$\int_0^L \sin^2(ax)\mathrm{d}x = \frac{1}{4a}(2aL - \sin(2aL)) \tag{2.22}$$

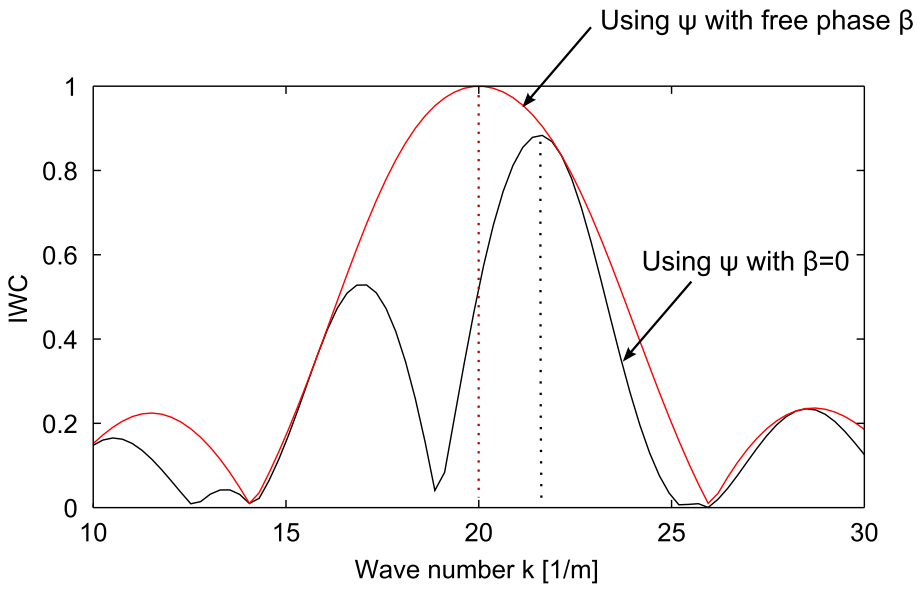

Figure 2.8: Comparison of the two methods of obtaining IWC function with correlation wave with and without free phase β.

2.3.2.3 Wave correlation with a plane-wave field

Let us consider a *single* plane wave propagating in the x-direction with wavelength λ defined over a two-dimensional domain Ω=[0,Δl]×[0,Δl] as shown in the Fig.2.9. This plane wave is correlated with a plane wave of the same wavelength. The difference of angles of propagation of these waves is θ.

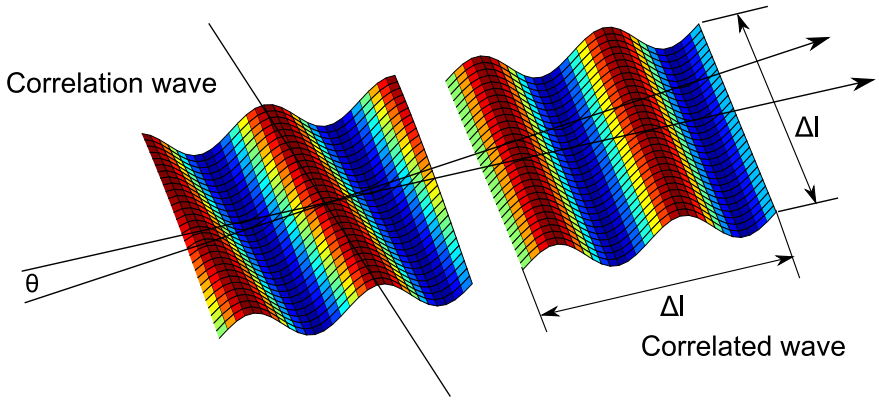

Figure 2.9: Scheme of the correlated plane wave.

First, we consider $\theta = 0$ and we change the dimensions of the domain Ω. It can be seen from Fig.2.10 that if more wavelengths are present in the wave-field, better is the resolution of the maximum of the IWC function.

Second, we fix the size of the domain to $\Delta l = 4\lambda$ and we vary the angle θ. It can be seen from Fig.2.11 that even for very small angles θ the IWC function drops fast to zero and its maximum

disappears. This can also be demonstrated in Fig.2.12 where the IWC function is shown as function of the **k** vector of the correlating wave. We see distinctly the two symmetrical maxima showing the presence of a unique plane-wave.

The conclusion we can make out of this paragraph is that:

- The good resolution of the IWC function is achieved for wave-fields larger than four wavelengths.
- The maximum of the IWC is achieved only in the presence of the wave propagating in the direction of the correlation wave as shown in Fig.2.12.

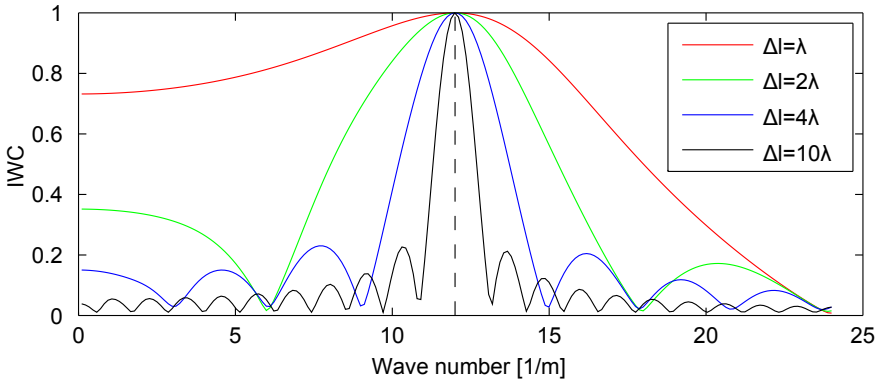

Figure 2.10: Influence of the size of the domain Ω with respect to wavelength on the resolution of IWC function.

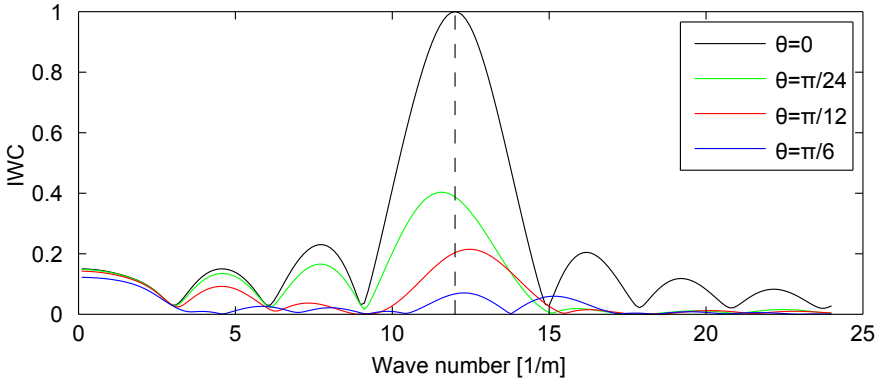

Figure 2.11: Influence of the misaligning of the plane wave on their correlation.

The behaviour of the IWC in the presence of multiple waves is discussed in the following paragraph.

2.3.2.4 Wave correlation with complex vibration field

To understand the behaviour of the IWC function on complex field we use the real experimentally measured wave fields on aluminium plate 2mm thick(experimental details are in the

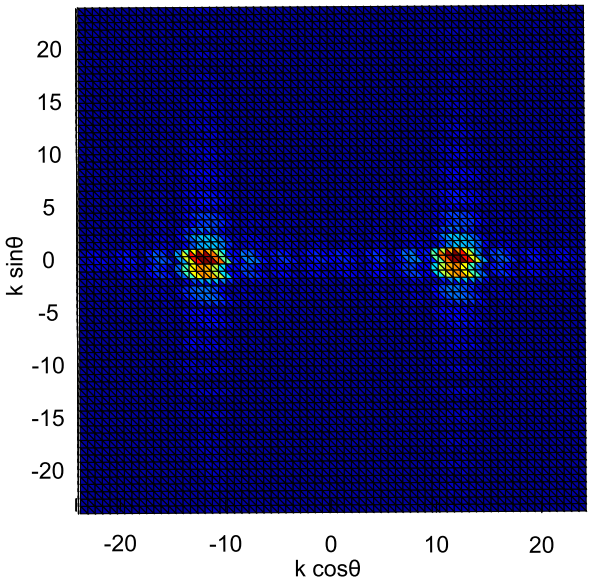

Figure 2.12: IWC function in the space [kcosθ ksinθ] defining the correlating wave.

Appendix A.2). Its average spectral density function of displacement is shown in Fig.2.13. Two wave-fields are chosen. One is a modal wave-field corresponding to 2768Hz (Fig.2.14A) and the other a non-modal steady state vibration field at 2850Hz (Fig.2.15A). This field is apparently constructed by superposition of a number of modes.

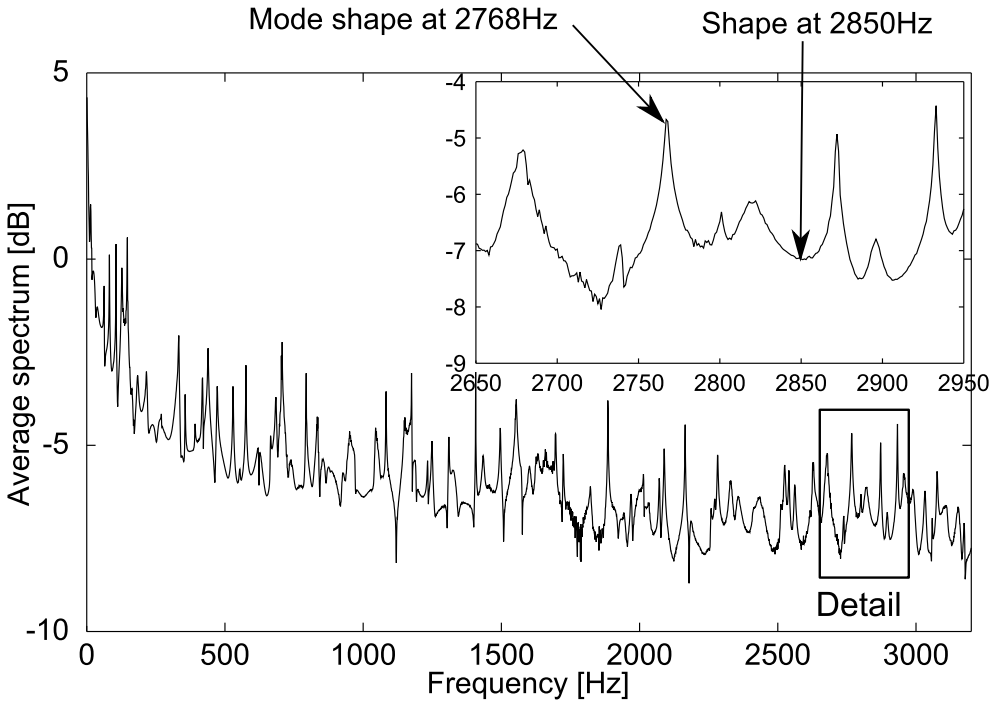

Figure 2.13: Average spectral density of the vibration response of the Aluminium 2mm plate.

In Fig.2.14B, we can see a IWC function in the k-space. It can be clearly seen that there are

two strong maxima (four if mirror images are counted) corresponding to the dominant waves which construct the mode at 2768Hz. Otherwise, there are no maxima in the y-direction showing that the mode is composed mostly of the waves in the x-direction.

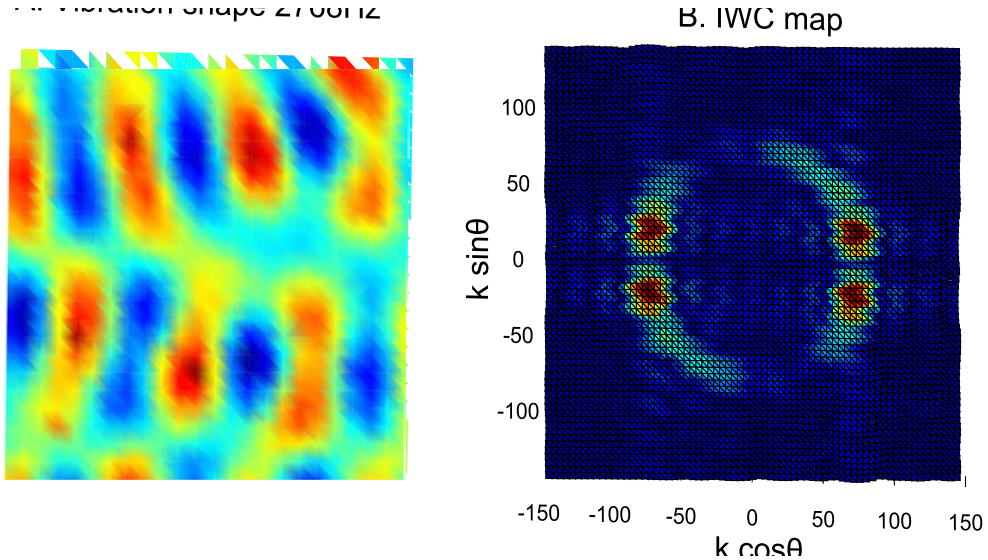

Figure 2.14: Aluminium 2mm plate. A - vibration shape at 2768Hz. B - IWC as a function of the wave numbers of the correlating wave.

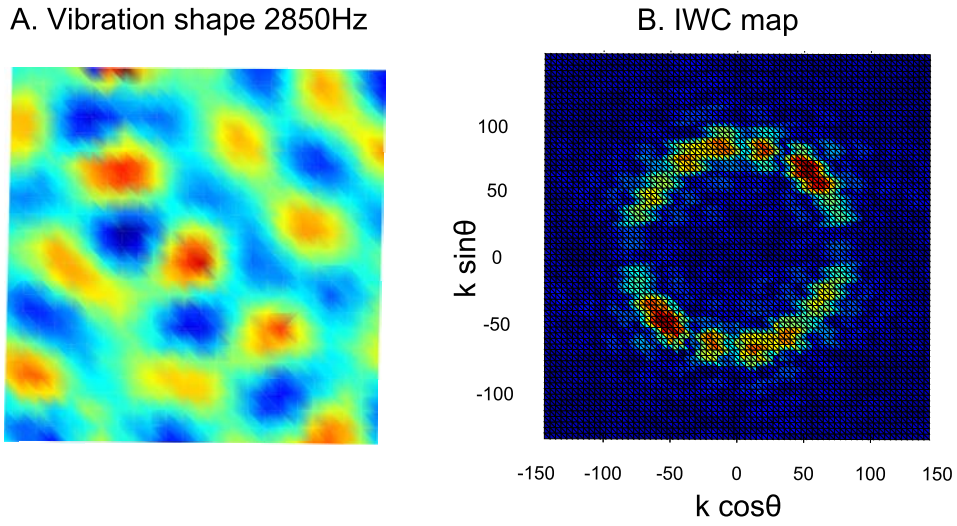

Figure 2.15: Aluminium 2mm plate. A - vibration shape at 2850Hz (modal frequency). B - IWC as a function of the wave numbers of the correlating wave.

In Fig.2.15B, we see a different situation. This time a vibration shape is composed of multitude of modes and it seems that there are waves in many directions. This case is beneficial because the natural wave number can be determined in more directions than in the preceding example.

In conclusion, we can say that in the case of modal vibration fields the waves are concentrated in a few points of the k-space and the maximum value of IWC is high but it repartition on the circle of the natural wave numbers is poor. For the non-modal vibration fields the repartition of the IWC function is more distributed.

2.3.2.5 Question of coupling of independent plane waves in the IWC method

So far, we have seen the behaviour of the IWC image corresponding to a plane-wave and a complex wave field. However, the question of the independence of the estimated $\hat{k}_{ij}$ defined by Eq.2.10 has not yet been answered. The independence with respect to the frequency can be easily addressed; $\hat{k}_{ij}$ is independent from $\hat{k}_{il}$ because the vibration fields corresponding to the j-th and l-th frequencies are independent. However, the independence with respect to the correlation wave direction represented by the first index i is more delicate to prove rigorously by mathematical means. None the less, we can get some insight to the problem considering the following.

The estimate $\hat{k}_{ij}$ is obtained by finding a maximum of the function IWC(w_j,.,.,θ_i) while the estimate $\hat{k}_{kj}$ is found by maximizing the function IWC(w_j,.,.,θ_k). Both estimates are obtained independently, if functions IWC(w_j,.,.,θ_i) and IWC(w_j,.,.,θ_k) are independent. This can be achieved if the plane wave functions $\Psi_i = \Psi(k_i, \theta_i, \beta)$ and $\Psi_k = \Psi(k_k, \theta_k, \beta)$ are *orthogonal*. Then, the projections defined by the IWC function (Eq.2.13) are independent. To see the orthogonality between Ψ_i and Ψ_k, let us define the correlation coefficient:

$$C_{ik} = \left| \frac{\int \Psi_i \Psi_k}{\sqrt{||\Psi_i||^2 ||\Psi_k||^2}} \right| \tag{2.24}$$

If the integral in Eq.2.24 goes over the infinite domain, then the $C_{ik} = 0$ unless $\theta_i = \theta_k$ and $k_i = k_k$ (then $C_{ik} = 1$). However, if the domain of integration is finite, then the correlation C_{ik} is not zero even if the angles θ_i and θ_k are different and its value depends on a number of parameters. Here we shall consider a numerical example close to typical experimental configuration used in this work. Let us consider a domain Ω=[0,L_Ω] $\times$ [0,L_Ω]. A plane wave Ψ_i and Ψ_k are defined over this domain with $k_i = 20$ rad/m. The number of (fictional) measurement points is N=400. The correlation C_{ik} as a function of the relative wavenumber k_k/k_i and $\gamma = \theta_k - \theta_i$ is shown in Fig.2.16A. In Fig.2.16B, there is the dependence on γ only. We can see that a certain limit can be found (represented by the dotted line) where the correlation coefficient ceases to decrease and reaches a certain plateau. We consider this limit as a limit for correlation of functions Ψ_i and Ψ_k. After this limit, these functions are considered (approximately) uncorrelated.

In Fig.2.17 we can see the influence of different parameters on the correlation C_{ik}. The number of points N (Fig.2.17A) does not have a crucial influence as long as the Shannon criterion is respected. However, the surface S of the zone Ω is very important, as shown in Fig.2.17B. Bigger the surface, more uncorrelated are the functions Ψ_i and Ψ_k. A similar situation is observed

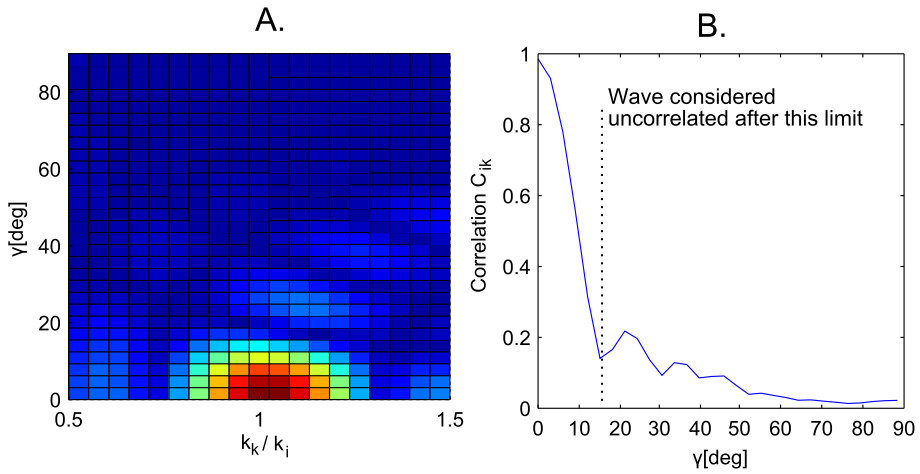

Figure 2.16: A.Cartography of C_{ik} as a function of k_k/k_i and angle difference γ. Dependence of C_{ik} on γ.

if the wavenumber of the functions Ψ increases (Fig.2.17C).

Practically, this analysis shows that we can use the estimates $\hat{k}_{ij}$ and $\hat{k}_{kj}$ as (aproximately) independent variables if the difference between angles θ_i and θ_k is upper than 20°. Of course, this result is not general but it depends on the parameters describing the geometry of the measurement as shown in Fig.2.17.

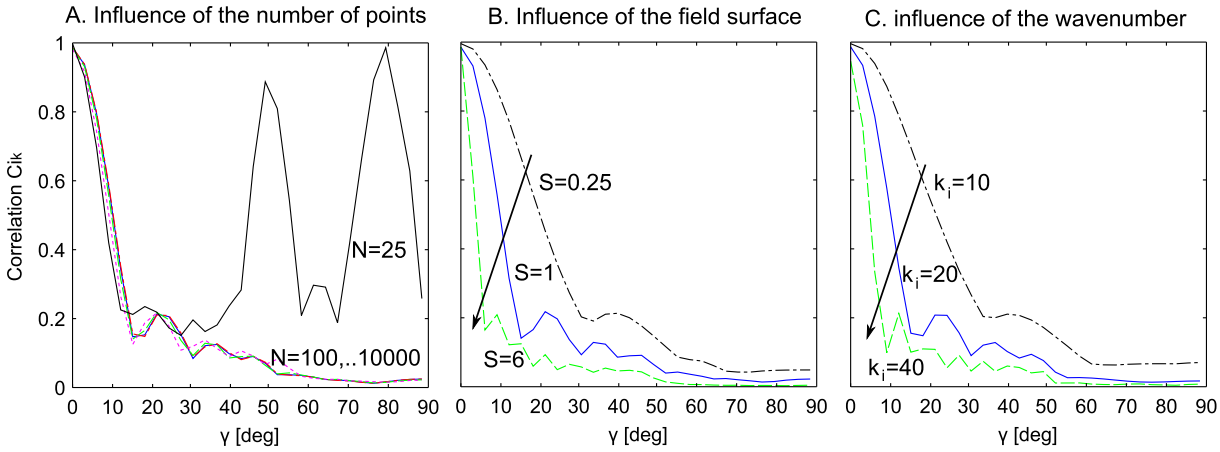

Figure 2.17: Influence of different parameters on the correlation C_{ik}. A. Influence of the number of points in the zone Ω. B. Influence of the zone size S. C. Influence of the wavenumber k_i.

2.3.2.6 Question of Gaussian distribution of $\hat{k}$ obtained by IWC method

So far, we have seen how the estimate $\hat{k}_{ij}$ is obtained from the measurement by Eq.2.10 and we have seen under which conditions is the estimate $\hat{k}_{ij}$ independent from $\hat{k}_{mn}$. Another important question is the distribution of $\hat{k}_{ij}$ in the probabilistic sense. As it was mentioned above $\hat{k}_{ij}$ is only an estimate of the real wavenumber k. A particular shape of the vibration field, noise, size

of the field and number of measurement points, they all influence in some way the estimate $\hat{k}_{ij}$. We do not know the way how all these factors influence the estimate, so we must consider $\hat{k}_{ij}$ as a variable with probabilistic distribution.

In order to have some insight into the distribution of $\hat{k}_{ij}$ let us consider a following numerical example. Consider a pseudo-vibration field w_n as the sum of plane waves [6]:

$$w_n(x,y) = \sum_{i=1}^{35} \alpha_i^{(n)} \sin(30(\cos\theta_i x + \sin\theta_i y) + \beta_i^{(n)}) \tag{2.25}$$

where $\theta_i = 2\pi(i-1)/35$ and $\alpha_i^{(n)}$ is a random variable distributed uniformly over (-0.5,0.5) interval and $\beta_i^{(n)}$ a random variable uniformly distributed over (0,2π) interval. All the these random variables are independent. We dispose with 10000 pseudo-vibration fields (w_1 to w_{10000}). The size of the vibration fields is (x,y)$\in$(0,1)$\times$(0,1). The number of "measurement" points is 2500. Each pseudo-vibration field w_n gives rise to an independent estimate $\hat{k}_n$ [7]. Ideally, the estimates $\hat{k}_n$ should form a normal distribution with mean 30 (wavenumber in the vibration field) and some standard deviance. However, as we can see in Fig.2.18 the probability density function of $\hat{k}_n$ is not really Gaussian. It is much more *peaked*. The irregularities in this figure comes from the fact that a finite set of random observations was used.

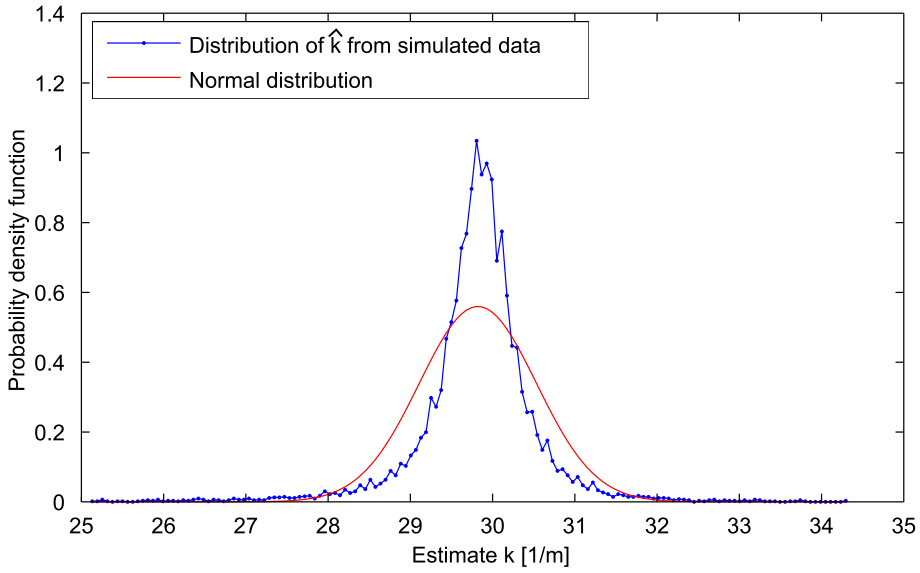

Figure 2.18: Comparison of the "experimental" distribution of estimates $\hat{k}$ obtained by application of the IWC method and the optimal fit of this distribution by a normal distribution (this distribution has the mean and the variance from the estimates of $\hat{k}_n$.

.

The values in Tab.2.3 show that the estimates $\hat{k}_n$ are slightly biased downwards (mean 29.8

[6] By this form we try to obtain the maximum possible vibration fields.

[7] Without the lack of generality we consider that this estimation is performed along the x-direction, there is no privileged direction in the random vibration field.

Mean	29.80
Standard deviance	0.78
Skewness	-2.42
Kurtosis	30.3

Table 2.3: Characteristics of the estimate $\hat{k}_n$.

instead of 30). This bias is also present in the estimation of skewness which is -2.42[8]. The skewness of the Gaussian distribution is 0. The kurtosis[9] 30.3 shows the "heaviness of the tails" of the distribution of $\hat{k}_n$. The kurtosis of the normal distribution is 3.

Considering the above points, we can conclude that the distribution of $\hat{k}$ is unfortunately quite far from the Gaussian distribution. However, we will still use the hypothesis of the Gaussian distribution later because it is a prerequisite for the statistical methods employed in the model selection. High value of kurtosis is also disadvantageous because its means that the distribution of $\hat{k}$ has heavy tails (observation far from the mean can occur).

[8]A sample skewness is calculated as $g_1 = (1/n \sum_{i=1}^{n}(x_i - \overline{x})^3)/(1/n \sum_{i=1}^{n}(x_i - \overline{x})^2)^{3/2})$ .Negative skewness often tends to bias the mean to the lower values.

[9]A sample kurtosis is calculated as $g_2 = (1/n \sum_{i=1}^{n}(x_i - \overline{x})^4)/(1/n \sum_{i=1}^{n}(x_i - \overline{x})^2)^2) - 3$.

2.4 Inverse wave decomposition method (IWD)

The inverse wave decomposition method (IWD) is inspired by the inverse methods used by Chardon described in the introduction section 1.3.2.3 and by McDaniel described in 1.3.2.3. This method can also be classified as a special so-called Trefftz method [10]. The difference between the method of Chardon and the IWD is that Chardon was interested in reconstruction of vibration field, whereas the goal of IWD is to find suitable parameters of the equation of motion. Suitable equation of motion should also lead to a good reconstruction of the vibration field as will be shown in this section. While Chardon was working uniquely with Kirchhoff-Love equation, in this work the IWD method is applied to a variety of equations describing vibration of isotropic and orthotropic bi-dimensional structures. The method of McDaniel is a special case of IWD method applied to one-dimensional structures considering the Euler-Bernoulli operator. However, more operators can be used in one dimension as shown in the section 2.4.3.

2.4.1 Description of the method

The equation of motion is described by a differential operator. The general form of this equation in the frequency domain (in one or two space dimensions) can be expressed by:

$$\mathcal{L}(u) = 0 \tag{2.26}$$

where $\mathcal{L}$ is the linear differential auto-adjoint operator describing the vibration and u is the transverse displacement field. We will call the parameters describing the operator $\mathcal{L}$ a vector $\mathbf{p}$. We can write symbolically $\mathcal{L}(\mathbf{p})$ to show the dependence of the operator on the vector of parameters. The goal is to determine the appropriate vector $\mathbf{p}$ for given experimental data and for a given operator $\mathcal{L}$.

Let us consider that we have a particular solution u of the Eq.2.26 (measured experimentally) at our disposal. This solution (vibration field) is measured at N_{points} discrete space coordinates $\mathbf{x^{(i)}}$. The discreet field can be expressed in the vector $\mathbf{u}$ with elements $u_i = u(\mathbf{x^{(i)}})$. Physically, u represents a steady-state vibration response for a given frequency.

Now, one applies the principle of Trefftz-like solution described in section 1.3.2.3. The general solution [11] of Eq.2.26 is expressed as:

[10] Trefftz methods are numerical methods for solution of partial differential equations with boundary conditions. The solution is approximated by a sum of particular solutions of the differential equation (for example plane waves for the wave equation or exponentials for heat-conduction equation). The coefficients of this decomposition are found by applying the boundary conditions.

[11] Actually, when we talk about the general solution, we have in mind an approximation of general solution in the proper mathematical sense, because the general solution of the Eq.2.26 does not often exist in the closed form.

$$g_{\mathcal{L}} = \sum_i \alpha_i g_{\mathcal{L}}^{(i)} \tag{2.27}$$

where all the functions $g_{\mathcal{L}}^{(i)}$ are particular solutions of Eq.2.26. The choice of the functions $g_{\mathcal{L}}^{(i)}$ should be done in the way that the function g_L should be close to the general solution of Eq.2.26[12].

The *inverse wave decomposition method* (IWD, Chardon's method) described in this thesis is based upon comparing the general solution of the operator which we want to identify with the measured vibration field (designed w). The main idea is that, even though we do not know of the real boundary conditions during the experiment the vibration field, u must lie in the general solution function space $g_{\mathcal{L}}$. So, if we succeed in finding the operator $\mathcal{L}$ whose general solution fits perfectly the measured field u we consider that this operator is the correct representation of the equation of motion. We want to solve the equation

$$\mathbf{u} = \sum_i \alpha_i \mathbf{g}_{\mathcal{L}}^{(\mathbf{i})}(\mathbf{p}) \tag{2.28}$$

where the measurement vector is $\mathbf{u}$ and the general solution functions are $\mathbf{g}_{\mathcal{L}}^{(\mathbf{i})}(\mathbf{p})$. The problem is that both α_i and $\mathbf{p}$ are unknown, so the problem given by Eq.2.28 is strongly non-linear. The solution is done by minimizing the residual cost function r^2:

$$r^2(\mathcal{L}(\mathbf{p}), \alpha, \mathbf{u}) = \|\mathbf{u} - \mathbf{g}_{\mathcal{L}}\|^2 = \|\mathbf{u} - \sum_i \alpha_i \mathbf{g}_{\mathcal{L}}^{(\mathbf{i})}(\mathbf{p})\|^2 \overset{\text{def}}{=} \sum_{j=1}^{N_{points}} |\delta_j|^2 \tag{2.29}$$

where the vector δ is composed of the differences between the measurement $\mathbf{w}$ and the general solution $\mathbf{g}_{\mathcal{L}}$. We can write a similar residual cost function for all vibration fields available $[\mathbf{u^{(1)}}, \mathbf{u^{(2)}}, \mathbf{u^{(3)}}...\mathbf{u^{(N)}}]$. If we call the residual cost function for every of these vibration fields $r_i^2(p) = r^2(., \mathbf{p}, \mathbf{u}^{(i)})$ then the total residual sum is defined as

$$\text{RSS} = r^2(., \mathbf{p}, \{\mathbf{u}^{(\mathbf{i})}\}_i) = \sum_i r_i^2(\mathbf{p}) \tag{2.30}$$

where RSS means the *residual sum of squares*. The cost function RSS is minimized with respect to the parameters $\mathbf{p}$ describing the operator $\mathcal{L}$ and the free parameters α. The inverse method consists in finding the optimal operator (optimal vector $\hat{\mathbf{p}}$, $\hat{\mathcal{L}} = \mathcal{L}(\hat{\mathbf{p}})$ and the optimal value of the parameters $\hat{\alpha}$

$$[\hat{\mathbf{p}}, \hat{\alpha}] = \underset{\mathbf{p},\alpha}{\text{argmin}}(r^2(\mathcal{L}(\mathbf{p}), \alpha), \{\mathbf{u}^{(\mathbf{i})}\}_i) \tag{2.31}$$

The more detailed scheme of the inverse method is shown in the Fig.2.19. The particu-

[12]The exact form of these functions is described in the section 2.4.3.1 for the 1D structures and in 2.4.4.1 for 2D structures

larity of this inverse problem is that the *direct* problem depends on the data as well. So the inverse problems consists of two consecutive problems: for a given parameter **p** the general solution space is defined and then the minimal distance of the measured vibration fields [$\mathbf{u^{(1)}}$, $\mathbf{u^{(2)}}$, $\mathbf{u^{(3)}}$...$\mathbf{u^{(N)}}$] from the general solution is determined (represented by residual fields δ and RSS). This distance is minimized over the space of the parameter **p**. While the first optimization is linear, the second is non-linear.

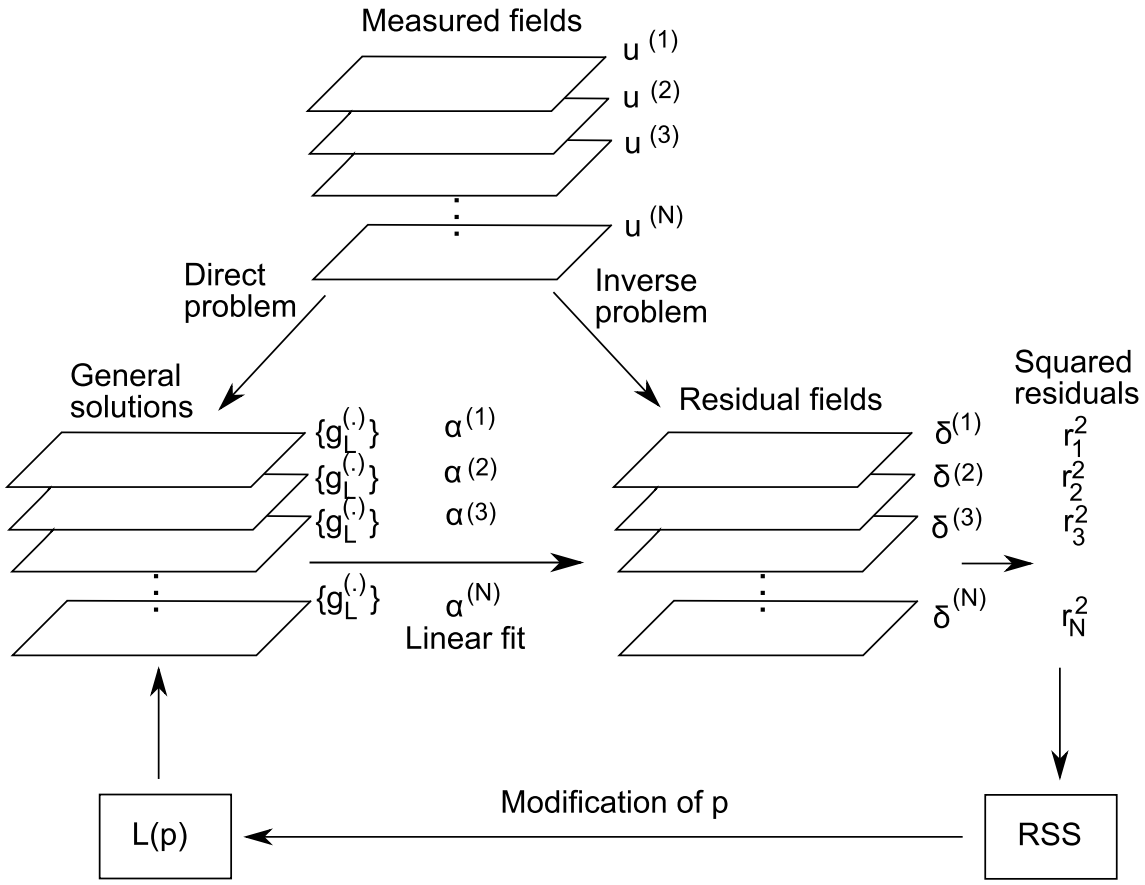

Figure 2.19: Scheme of the inverse problem of the IWD method.

For further considerations we define several quantities. The best fit corresponding to the data belonging to the parameter $\hat{\mathbf{p}}$ and $\hat{\alpha}$ is called (for a particular vibration field)

$$\hat{\mathbf{g}}_{\mathbf{L}} = \sum_i \hat{\alpha}_i \mathbf{g}^{(\mathbf{i})}_{\mathcal{L}(\hat{\mathbf{p}})} \tag{2.32}$$

The normalized square residual of the inverse problem $\tilde{\mathbf{r}}^{\mathbf{2}}$ represents at the solution normalized by the norm of the vibration field vector. It is defined as follows for one vibration field **w**

$$\tilde{r}^2(\mathcal{L}(\hat{\mathbf{p}}), \alpha, \mathbf{u}) = \frac{||\mathbf{u} - \hat{\mathbf{g}}_{\mathcal{L}}||^2}{||\mathbf{u}||^2} \tag{2.33}$$

If $\tilde{r}^2$ tends to zero the models fits perfectly the vibration field. If it tends to unity the model is completely uncorrelated with the vibration field.

2.4.2 Estimation of errors

The statistical treatment of the IWC and IWD methods differs and so does the estimation of errors. The IWC inverse problem can be written in terms of a system of non-linear equations with unknown parameter $\mathbf{p}$

$$k_{ij}^{mod}(\mathbf{p}) = k_{ij}^{exp} \tag{2.34}$$

where $k^{(mod)}$ are the wave vectors *modelled* by some equation of motion and $k^{(exp)}$ are the wave vectors determined *experimentally*. A number of techniques can be employed to treat statistically the problem given by Eq.2.34 especially if the RHS components are independently identically distributed random variables.

The problem of the IWD inverse method cannot be expressed in the same way. From Eq.2.28 we can write an equation describing the goal of the inverse method (measured field equals the general solution field)

$$\mathbf{g}_{\mathcal{L}}(\mathbf{p}, \mathbf{u}) = \mathbf{u} \tag{2.35}$$

We can see that the problem is *implicit* in its nature. Both the LHS and RHS depend on the measurement. A unique solution of Eq.2.35 with respect to $\mathbf{p}$ as we be obtained by minimizing the least squares of the residuals as is shown by Eq.2.31. However, the statistical treatment of Eq.2.35 is very difficult and most methods fail to give prediction about the estimates of $\mathbf{p}$. Fortunately, the Jackknife method can still be used in this case for estimation of variance of $\hat{\mathbf{p}}$ as it is shown below.

2.4.2.1 Jackknife method

The jackknife method is used for the IWD inverse method in the same manner as was shown for the IWC in section 2.3.1.2. In Fig.2.20, we can see an example of pseudo solutions $\hat{\mathbf{p}}^{(k)}$ calculated by Jackknife method and the confidence interval calculated by Eq.2.19. The same experimental data as in the section 2.3.1.2 were used (aluminium plate of 2mm thickness).

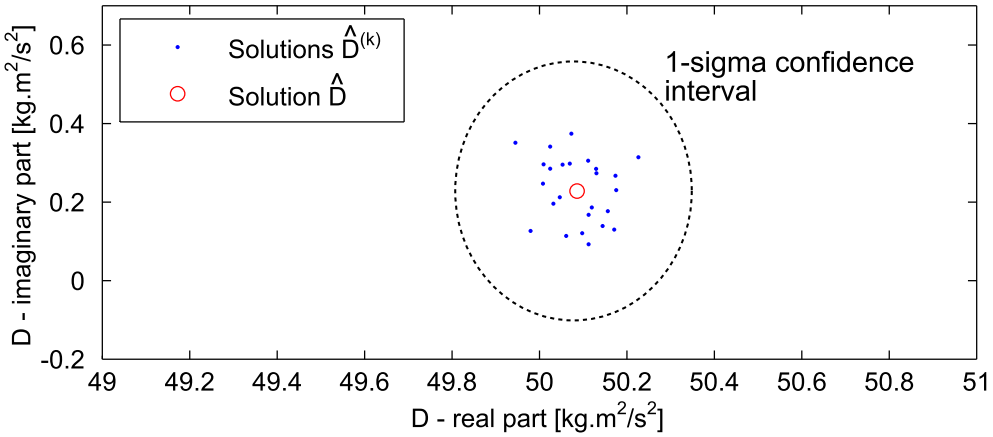

Figure 2.20: Example of pseudo-solutions $\hat{\mathbf{p}}^{(k)}$ (here the vector $\mathbf{p}$ is represented by plate stiffness D) obtained when using the jackknife method with IWD method. The data comes from real measurement on thin 2mm thick aluminium plate. Supposed operator $\mathcal{L}$ is Kirchhoff model.

2.4.3 Inverse wave decomposition for 1D structures

As it was mentioned in the preceding chapter, the IWD method in 1D is somewhat special because the wave solution g_L defined by Eq.2.27 is not only the general solution of the homogeneous equation but it is also composed of finite number of functions. Number of those functions is relatively small, it ranges from 2 to 6 depending on the degree of the equation of motion. This is a great advantage with respect to the problems in 2D where the number of functions in the space g_L can be around 50 and they represent only *approximatively* the general solution. Given all those facts, the IWD method applied on 1D structures is more stable and precise than the method applied to the 2D structures.

Let us suppose that we are dealing with the following self-adjoint linear operator $\mathcal{L}$ which has the form (for list of the possible operators see Section 2.2.1)

$$\mathcal{L}(u) = c_0 u(x) + c_2 \frac{d^2u(x)}{dx^2} + c_4 \frac{d^4u(x)}{dx^4} + c_6 \frac{d^6u(x)}{dx^6} + ... = 0 \tag{2.36}$$

where u is the transverse (flexural) displacement of the string or beam described by the x coordinate. Several 1D models will be studied in this thesis, their overview is in the Tab.2.1.

2.4.3.1 Construction of general solution of equation of motion

The construction of general solution g_L for the equation Eq.2.1 is very simple. For a given frequency (fixed coefficients c) all the functions of the form $g = \exp(kx)$ where k is the solution of the dispersion equation

$$c_0 + c_2 k^2 + c_4 k^4 + ... = 0 \tag{2.37}$$

verify the equation of motion Eq.2.36. If we design k_i all the independent solutions of Eq.2.37 we can write the general solution in the form

$$g_L = \sum_i \alpha_i g_L^{(i)} = \sum_i \alpha_i \exp(k_i x) \tag{2.38}$$

For example, in the case of *string* model we have two independent solution of the dispersion equation with $k_{1,2} = \pm i\omega\sqrt{T/\rho_l}$. In the case of Kirchhoff model we have four independent solutions $k_{1,2} = \pm\sqrt{\omega}\sqrt[4]{EI/\rho_l}$ and $k_{3,4} = \pm i\sqrt{\omega}\sqrt[4]{EI/\rho_l}$. The first two solutions represent evanescent waves while the second two solutions represent propagating waves. For the string model, only the propagating waves exist.

2.4.3.2 Lower-frequency threshold for the IWD

IWD is not stable unless we have sufficient information about the wave of the vibration field. This is especially true when dealing with low-frequency measurements. On Fig.2.21 we can see

the inversion results for the Euler operator applied to a measurement of a steel beam. We can see that inversion becomes stable for frequencies upper than a given frequency which is about 200Hz and the vibration field is about "one-wavelength" long. In general, we can say that we need at least one wavelength in the observed zone to be able to use the IWD technique.

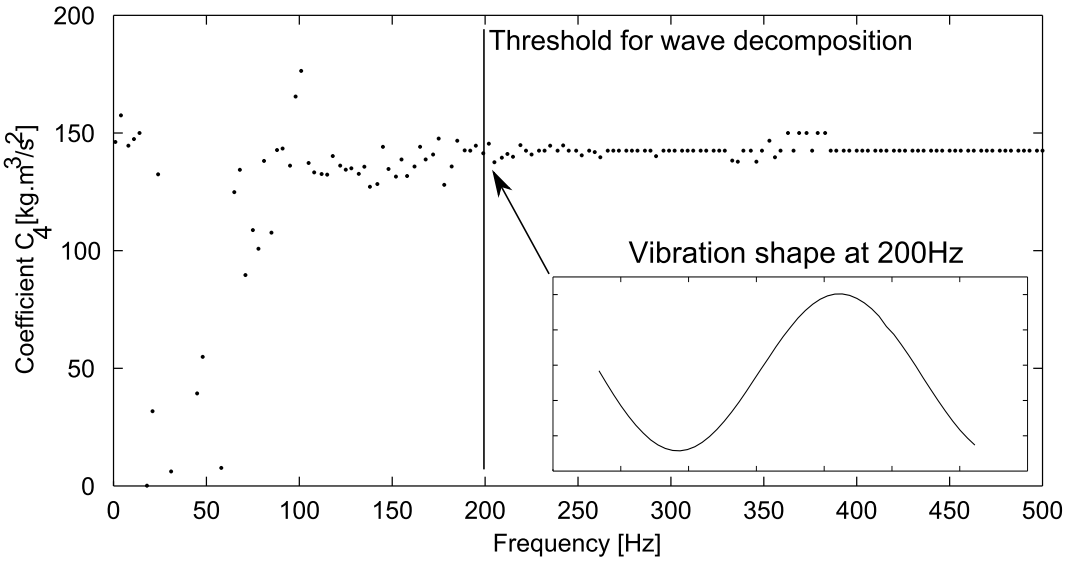

Figure 2.21: Inversion results in frequency dependence. We see that unless 200Hz is reached the inverse problem is unstable and apparently ill-posed. In general, one wavelength is necessary to have stable decomposition.

2.4.3.3 Question of uniqueness of IWD solution

Uniqueness considerations can be well demonstrated in the case of Euler+Force operator (A_3). The corresponding equation is of the type

$$EI\frac{\mathrm{d}^4u}{\mathrm{d}x^4} - T\frac{\mathrm{d}^2u}{\mathrm{d}x^2} - \rho_L\omega^2 u = 0 \tag{2.39}$$

where the unknowns are EI and the axial force T. For our purposes we consider EI=0.05kg.m^3/s^2, T=-300N, ρ_L=1kg/m. To simplify the uniqueness considerations, imagine that we measure somewhere in the middle of the beam where only propagative waves exist, so experimentally we measure only the sine standing waves of the wave number $k^{(exp)}$. The wave vector $k(\omega)$ corresponding to the dispersion equation of Eq.2.39 is solution to

$$EIk^4 - Tk^2 - \rho_L\omega^2 = 0 \tag{2.40}$$

Apparently, if we search inversely the unknowns EI and T for which we get $k^{(exp)}$=k then there is an infinite number of solutions forming a line in the space of (T, EI). These lines can be seen in Fig.2.22. We can clearly see, that there exists a common solution, which can be

revealed only if *multiple frequency* measurements are considered. In other words, this means that when more than one unknown are to be determined, these unknowns have to be considered independent of frequency at least in a certain frequency range. From Fig.2.22 we can see also that the influence of the axial force is more important at low frequencies, while it is almost non-existent at high frequencies. It means that it is very difficult to determine the axial force from high frequency measurements only. All the above considerations correspond to inversion done on a dispersion curve and infinite objects. Our case is a bit different, we are dealing with finite objects, where the evanescent waves take place. Their presence is beneficial for the stabilisation of the inverse problem. However, the presence of the evanescent waves drops down very fast with frequency.

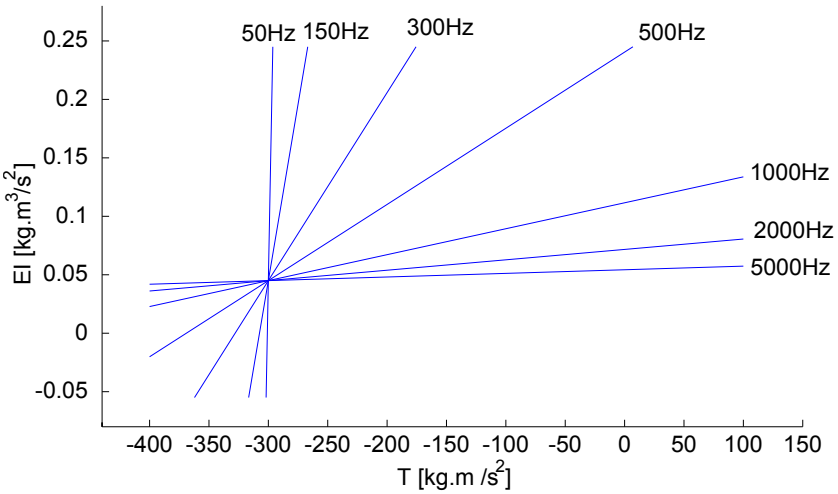

Figure 2.22: Lines giving all the solutions for particular frequencies.

2.4.4 Inverse wave decomposition for 2D structures

2.4.4.1 Construction of pseudo-general solution g_L

In the Section 2.4.1 the vibration field was decomposed into a set of functions which were all the solutions of the operator $\mathcal{L}$ in the domain Ω. This functional space was called g_L. In the case of one-dimensional structures, this functional space was composed of sine and cosine functions together with their hyperbolic counterparts. This functional space constitutes the general solution of the equation of motion Eq.2.1 with zero RHS.

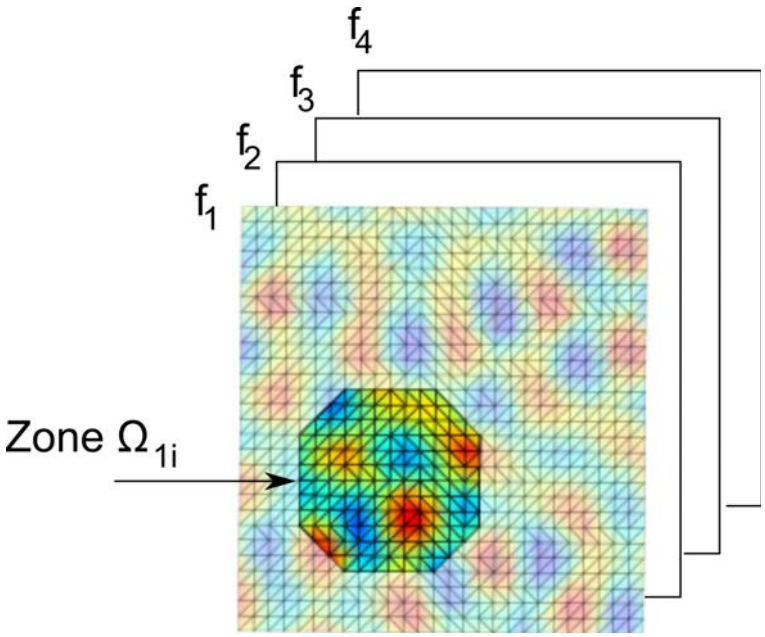

Figure 2.23: Wave decomposition is effected on a small (local) part of an complex vibration field. Circular zone Ω is chosen inside the vibration field. There may be several zones Ω inside the field belonging to the same frequency.

In the case of 2D structures the construction of the general solution of Eq.2.6 is impossible. There is an infinite number of linearly independent solutions of Eq.2.6. [13] So, approximative solutions of Eq.2.1 are considered; they should be, however, sufficiently close to the general solution and not to contain too many independent functions.

In this thesis, the choice was to use the plane waves travelling in several discrete directions. This approach was previously proposed by Chardon [6]. This decomposition is always localized on a small zone (patch) Ω (see Fig.2.23). For the reasons of symmetry and simplicity, the geometry of these zones is a circle. In the following, the indices of zones will not be mentioned

[13] For example there exist plane waves with adequate wave vector which can travel in all directions - so there is an infinity of solutions possible. Another solutions can be fundamental solutions $u_F(x,\xi)$ where u_F is solution of the equation $\mathcal{L}(u_F(x,\xi)) = \delta(x-\xi)$. As we can choose freely the point ξ outside the zone Ω we can get infinity of solutions $u_F(x,\xi)$ all satisfying the the equation of motion $\mathcal{L}(u_F(x,\xi)) = 0$ in Ω.

in the formulas unless it is not necessary. All the considerations below applied to one zone can be applied to all the zones Ω_{ij}.

So, if we consider one particular zone (patch), we can define the pseudo-general solution for some isotropic model as

$$g_L(x) = \sum_{i=1}^{N_{dir}} \sum_j \alpha_{ij} \exp(k_j(x.\cos\theta_i + y.\sin\theta_i)) \tag{2.41}$$

where $\theta_i = (i-1)\pi/N_{dir}$ is the angle of the plane wave, k_j is the j-th solution of the dispersion equation corresponding to the equation of motion Eq.2.26. This solution g_L will be called *pseudo-general* solution. It is not the general solution in the proper sense. But as N_{dir} grows higher the function g_L approaches the general solution. Colton [8] has shown that a solution like 2.41 is dense in the general solution of the *membrane* equation in the *convex* zone Ω. A similar proof for the *fourth-order Kirchhoff* equation was done by Chardon [5].

If the equation of motion is anisotropic, then the pseudo-general solution must be modified to:

$$g_L(x) = \sum_{i=1}^{N_{dir}} \sum_j \alpha_{ij} \exp(k_j(\theta_i)(x.\cos\theta_i + y.\sin\theta_i)) \tag{2.42}$$

where $k_j(\theta_i)$ is the j-th solution of the orthotropic dispersion equation:

$$-\rho_S \omega^2 + [k(\theta_i)]^4 \left(D_1 \cos^4\theta_i + D_3 \sin^4\theta_i + (D_2 + D_4)\sin^2\theta_i \cos^2\theta_i\right) = 0 \tag{2.43}$$

In Fig.2.24, we can see the principle of the IWD in 2D. The vibration field measured in the the circular zone Ω is decomposed into several propagating and evanescent waves which are all particular solution of the equation of motion in the zone Ω. We try to find the best equation of motion (the best pseudo-general solution g_L) to obtain the optimal fit of the measured displacement field.

As we are dealing with approximative pseudo-general solution of equation of motion in 2D, the very important point is the optimized number of plane waves used in the construction of g_L. The zone Ω is a circle with diameter R_Ω which depends on the wavelength of the vibration field. For our purposes, it is useful to work with the correlation length parameter λ. In case of a plane wave the value of λ would be the wavelength of the vibration field. In case of a general steady state vibration field this value is close to the natural (or dominant) wavelength corresponding to the given frequency.

The value of λ gives the dimension scale of our vibration field. All the dimensions are taken with respect to this variable. The relative radius is defined $r_\Omega = R_\Omega/\lambda$. The number of necessary approximative plane wave functions can be obtained by examining the evolution of the error function defined by Eq.2.29 with number of plane wave directions N_{dir}. We see an example of

this function in Fig.2.25. The optimal number of independent plane-wave directions lies in the inflexion point of the curve because the error function diminishes very slowly after this point, while the ill-posedness of the inverse problem increases.

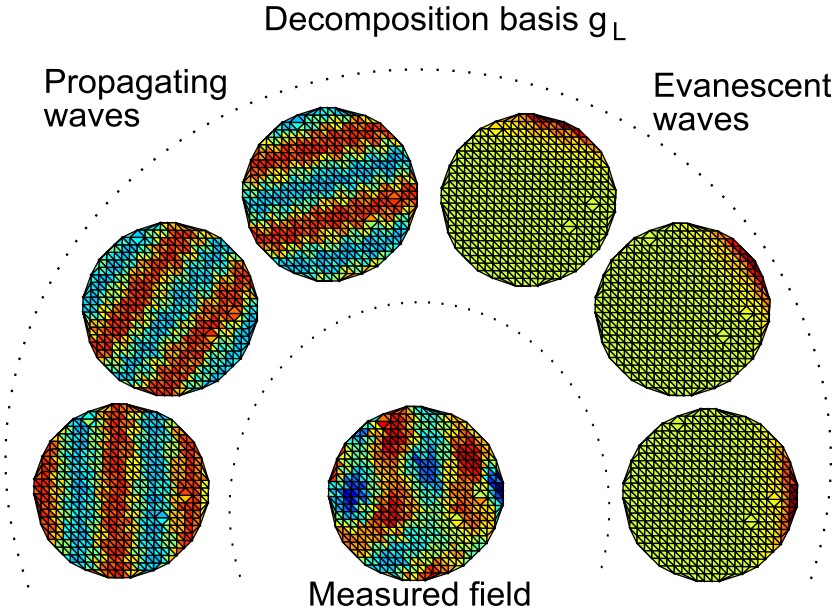

Figure 2.24: Principle of decomposition of the vibration field into the basis g_L

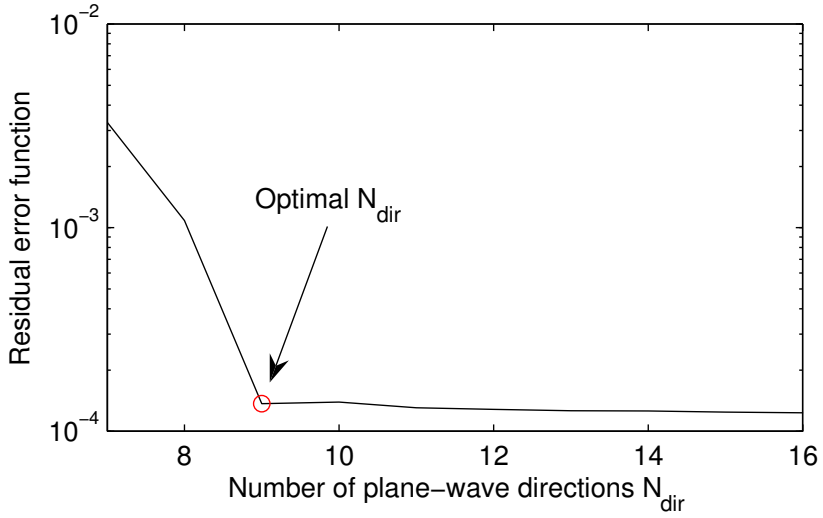

Figure 2.25: Optimal number of plane-wave directions for given sizes of the circular zone Ω. This example is for $r_\Omega = 1$.

2.4.4.2 Question of uniqueness of the IWD solution

Poor conditioning of the IWD method is discussed and some remedies are presented. The problem of non-uniqueness is also discussed and some examples are shown.

A. Regularisation omitting the evanescent waves As it was mentioned above the number of functions in the general solution space $g_{\mathcal{L}}$ (Eq.2.41) is crucial to a successful inversion. If this number is too high, then the inverse problem is ill-posed, if the number is too low, the inverse problem is well-posed but biased. So, we are interested in minimizing the size of the basis of the general solution without diminishing the precision of the inversion. This can be achieved for example by dropping off unnecessary functions from the sum of Eq.2.41. These unnecessary functions can be the *evanescent waves* when we are dealing with vibration field at high frequency or far from the physical boundary, where the presence of the evanescent waves is not likely. This regularization is beneficial as it divides the number of plane waves by two.

An example is taken from the measurement of the aluminium plate 2mm thick. The normalized residual squares function defined by Eq.2.33 is shown in Figs.2.26 and 2.27 for two frequencies 1000 and 2400Hz. Both figures show the non-symmetry of the residual function. This non-symmetry is particularly visible when the evanescent waves are used. We can see that in both cases the residual function of the IWD without the evanescent waves has more distinct minimum (the inversion is more well-posed). Otherwise, the minima of the original (with evanescent waves) and regularized (without evanescent waves) curves are different at 1000Hz. This is due to the regularization assumption, the general solution in Ω does not contain the evanescent waves. This assumption is correct at high frequencies (far from boundary, Fig.2.27) but it is not at low frequencies (close to boundary, Fig.2.26).

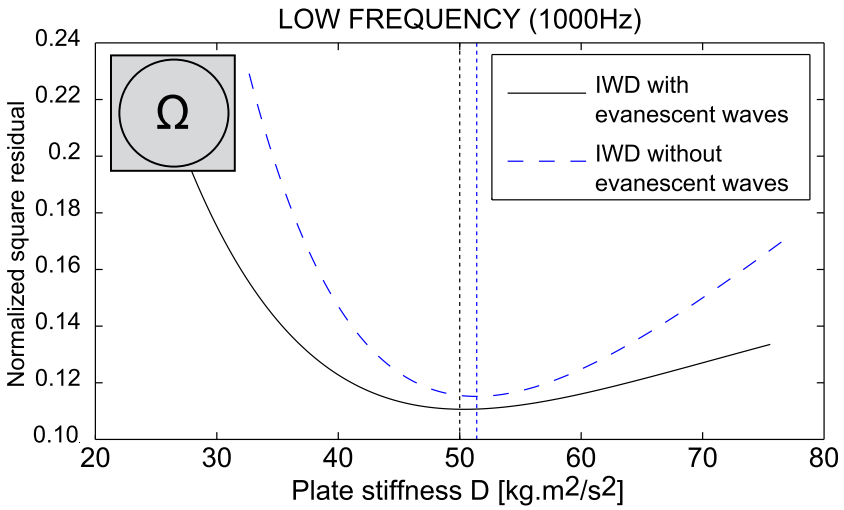

Figure 2.26: Normalized residual square of the IWD as a function of model parameter D (Kirchhoff plate stiffness) for 1000Hz vibration field. In the upper left corner a size of the zone Ω is compared to the size of the plate. Results taken from measurements on an aluminium plate 2mm thick.

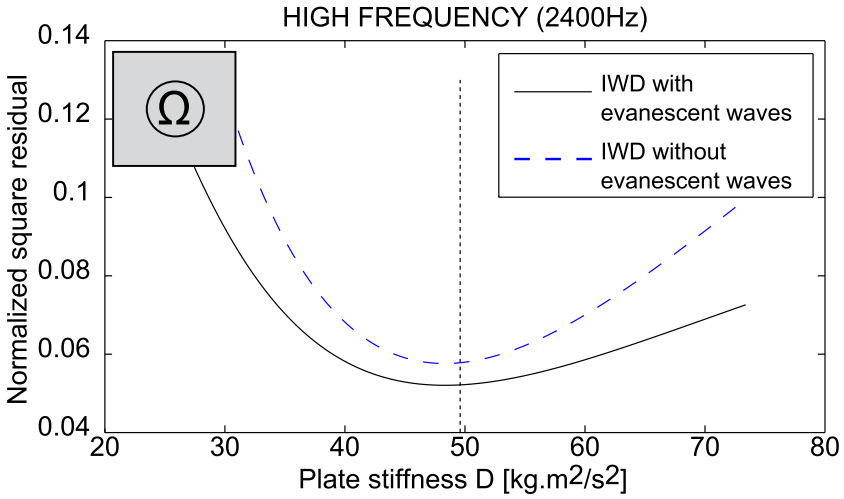

Figure 2.27: Normalized residual square of the IWD as a function of model parameter D (Kirchhoff plate stiffness) for 2400Hz vibration field. In the upper left corner, the zone Ω is positioned with respect to the plate. Results taken from measurements on an aluminium plate 2mm thick.

B. Unique determination of multiple inversion parameters The inverse problem defined by Eq.2.31 should have unique solution in order to exploit the method. However, the uniqueness of the solution of Eq.2.31 depends partly on the measured data. Typically, the problem of the non-uniqueness of the inverse problem arises when we want to determine the othotropic coefficients from a single vibration field. If this vibration field is as shown in Fig.2.28, we can only determine the D_1 coefficient. It is an important point that in order to determine more then one parameter we need to run the inverse technique for more independent vibration field measurements (basically this means for different frequencies). If only one parameter is to be determined, one vibration field is sufficient.

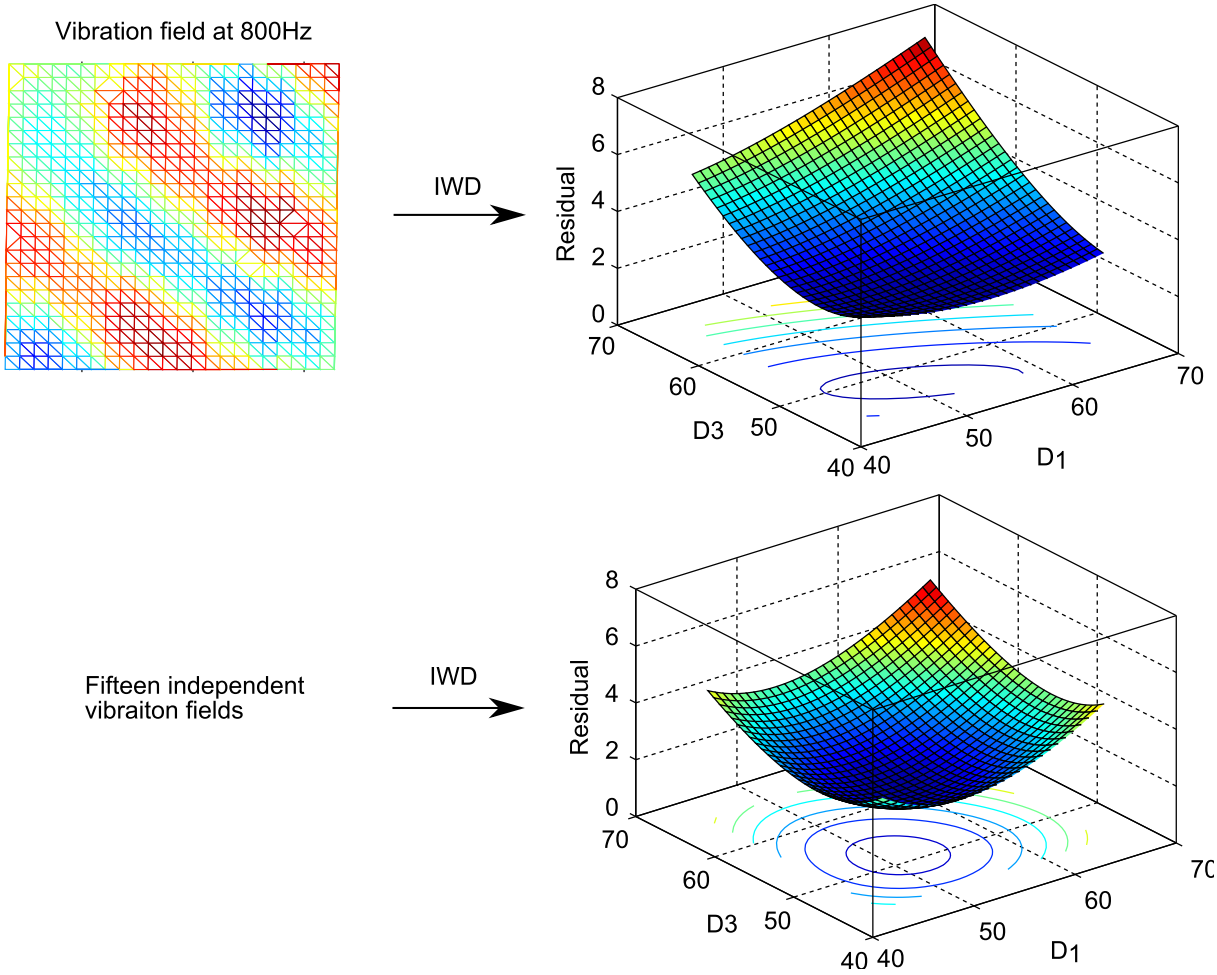

Figure 2.28: Influence of the complexity of the vibration fields on the stability of IWD technique. Results taken from measurements on an aluminium plate 2mm thick.

2.5 Conclusion

The Section 2 starts with a brief description of inverse problems in general. The inverse problem treated in this thesis is then explained. In the following of this section we have seen in detail two inverse methods used in this thesis: IWC - Inverse wave correlation and IWD - Inverse wave decomposition.

The IWC method was invented by Berthaut [3]. It permits to determine the dominant wavenumber of the vibration field. In Section 2.3, the original theory of Berthaut is further developed. The asymptotic properties of the IWC function are presented in Section 2.20. They justify the use of the IWC function to estimate the dominant wavenumber of the vibration field. The question of phase of the correlation plane wave is discussed in Section 2.3.2.2. It is shown that the adding a phase shift as a free parameter to the correlation wave formulation brings more stability to the inverse problem. Sections 2.3.2.3 and 2.3.2.4 show the behaviour of the IWC function when different vibration fields are considered. The influence of geometrical/measurement parameters is also shown. Section 2.3.2.5 treats with an important question of statistical independence of the estimates of the dominant wavenumbers by the IWC method. Section 2.3.2.6 deals with a question of statistical distribution of the estimates of the dominant wavenumber. It is shown that the Gaussian distribution is not obtained.

The IWD method was first used by Chardon in [6].

The IWD method determines the optimal general solution to the equation of motion. Both these methods originate from the previous research.

3 Model selection

Figure 3.1: What is the differential equation describing the roof of Aquarena swimming pool in Arras?

"Entia non sunt multiplicanda praeter necessitatem."

"Entities must not be multiplied beyond necessity." (William Ockham O.F.M.)

3.1 Introduction

As it was described in Section 1.4 there are several model selection techniques depending on the *nature of mathematical problem* and on the *target* of the model selection. It was also mentioned in Section 2 that we consider two distinct inverse methods identifying the parameters of the equation of motion: IWC and IWD.

In the case of IWC, the inverse problem is described *equivalently* by minimization of non-linear least-squares optimization (Eq.2.14) and the maximization of the likelihood function (given by Eq.2.16). The target of the model selection is to find an equation of motion which:

- describes the best the dispersion curve of the unknown structure (AIC criterion).
- leads to the most probable description of the dispersion curve if the measurements are given (BIC).

The application of information criteria to the IWC problem is described in Section 3.2.

In the case of IWD, however, the problem is given by minimizing the residual function given by Eq.2.30. Contrary to the IWC method the likelihood formulation does not exist because we do not know the likelihood function. As it is explained in Section 3.2.4, the properties of the residuals used by the IWD method disable the construction of the likelihood function. Without the likelihood function, information criteria (AIC and BIC) cannot be used. Therefore, a cross-validation approach was chosen to select the target of a model selection. The target of this model selection can be seen as the optimal functional subspace which would fit the displacement field at any point. The *Cross-validation* technique used to obtain this target is described in Section 3.3.

3.1.1 Choice of the candidate models

As it was mentioned earlier, it is sometimes very difficult to make a preliminary choice of *candidate models*. There are basically three possible situations:

- We know which model is true. Then no model selection is necessary. This situation is very rare in a real world. This situation is depicted in Fig.3.2a.
- We know that a model should belong to some finite class of models, but we do not know which one is the best. This situation is optimal for a model selection. It corresponds to Fig.3.2b.
- We do not know which model could describe the problem. We are in the situation described by Fig.3.2c.

Let us have a look at Fig.3.2. It shows a hypothetical problem of model selection [1]. The measurement is shown by a point M. The ellipses belonging to the different models show possible outputs of these models. In the first case on left, the model E describes entirely the measured phenomenon. This situation does never happen in the real world when experimental data are considered. In the second case in the middle, the whole reality of possible outcomes is *covered* by candidate models. This situation is optimal from the point of view of the model selection, because the best model is likely to be chosen (model D in this case). In the third situation on right, we do not know which models might describe the phenomenon, so some models like C and D are missing. In this case model B is wrongly chosen instead of D which is missing from the candidate models.

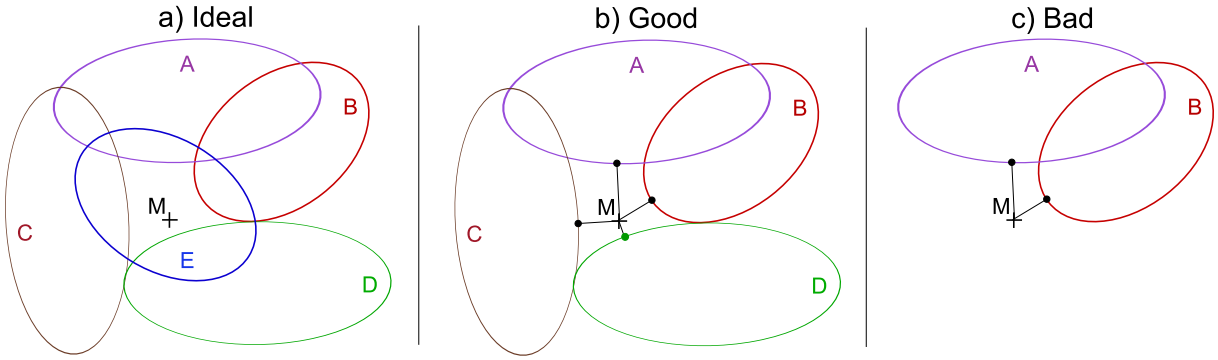

Figure 3.2: On left - Ideal model choice. In the middle - a good choice of candidate models. On right - a bad choice of candidate models.

Our goal in the choice of candidate models is therefore to be in the situation of Fig.3.2b where the candidate models represent together all ”reality”. What does that really mean in the terms of vibration problem treated in this work? We shall demonstrate a choice of candidate models with a help of some examples.

1. Let us consider that we want to determine the model of vibration of an aluminium plate having an unknown thickness (for example the plate is mounted in such a way that the thickness cannot be measured). In this case, the full reality of models can be described by a Kirchhoff and a Mindlin models. If the plate is thin then the Kirchhoff model would be chosen, if the plate is thick then the Mindlin model would be chosen. There are no other reasonable possibilities.

2. We want to identify the model of vibration of a bass guitar string. There are three possibilities: if the section is too important it would behave as Euler beam, if the axial tension force is high it would behave as a string and if none of the two does take over it would

[1] In this simplified case we do not consider the model complexity which comes afterwards. We can imagine as if all the models were equally complex.

be a mixed model of Euler and string. A full reality of possible situations is therefore achieved with these three models.

3. We are dealing with a thin composite plate. We know that there are two principal axes of symmetry due to the fabrication. The possible models are then either isotropic or orthotropic Kirchhoff plate model. One of them is right while the other is wrong.

However, often we face the situation of missing models in Fig.3.2c. This is especially true for complicated thick composite plates, where the full reality can be difficult to achieve by a few candidate models.

3.2 Information criteria adapted for Inverse wave correlation

Even though, the AIC and BIC information criteria have different selection targets (see Section 1.4), both can be applied as post-processing of the IWC method. Both information criteria are particularly adapted for problems of non-linear curve fitting. A short description of both criteria are presented below.

3.2.1 Akaike information criterion (AIC)

The target of the AIC is to find the model which minimizes the Kullback-Leibler distance. AIC criterion was introduced by Akaike in 1973 [54] a brief description is given below. For further information see Burnham [56].

3.2.1.1 Kullback-Leibler distance and AIC

Kullback-Leibler distance [58] (or information) describes how close two models are. It is based upon their probability distributions. Assume that we have two models represented by their probability density functions f and g. We consider that both models are known and that f represents a *full reality* or *truth* [2] and g is a model approximating the full reality. We can say that this model depends on some free parameters $g(\theta)$. Then the Kullback-Leibler (K-L) distance from g to f is defined as:

$$I(f,g) = \int f(x)\ln\left(\frac{f(x)}{g(x|\theta)}\right)\mathrm{dx} \tag{3.1}$$

If the two models are equal $f = g$ then their distance is zero $I(f,g) = 0$. Otherwise, it is always positive.[3] The goal of the model selection based on the K-L distance would be to choose the model which minimizes this distance. This distance cannot be determined if we do not know f but AIC permits to approximate this distance.

Expression 3.1 can be further developed as:

$$I(f,g) = \int f(x)\ln f(x)\mathrm{dx} - \int f(x)\ln g(x)\mathrm{dx} = \mathrm{E}_f[\ln(f(x))] - \mathrm{E}_f[\ln(g(x|\theta))] \tag{3.2}$$

where E stands for expected value in the probability sense. The first term of 3.2 depends only on the true f and it is independent of model g so it can be omitted from the model selection considerations. Akaike [54] showed that the second term in Eq.3.2 can be written as:

[2] Unless we are dealing with artificial problems with simulated data, this function is never known.

[3] K-L distance is not a metric on the space of the probability distributions because $I(f,g) \neq I(g,f)$.

$$\mathrm{E}_f[\ln(g(x|\theta))] = \mathrm{E}_y\mathrm{E}_x[\ln(g(x|\hat{\theta}(y)))] \tag{3.3}$$

where x and y are independent random samples from the true distribution f. Expression 3.3 cannot be evaluated exactly unless we know the true distribution f. Akaike found that a log-likelihood function is a asymptotically biased estimator of 3.3. The bias of this estimation is equal to the number of estimated parameters K. For a large samples we can write:

$$I(f,g) = C - \mathrm{E}_y\mathrm{E}_x[\ln(g(x|\hat{\theta}(y)))] \approx C - \ln(L(\hat{\theta})|\mathrm{data}) + K \tag{3.4}$$

Dropping the unnecessary constant C and multiplying [4] the Eq.3.4 by 2 we obtain the AIC criterion:

$$AIC = -2\ln(L(\hat{\theta})|\mathrm{data}) + 2K \tag{3.5}$$

As it was later shown the AIC defined by Eq.3.5 is valid only asymptotically (i.e. for large samples). If only smaller samples are available it is advised to use modified second order AIC_C defined as

$$AIC_c = AIC + \frac{2K(K+1)}{N-K-1} \tag{3.6}$$

where N is the number of measurements (sample size). If $N \gg K$ then $AIC = AIC_c$. Later in this work, AIC_c is always used regardless to the sample size.

The principle of use of the AIC criterion is very simple. If we dispose several models g_i, we can calculate the maximal likelihood function for each of them and compare their AIC_i values. The model with lowest value of AIC is the one selected by AIC criterion. It should be noted that the absolute value of AIC is not important. However, the relative differences between the AIC values of different models are important because they correspond to likelihood of models. If we define the AIC difference as

$$\Delta_i = AIC_i - \min_k(AIC_k) \tag{3.7}$$

then the selected model has $\Delta_i = 0$ and the other models have $\Delta_i > 0$. Akaike interpreted these differences with the so called "Akaike weights":

$$w_i = \frac{\exp(-\Delta_i/2)}{\sum_r \exp(-\Delta_r/2)} \tag{3.8}$$

Akaike weight w_i ranges from 0 to 1 and has a meaning of model probability of being the best model to minimize the K-L distance. Empirically, we can class the models according to their Δ_i using the rule given in Tab.3.1 (from Burnham [56]):

[4] This is unnecessary, Akaike did this for "taking the historical reasons into account."

Δ_i	Level of support for model i
0-2	Substantial
4-7	Minor
>10	Essentially none

Table 3.1: Rule of thumb for an AIC model selection.

3.2.2 Bayesian information criterion (BIC)

The Bayesian information criterion (also called Schwartz-Bayes information criterion) was developed by Schwarz in 1978 [53]. Although BIC has similar behaviour as AIC the derivation of this criterion is different. BIC is a criterion which chooses among a set of models the model which is the *most probable* for given data. Moreover, if the true model [5] is among the candidate models then BIC chooses this model with probability 1 if the sample size goes to infinity. This is not necessarily true for the AIC model.

Let us consider that we dispose some data X and a finite set of candidate models $\mathcal{M} = [\mathcal{M}_1, \mathcal{M}_2, ...\mathcal{M}_n]$. The target of the BIC is to find which of the models maximizes the posterior probability:

$$\mathcal{M}_{BIC} = \underset{\mathcal{M}_i}{\operatorname{argmax}}\, P(\mathcal{M}_i|X) \tag{3.9}$$

The expression 3.9 is developed according the principle of the Bayes theorem. The derivation of the Eq.3.9 is beyond the scope of this work, detailed derivation can be found for example in [52]. It is shown that $\ln P(\mathcal{M}_i|X)$ can be approximated asymptotically as:

$$\ln P(\mathcal{M}_i|X) \approx \ln L(X|\hat{\theta}_i, \mathcal{M}_i) - \frac{K_i}{2}\ln N \tag{3.10}$$

where L is the likelihood function, N is the number of measurements (sample size), K_i is the number of parameters θ_i describing the i-th model $\mathcal{M}_i$. Multiplying this equation by -2 we obtain the BIC criterion:

$$BIC_i = -2\ln L(X|\hat{\theta}_i, \mathcal{M}_i) + K_i \ln N \tag{3.11}$$

Then the optimal model (with highest posterior probability) is chosen by minimizing the BIC criterion over the set of models:

$$\mathcal{M}_{BIC} = \underset{\mathcal{M}_i}{\operatorname{argmin}}\, BIC_i \tag{3.12}$$

The absolute value of BIC is not important, it is only the difference between the BICs of different models which counts. As it was the case for the AIC criterion it is common to define

[5] In other words the data come from the model which is included in the set of candidate models.

the BIC difference as:

$$\Delta_i = BIC_i - \min_k(BIC_k) \tag{3.13}$$

The best model according to the BIC has $\Delta BIC = 0$ all the other models have $\Delta BIC > 0$. The BIC differences can also serve to estimate the posterior probabilities of different models in the candidate set. Similarly to the AIC, the probability that the i-th model is the true model can be expressed as:

$$w_i = \frac{\exp(-\Delta_i/2)}{\sum_r \exp(-\Delta_r/2)} \tag{3.14}$$

3.2.3 Application of the AIC and BIC to the IWC-based model selection

In both AIC and BIC approaches the log-likelihood function is necessary. Under the hypotheses given in Section 2.3.1.1, the log-likelihood function can be expressed according to the Eq.2.18 as:

$$\ln L(\mathbf{p}) = -\frac{N}{2}\ln(2\pi) - \frac{N}{2}\ln\sigma^2 - \frac{1}{2}\sum_{ij}\left(\frac{r_{ij}^2(\mathbf{p})}{\sigma^2}\right) \tag{3.15}$$

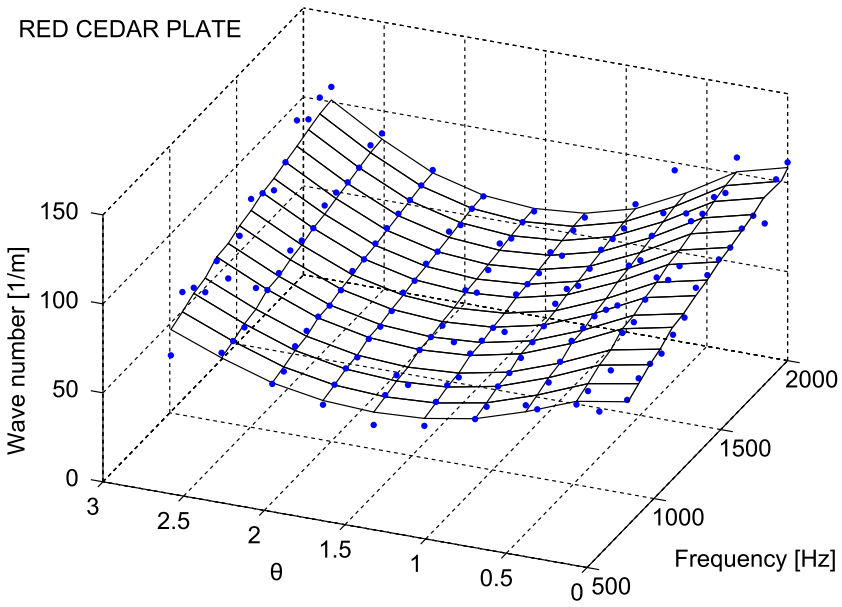

Figure 3.3: Red cedar plate: example of a least square fit of wavenumber function obtained by IWC method (blue points) by an orthotropic model. Angle θ represents the angle of a plane wave correlated with the vibration field.

Residuals $r_{ij}(\hat{\mathbf{p}})$ are represented by differences of the "experimental" wave numbers obtained by IWC and the wave numbers given by the model. An idea of these residuals is shown in

Fig.3.3 showing the experimental data of the red cedar plate. For the maximized value of the log-likelihood we have $\sum_{ij} r_{ij}^2(\hat{\mathbf{p}}) = (N-1)\sigma^2$ and therefore the maximum of the log-likelihood function is

$$\ln L(\hat{\mathbf{p}}) = -\frac{N}{2}\ln(2\pi) - \frac{N}{2}\ln\sigma^2 - \frac{1}{2}N \tag{3.16}$$

and omitting the unnecessary constants not depending on the model we obtain

$$\ln L(\hat{\mathbf{p}}) \approx -\frac{N}{2}\ln\sigma^2 \tag{3.17}$$

Then the AIC and BIC criterions can be expressed in terms of the residual variance

$$AIC = N\ln\sigma^2 + 2K\left(\frac{N}{N-K-1}\right) \tag{3.18}$$

$$BIC = N\ln\sigma^2 + K\ln N \tag{3.19}$$

This form shows very well the model selection "trade-off" between the model precision and its complexity. The precision term is represented by an estimated variance of the data σ^2 when the model is employed and its complexity is represented by a number of estimated parameters K.

Comparing Eq.3.18 and 3.19 we can see that although the principles for derivation of AIC and BIC are quite different resulting criteria look similarly. They differ only in the second term representing the penalty for the model complexity. Typically, the penalty of the BIC is more important than the penalty of the AIC. That is the reason why the BIC criterion is sometimes called more conservative, it tends to choose simpler models than AIC.

On Fig.3.4 we can see an example of use of AIC and BIC on the data obtained from measurement done on 2mm-thick aluminium plate (description in Appendix A.2). Five models are considered B1, B2, B3, B4 and B6. On the left, we can see that appart from the B1 (membrane) model all the other four models fit the dispersion data in a similar way. Therefore the selection of the model based on their residual of fit would be difficult. Moreover, we can see clearly in Fig.3.4 right that both AIC and BIC criteria favour the simplest model of the three - B2 (Kirchhoff plate). We can also see that BIC is more conservative, it chooses the simplest model with a greater margin.

A different example is shown in Fig.3.5 corresponding to the IWC analysis applied on the measurement of a *paper membrane* (description in Section 4.2.3). Three models are considered: B1, B2 and B3. We can see that the fit of the three models is very different with model B3 being visibly the best model. In this case, the difference in the number of parameters in the penalty term in Eq.3.18 and 3.19 is too small compared to the difference of fit obtained by those models. Therefore even if the number of parameters of the model B3 is the highest, this model is a surely

	Aluminium 2mm				Paper membrane			
	AIC		BIC		AIC		BIC	
Model	Δ_i	w_i	Δ_i	w_i	Δ_i	w_i	Δ_i	w_i
B1 (membrane)	271	0.00	272	0.00	292	0	288	0
B2 (Kichhoff)	0	0.46	0	0.82	143	0	140	0
B3 (Kirch./memb.)	1.82	0.18	4.78	0.08	0	1	0	1
B4 (Mindlin)	1.60	0.20	4.57	0.08	-	-	-	-
B6 (Kirch.ortho.)	2.29	0.14	8.17	0.01	-	-	-	-

Table 3.2: AIC and BIC values for IWC analysis effectuated on 2mm aluminium plate and paper membrane.

chosen with probability 1 (see Tab.3.2).

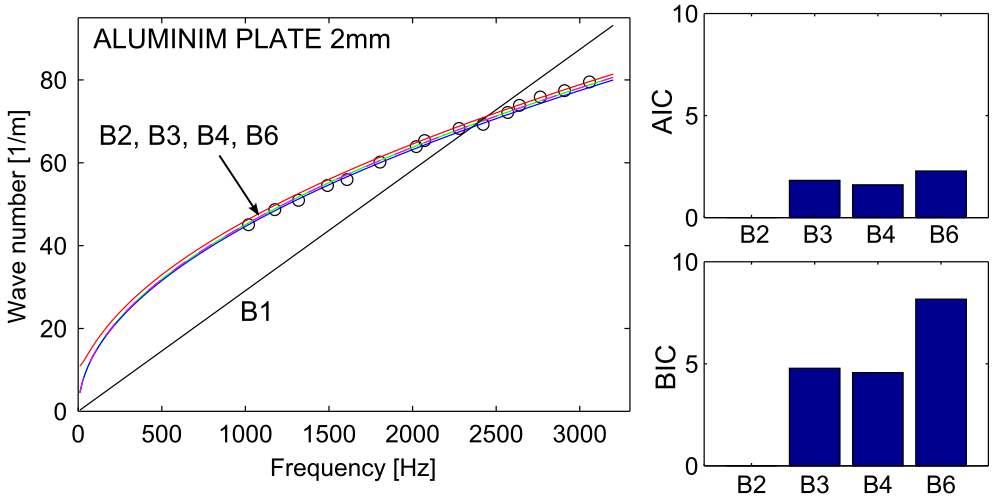

Figure 3.4: Example of the fit of the dispersion curve for aluminium 2mm plate obtained by IWC by different models on left and the AIC/BIC analysis on right. The B1 model is not shown in the graph on right because its values are too high.

3.2.4 Why information criteria cannot be used with IWD inverse problem?

As we have seen in the preceding section, AIC and BIC criteria are very simple to use, their application give the possibility to choose the best model and to see whether other models are close or far from the best model. Moreover, in case of several models which are close to the best model, we can even do a multi-model inference (making a somewhat mixed model) as described in Burnham [56] [6]. So, why not to use these criteria for all model selection problems (i.e. for all inverse problems)?

[6]This procedure is, however, nor applicable in our case, because parameters of the different equations of motion do not have the same units.

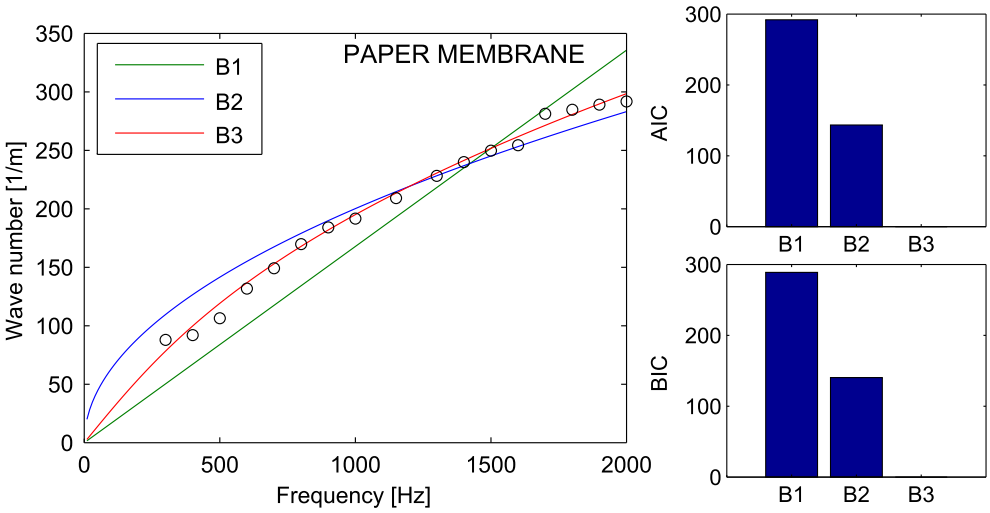

Figure 3.5: Example of the fit of the dispersion curve for paper membrane obtained by IWC by different models on left and the AIC/BIC analysis on right.

Let us take for example the case of the AIC applied on the aluminium 2mm plate measurement (see Appendix A.2). Without any further investigation we try to use the formula for AIC given by Eq.3.18:

$$AIC = N\ln\sigma^2 + 2K\left(\frac{N}{N-K-1}\right) \tag{3.20}$$

In this case, we apply this formula on the IWD inverse problem, N is the number of measured points, K is number of parameters (i.e. the number of all the constants α and all the parameters of $\mathcal{L}$ in Eq.2.27). Actually, the number of all the coefficients α is the same for all models, so it might be omitted as long as we are only interested in differences in AIC values. Then $\sigma^2 = \sum_{ij}(\delta_{ij})/(N-1)$ where δ_{ij} is the residual from fitting the i-th vibration shapes measured at j-th point as described in Section 2.4. Then, if we consider that we have N_S vibration shapes and each has Np_i points then $N = \sum_{i=1}^{N_S} Np_i$. Consequently, N is very large. In this example N=12808. The resulting AIC values are shown in Tab.3.3 in the first column. We can see that the model selection is erroneous. The orthotropic model B6 is chosen instead of the Kirchhoff model B2 which is found to be the best model when using the AIC with IWC. Why do we come to a different and highly suspicious conclusion (our plate is not orthotropic)?

The problem with IWD lies in its mathematical formulation. Let us have a look at the mathematical formulation of both inverse problems. Both problems can be expressed as nonlinear optimization problem to find the estimate $\hat{\mathbf{p}} = \text{argmin}\sum_{ij} r_{ij}^2$. However, the residuals r_{ij} are different in the two cases (see Eq.2.14 for IWC and Eq.1.11) for IWD):

	IWD	IWC
Model	Δ_i	Δ_i
B1 (membrane)	43814	271
B2 (Kichhoff)	4	0
B3 (Kirch./memb.)	5	1.8
B4 (Mindlin)	15	1.6
B6 (Kirch.ortho.)	0	2.3

Table 3.3: Fictional values of AIC when applied to IWD inverse problem on aluminium 2mm plate (first column). The second column contains the comparison to AIC applied to IWC inverse problem.

$$\underset{\text{IWC}}{r_{ij} = \hat{k}_{ij}^{exp} - k_{ij}^{mod}(\mathbf{p})} \qquad \underset{\text{IWD}}{r_{ij} = u_{ij} - \mathbf{P}(\mathbf{p})\mathbf{u}_{.,j}} \quad \mathbf{P}=\psi\psi^{-1}$$

where the estimates $\hat{k}_{ij}^{exp}$ are independently obtained by the IWC method as described in Section 2.3.2.5. Fig.3.6 shows graphically the difference of the residuals considered by these two inverse problems. Even though the displacements u_{ij} are independent, the residuals r_{ij} obtained by the IWD method are not because the projector $\mathbf{P}$ couples the individual point measurement u_{ij} with all the measurement in the zone Z represented by $\mathbf{u}_{.,j}$. According to the nomenclature of Section 2.4.1 the elements of the matrix ψ are $\psi_{ik} = g_{\mathcal{L}}^{(k)}(\mathbf{x}_i)$.

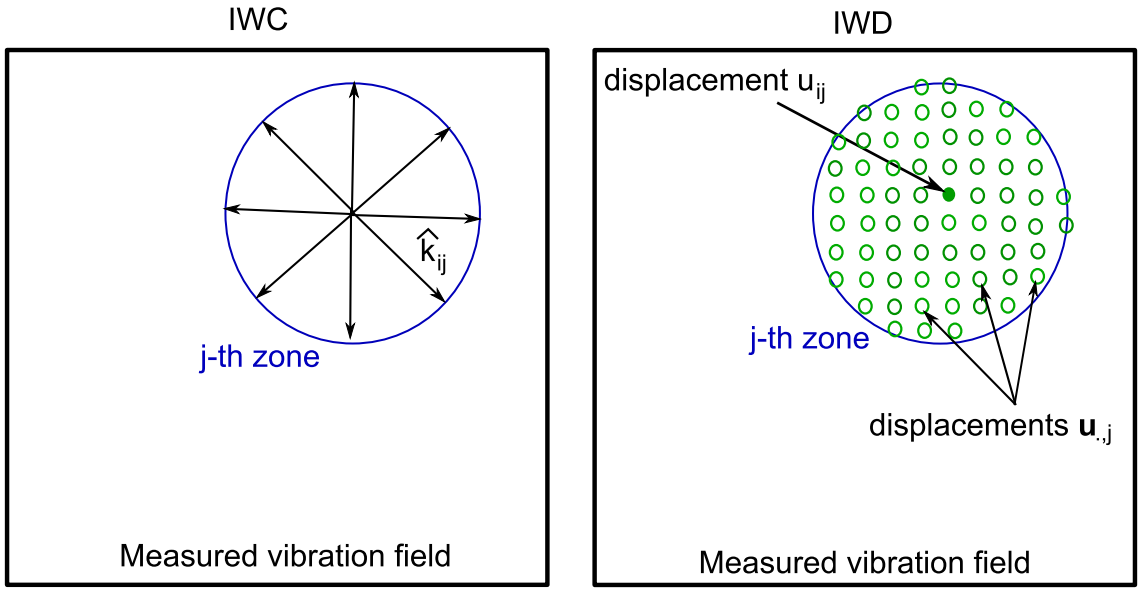

Figure 3.6: Explication of the difference of the residuals of the IWC and IWD methods.

An example of the projector matrix $\mathbf{P}$ taken from the measurement of the aluminium 2mm plate is shown in Fig.3.7. We can see that this matrix is not unity matrix. This means that each column is coupled with multiple lines. From the statistical point of view, this coupling

introduces a dependence between the residuals r_{ij} obtained by by IWD method. And dependent residuals r_{ij} lead to erroneous estimation of AIC criterion as it was shown at the beginning of this section.

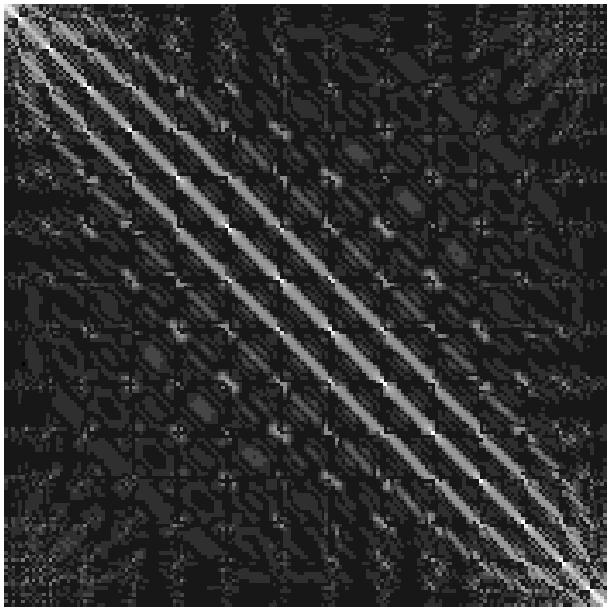

Figure 3.7: An example of the projector matrix **P** used by the IWD method. In this figure only the absolute values are shown.

3.2.5 Why information criteria can(not) be used with asymptotic inverse methods?

In this section, we shall see a possible application of information criteria in the case of asymptotic inverse method as described in Section 1.3.2.4. We will concentrate on the use of the modal density function $n(\omega) = n(2\pi f)$. This function is described analytically by Eq.1.16. If we want to build some inverse method, we must determine a discrete data-based function $n(f_i)$. We shall see that an inappropriate choice of $n(f_i)$ leads to the destruction of the information criteria usability. Let us imagine that some reliable and robust method permits to identify all the modes of the structure and that these modes are determined *independently*. Then, we can define the modal density as:

$$n(f_i) = \frac{N_m(f_i - \Delta f/2, f + \Delta f/2)}{\Delta f} \tag{3.21}$$

where $N_m(f_1, f_2)$ is the number of eigen frequencies between frequencies f_1 and f_2. Then, the modal density can be approximately determined by Eq.3.21 for a number of eigen frequencies and the parameter Δf needs to be adjusted. However, if the averaging interval Δf is larger than the distance between f_i and f_{i+1}, one mode is used for calculation of several modal densities

$n(f_i)$. Therefore, the calculated modal densities are *not independent* from each other.

A numerical example shows this phenomenon. Let us consider a 2mm-thick rectangular simply-supported aluminium plate with E=70GPa and ρ=2700kg/m^3. Its dimensions are L_x = 1m and L_y = 0.8m. Its eigen frequencies can be calculated analytically (Gerardin [75]):

$$f_{nm} = \frac{1}{2\pi}\left(\left(\frac{m\pi}{L_x}\right)^2 + \left(\frac{n\pi}{L_y}\right)^2\right)\sqrt{\frac{D}{\rho_S}} \tag{3.22}$$

The asymptotic modal density is independent of frequency $n(f = \infty) = 0.128$/Hz. In this case we choose Δf=200Hz. So, considering the approximative formula Eq.3.21, we can conclude that a single mode influences $200x0.128 \approx 25$ estimations of modal densities. Clearly, these estimations cannot be independent one from another. This example of using a moving average is shown in Fig.3.8 by black crosses. What is happening here is a multiplication of information into interdependent variables. This approach would lead to erroneous results when information criteria such as AIC or BIC were to be used.

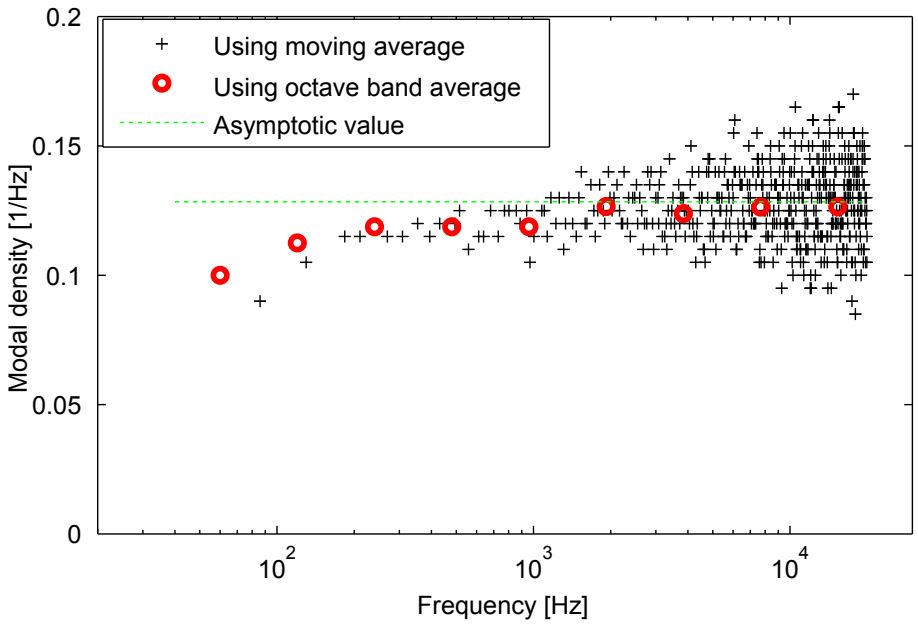

Figure 3.8: Two different ways of estimating the modal density lead to the same fitted function but resulting statistical meaning of information criteria is not the same.

The correct approach to this problem would be to split modes into *non-overlaping* sets. For example, we can choose octave bands of audible sound. Then the modal density is evaluated in each octave band *independently*. The results are shown in Fig.3.8 by red circles. In this case we obtain fewer points but these points are independent one from another and the information criteria based statistics as AIC and BIC can be used.

3.2.6 Why information criteria can(not) be used with FAT(RIFF) inverse method?

The FAT(RIFF) method is described in section 1.3.3.1. It was shown that this methods consists of verifying locally the equation of motion. Here, we discuss the possibility to use the information criteria for the selection of models. Let us imagine that at the i-th spatial point, the residual of the RIFF problem is defined as (see Eq.1.27):

$$r_i = D\delta^4 u_i^{(exp)} - \omega^2 \rho_S u_i^{(exp)} \tag{3.23}$$

If we want to use the criteria as AIC and BIC with the least-squares defined by the residuals given by Eq.3.23, we must ensure that these residuals are independent. Due to the difference scheme used to estimate the fourth derivative, the residual r_i depends on thirteen adjacent points. However, if the i-th and j-th points are sufficiently far away (Fig.3.9A) they use different points then the residuals r_i and r_j are independent. This is only valid for a non-regularized version of RIFF. As the regularization is crucial for stable inversion a low-pass spacial filter is applied. This filter, however, links the points i and j which were disconnected before (Fig.3.9B). So the independence of residuals r_i and r_j is lost.

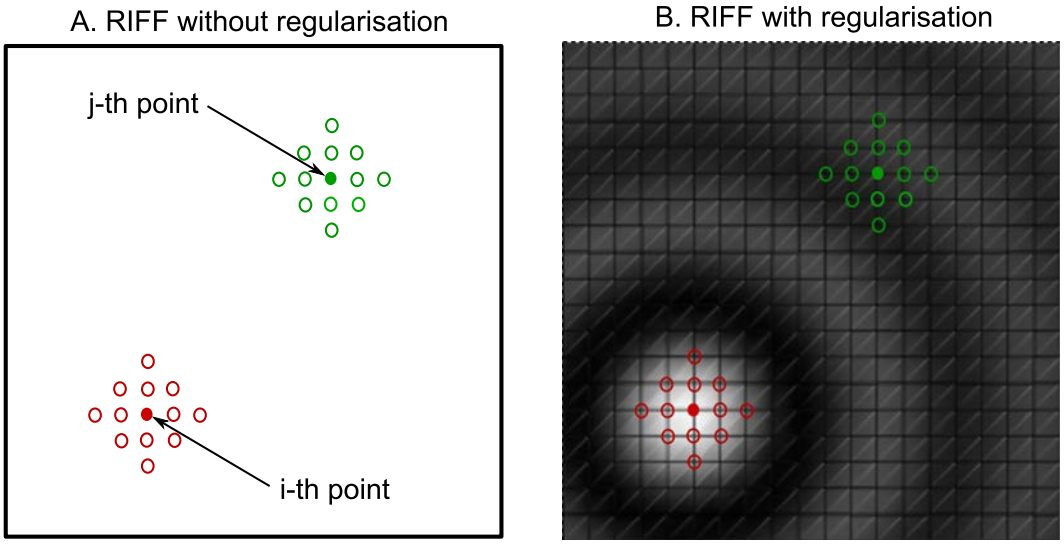

Figure 3.9: A. In case of the RIFF without regularisation, the solution at points i and j are independent. B. In the case of the regularized RIFF, the solution at point i is linked to point j by a low-pass spatial filter function.

In order to be able to use the information criteria and the residuals r_i obtained from regularized RIFF method, then we would need a sufficient spacial distance between the points where the residual is evaluated. This spatial distance should be superior the characteristic size of the low-pass filter function.

3.3 Cross-validation adapted for Inverse wave decomposition

The *Cross-validation technique* is one of the most popular and simple techniques for model selection ([63]). Its objective is to judge the capability of the identified model to predict the measurement. Due to its versatility it was employed with the IWD inverse technique which is otherwise too complicated to be used with other model selection methods. The principle of the cross-validation is very simple. Let us consider that we have some data vector $\mathbf{d} = (d_1, d_2, ...d_n)$ and a model $\mathcal{M}(\mathbf{p})$ depending on the parameter $\mathbf{p}$. We suppose that the data can be simulated by the model and that the model can be identified from the data by some inverse technique. Then, the principle of the cross-validation is to separate the observation vector $\mathbf{d}$ into two sets: the *training set* $\mathbf{d_t}$ and the *validation set* $\mathbf{d_v}$. These sets should have null intersection and $\mathbf{d} = \cup\{\mathbf{d_t}, \mathbf{d_v}\}$. The training set serves to estimate the parameter of the model $\hat{\mathbf{p}}$. Then, we can simulate the outcome of the model $\mathcal{M}(\hat{\mathbf{p}})$ on the set $\mathbf{d_v}$ and compare it to the measured values.

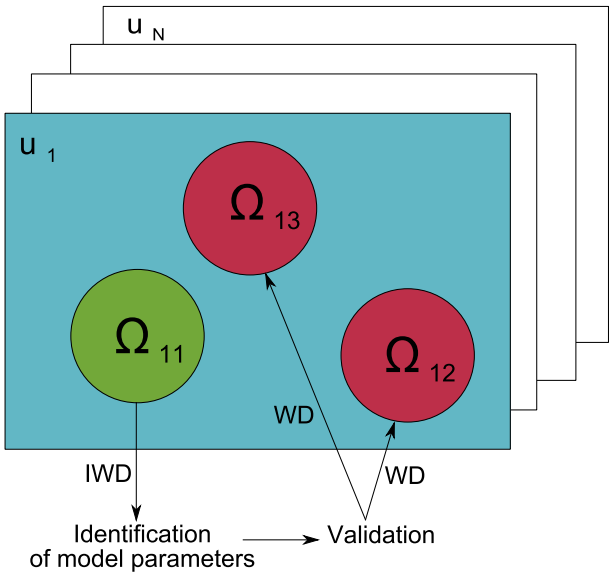

Figure 3.10: Principle of the cross-validation method used together with the IWD inverse method.

The problem of this method is its non-uniqueness of choosing the decomposition of the training and validation sets. In the review paper [50], Arlot gives exhausting list of possible ways to choose this decomposition. As this method is rather empirical, there is almost no general rule which applies to all kind of problems. In our case of vibration problems considered in this thesis, the individual vibration shapes are considered as elements of the data vector $\mathbf{U} = (\mathbf{u}_{f_1}, \mathbf{u}_{f_2}, ...\mathbf{u}_{f_n})$ [7] where f_i are the steady-state oscillation frequencies. As it was mentioned in the section 2.4, the IWD method does not use all the vibration field $\mathbf{u}_i$ but only its part forming

[7] $\mathbf{w}_i$ are considered like column vectors. Each vector represents the measured displacement at all the points.

a circular zone Ω with a diameter related to the approximative wavelength of the field. So we basically dispose with a few independent zones Ω which can serve for an IWD within each i-th wave field $\mathbf{u}_i$. Schematic example of the zones and the application of the IWD is shown in Fig.3.10. Here the vibration field contained in the green zone Ω_{11} is used to identify the model parameters by the IWD and then these model parameters are used for *wave decomposition* (i.e.WD) of the vibration fields in the zones Ω_{12} and Ω_{13}. The misfit of this decomposition is an indicator of the quality of the identified model and its comparison among multiple models can be a basis for a model selection. In this work a number of zones used for testing and training was either equal or 1:2 (more testing zones).

In the following examples the residual error function defined by Eq.2.33 is applied to the validation set.

3.3.1 Example of red cedar wood plate

The red cedar musical wood plate of 2mm thickness represents an anisotropic plate (measurement described in Appendix A.5). We consider five possible models for model selection (B1,B2,B3,B4,B6). Fifteen steady-state vibration fields were in data the space vector $\mathbf{U}$. In each vibration field, there was one zone Ω for *training* and two for *validation (testing)*. There was fifteen vibration fields used for building the models and thirty for testing the identified models. The resulting cross-validation error function (see Eq.1.41 for definition) is shown in Fig.3.11B. We can see that the orthotropic model B6 is by far the best among the five models. On the second position there is a group of models B2,B3 and B4 all having similar testing residuals. The last is the membrane model B1. It seems easy to choose the best model in this case, however, the situation may be less clear as we shall see in the next example.

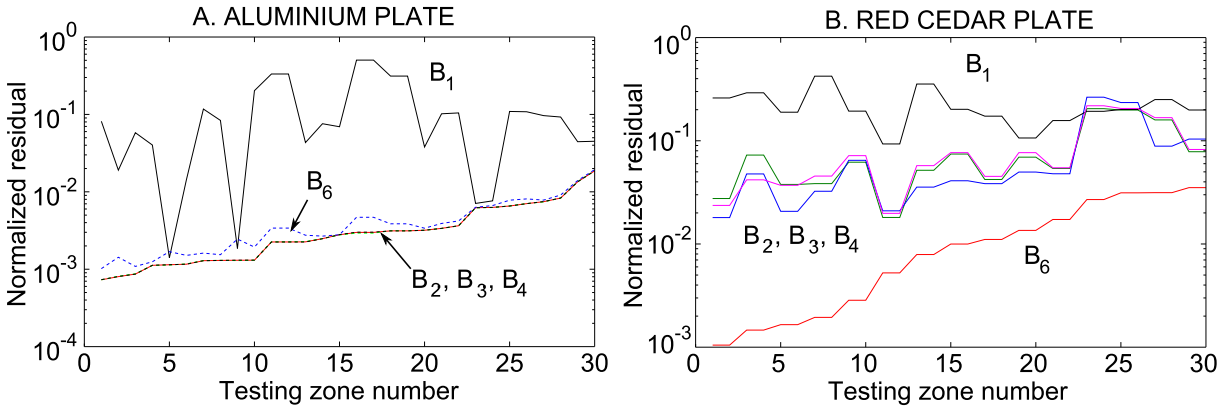

Figure 3.11: Two examples of residuals obtained by different models when using cross-validation.

3.3.2 Example of the thin aluminium plate

The thin 2mm aluminium plate (measurement described in Appendix A.2) was investigated by the inverse method IWD and the results were post-processed to show the performance of the cross-validation method on this measurement sample. As in the preceding example, there were the same number of testing and training zones. The same set of five candidate models (B1, B2, B3, B4, B6) is considered. This time, however, we cannot see clearly the best model in Fig.3.11A. There is one bad model (B1-membrane), three models (B2,B3,B4) giving almost identical predictions and model B6 slightly behind them. Which of the competing models should be chosen in this case? The question can be answered in two ways. If we are in the situation of a red cedar in Fig.3.11B where one and only model gives *statistically lower* residuals then it should be chosen. However, if there are more models whose residuals are comparable (hypothesis of their equality cannot be rejected) then the simplest model of them should be chosen. The next chapter deals with a question of statistical comparison of residuals of different models.

3.3.3 Statistical treatment of residuals of the IWD problem

3.3.3.1 Considering one testing zone

In the last section, we encountered a situation when it was necessary to decide, if residuals obtained by one model are statistically different (lower) from residual obtained by another model (typically the case of Fig.3.11A for models B2,B3,B4 and B6). In order to decide we shall employ a statistical test as described in the following.

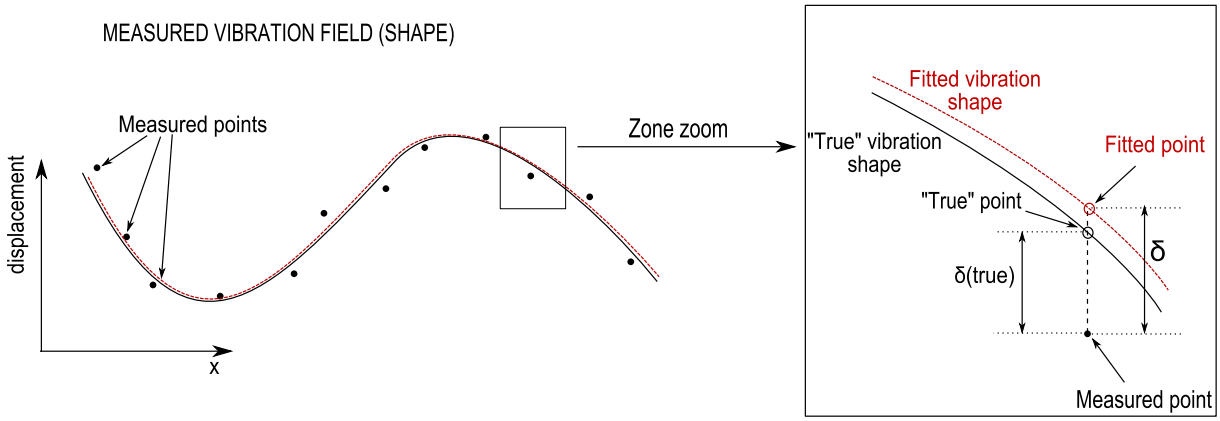

Figure 3.12: Explanation of the residuals δ. The true vibration field is represented by the black line. The fit obtained by IWD method is represented by the red dashed line. Measurement points are black circles.

In Fig.3.12 there is a fictional 1D vibration field. This field is represented by a black line. This function is unknown to us, but we dispose the measurement at a number of points (black

circles). However, these measurements are not *exactly* situated *on* the black line because there is some noise which makes each measurement a random variable. We define a variable δ(true) as the difference between the true value of displacement and its measured value at a particular point (see the detail in Fig.3.12). Due to the measurement uncertainty, this variable is a random variable. We suppose that the distribution of δ(true) is:

- Gaussian with zero mean
- independent of the space coordinate x [8]
- variables δ(true) are statistically independent from one point to another[9]

It should be noted that the true displacement represented by the black line is unknown, but we know a displacement fitted by the IWD method (red line in Fig.3.12). So we can define δ as a difference between the measured value and the fitted value (see Eq.2.29 for definition of δ). Generally, δ(true)$\neq \delta$, but if the fit is close enough to the true underlying function, we can consider these two (random) variables equal and therefore their distributions identical.

Let us suppose that we are dealing with a zone Ω where the IWD is performed for two different models designed by indices 1 and 2. The number of measurement points in the zone Ω is N_Ω. The residuals between the fits and measurement are designed $\delta^{(1)}$ and $\delta^{(2)}$[10]. As it was discussed in the preceding paragraph, we can suppose that elements of $\delta^{(1)}$ are identically independently normally distributed random variables with zero mean and variance σ_1^2. Similar supposition holds for the model 2.

However, we do not know the real values of σ_1^2 and σ_2^2. Our goal would be to determine if $\sigma_1^2 > \sigma_2^2$ [11] or $\sigma_1^2 = \sigma_2^2$. If the latter is true, then the model 1 gives statistically the *same* fit on the zone Ω as the model 2. Otherwise, the model 2 performs better. To this end, we employ a standard F-test with the following hypothesis:

$$H_0\text{: } \sigma_1^2 = \sigma_2^2 \text{ (null hypothesis)}$$
$$H_1\text{: } \sigma_1^2 > \sigma_2^2 \text{ (alternative hypothesis)}$$

Because the true variances σ_1^2 and σ_2^2 are not known we must use their estimates s_1^2 and s_2^2 [12]. If the null hypothesis H_0 is true than the ratio

$$F = s_1^2/s_2^2 \tag{3.24}$$

[8]This means that the measurement noise is the same for every points. This is, however, true only in the ideal experimental conditions.

[9]This can be assumed because the scanning laser vibrometer measures each point separately.

[10]In this case $\delta^{(1)}$ and $\delta^{(2)}$ are vectors with N_Ω elements.

[11]Without the loss of generality we suppose that the residual of the model 2 is smaller.

[12]The estimate of variance can be calculated as $s_i^2 = \sum_k |\delta_k^{(i)}|^2/(N_\Omega - 1)$.

has Fisher distribution with (N_Ω,N_Ω) degrees of freedom. If the Fisher statistic F is close to 1, than the hypothesis H_0 is likely (variances are equal). Otherwise, as F grows the hypothesis H_0 becomes less and less likely. More precisely, the null hypothesis H_0 is rejected on the significance level α if

$$F > F_{\alpha,N_\Omega,N_\Omega} \tag{3.25}$$

where $F_{1-\alpha,N_\Omega,N_\Omega}$ is a quantile obtained from the cumulative distribution function of the Fisher distribution. Otherwise, if F<$F_{\alpha,N_\Omega,N_\Omega}$ then the null hypothesis *cannot be rejected*[13]. If the cumulative distribution of $F(x, N, N)$ is designed $CF(x, N, N)$ then the quantile is defined as

$$CF(F_{1-\alpha,N_\Omega,N_\Omega}, N_\Omega, N_\Omega) = 1 - \alpha \tag{3.26}$$

The significance level α used in this work is always 0.05[14].

Two concrete examples of testing the fit of the IWD method are shown in the following.

In Fig.3.13, we can see a detailed example of residuals obtained on *one* testing zone for the aluminium plate and the red cedar (see for comparison Fig.3.11). In Fig.3.13, the residuals for different models are shown: $\delta^{(1)}$ for B1 (membrane), $\delta^{(2)}$ for B2 (Kirchhoff), $\delta^{(4)}$ for B3 (Mindlin) and $\delta^{(5)}$ for B6 (Kirchhoff orthotropic). The indices of the measurement points inside the zone were permuted in order to make the displacement function monotonically growing with index number to facilitate the reading of the graphs. From Fig.3.13, we can conclude that the residuals do not depend on the amplitude of the measured displacement. This confirms one of the hypothesis used for the random variable δ(true) in the preceding section.

In the case of the measurement made on 2mm aluminium plate (Fig.3.13 A), three residuals displayed are displayed: $\delta^{(1)}$, $\delta^{(2)}$ and $\delta^{(4)}$. We can see that while the residual $\delta^{(1)}$ is much bigger that the other two, $\delta^{(2)}$ and $\delta^{(4)}$ are almost identical. Indeed, the statistical analysis yields the Fisher statistics $F_{12} = s_1^2/s_2^2 = 29.02$ and $F_{23} = s_2^2/s_3^2 = 1.0001$. This zone has $N_\Omega = 343$ points. From the Fisher distribution we obtain the quantile $F_{0.95,343,343} = 1.195$. We can see that the statistical difference of the residuals $\delta^{(1)}$ and $\delta^{(2)}$ is without a question because $F_{12} = 29.02 > 1.195$ (hypothesis H_0 is rejected). In the second case, however, we cannot reject the null hypothesis because $F_{23} = 1.0001 < 1.195$. This means from the statistical point of view the models B2 and B3 perform equally on this particular zone.

The second example is shown in Fig.3.13B, there are two competing models: B2(isotropic plate) and B6 (orthotropic plate). The situation is less clear than in the latter case, but still the orthotropic model B6 outperforms the isotropic Kirchhoff model B2. In this case we have $N_\Omega = 211$ points and the quantile is $F_{0.95,211,211} = 1.256$. Since the Fisher statistics is $F = s_2^2/s_5^2 = 4.91 > 1.256$ the null hypothesis is rejected. This means that the residuals of the B2

[13]This does not mean that this hypothesis is true, but that there is not enough evidence to confirm that it is false.
[14]Of course, this level is arbitrary, however, 0.05 is the most popular choice in statistics.

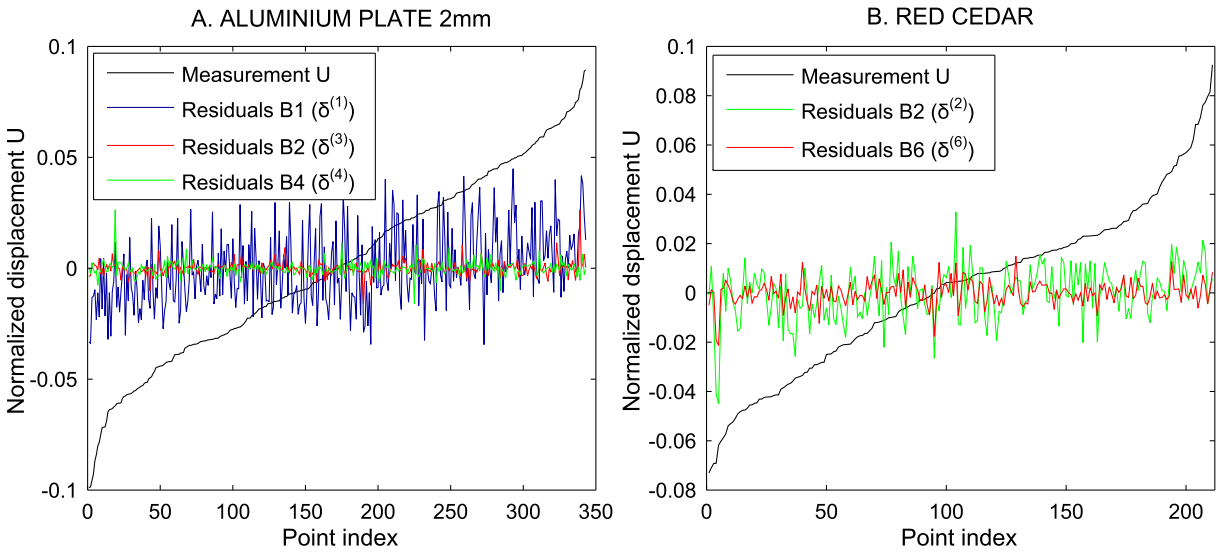

Figure 3.13: Examples of the residuals obtained on one *testing* zone Ω using different models. A. Aluminium plate 2mm measurement, B. red cedar wood plate. The black line represents the measured displacement in the zone Ω.

model are statistically higher than the residuals of the B6 model.

3.3.3.2 Considering multiple testing zones

So far, we were only considering one zone Ω. But the method presented above can be applied to any testing zone.

In this section we shall see how a hypothesis testing shown in the preceding section can be displayed graphically. As it was shown, the variable F defined by Eq.3.24 is a random variable with the Fisher distribution. Let us consider hypothetical models 1 and 2 and a fictional measurement on number of zones. The distribution (probability density function) of the the F statistics applied to the zone 6 is shown in Fig.3.14A. A confidence interval for F is delimited by values F_A and F_B. This means that the true value of F is inside the interval $F_A < F < F_B$ with the probability 95%. In Fig.3.14B we can see the probability density function of F for zones 6 and 24. We can see that in the case of the zone 6, the distribution of F is around unity and the hypothesis of $F = 1$ cannot be rejected. In other words, it means that $F_A < 1 < F_B$. However, in the case of zone number 24, the distribution of F is far from unity and $F_A > 1$. In this case, the hypothesis $F = 1$ is rejected on a significance level 5%. In the following, the kind of figure Fig.3.14B would be used. For each model, the estimated value of F is not shown, but instead, the confidence interval (points F_A and F_B) is shown. If the lower confidence interval limit $F_A < 1$, then the hypothesis about the equality of models (hypothesis H_0) *cannot* be rejected. Otherwise, if $F_A > 1$, then the hypothesis is rejected (it means that model 1 is worse than model 2). The curve like Fig.3.14B helps us to see how many testing zones are equally fitted by model 1 and 2, and how many zones are fitted *better* by model 1 and 2 respectively.

The two previously mentioned examples of 2mm aluminium plate and red cedar plate are used to show the statistical treatment explained above. The confidence intervals are shown in Fig.3.15.

In the case of the aluminium plate, the variance s_2^2 corresponds to the B2 model (Kirchhoff plate). The variance s_1^2 corresponds to different models (B1,B3,B4,B6). In Fig.3.15A, we can see that while the statistic F for model B1 is far away from 1 for most of the testing zones, all the other models are equivalent with the B2 model.

In the case of the Red Cedar plate the denominator of the F statistics is the B6 (Kirchhoff orthotropic plate) and the nominator is the B2 model (Kirch. isotropic). We can see that all the testing zones are statistically better fitted by the orthotropic model and the F statistics is always higher than 1. The choice of the model B6 is uncontested.

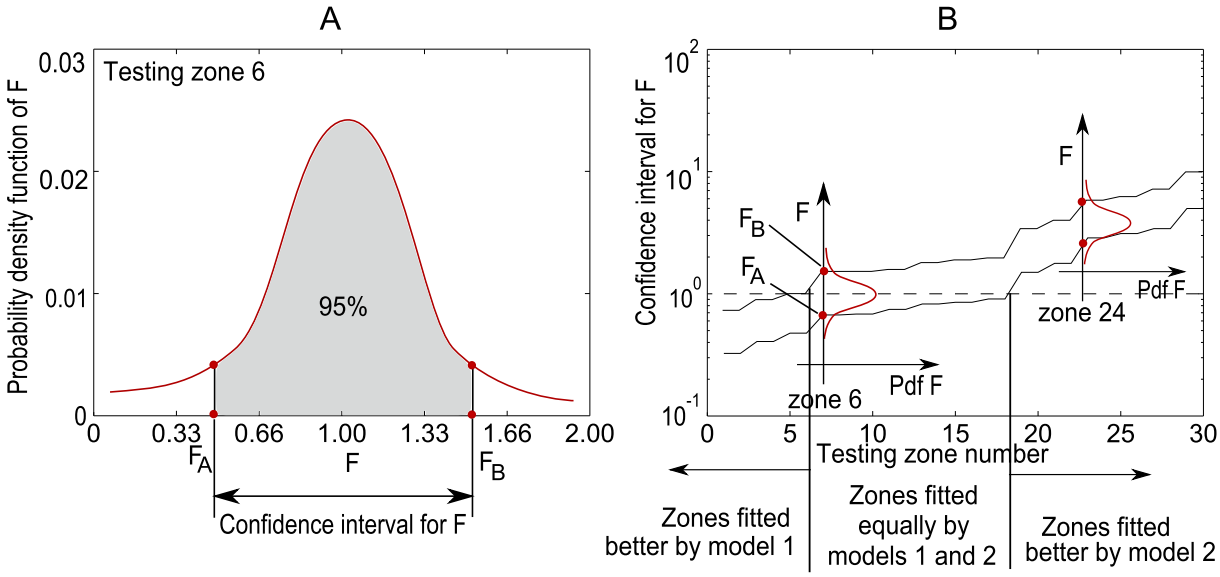

Figure 3.14: An illustrative example explaining the F statistics as a random variable.

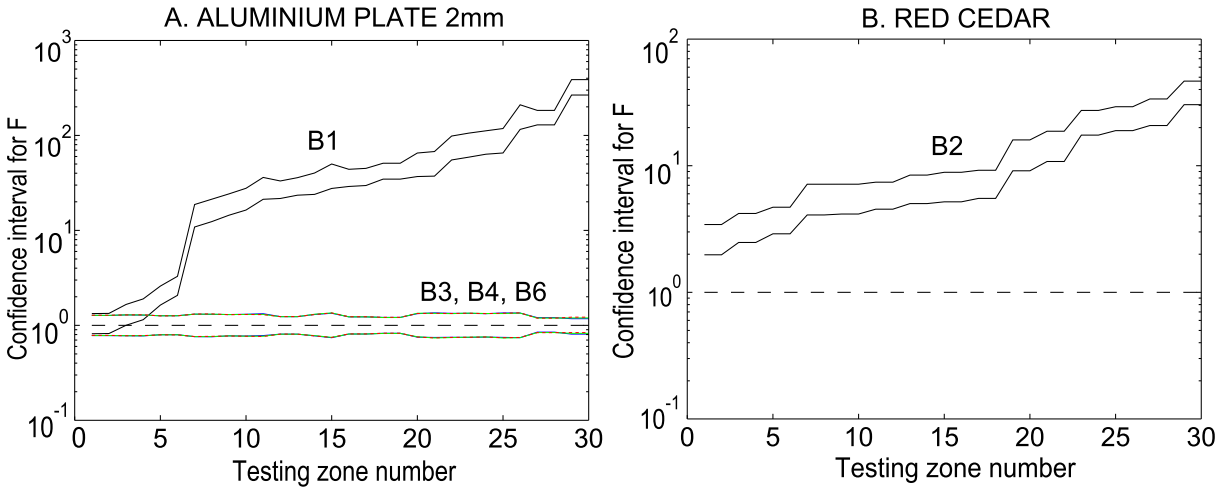

Figure 3.15: F-statitics applied to 2mm aluminium plate and red cedar measurements. On left we can see equivalence in the fits of several models. On the right the F-statistics comparing the orthotropic and isotropic Kirchhoff models shows clearly the statistically better fit of the orthotropic model.

3.4 Conclusion

In this section, we have seen the application of the general model selection techniques in the case of the IWC and IWD inverse methods.

The problem of preliminary choice of candidate models was discussed in Section 3.1.1. It was shown that a wise choice of the candidate models (equations of motion) is necessary for a good model selection. If a good models is to be chosen, it must be already present in the set of candidate models.

The Section 3.2 was devoted to the information criteria AIC and BIC. These criteria are exposed with a brief mathematical background. The application of these criteria as a post-processing of the IWC inverse problem is presented in Section 3.2.3. Several typical experimental examples are discussed. The advantages and setback of these criteria are shown. Sections 3.2.4, 3.2.5 and 3.2.6 discuss the possibility to use the information criteria for model selection based on other inverse methods. It is shown that the requirements of the information criteria are too restrictive for the IWD and RIFF methods. It is shown, that statistically independent residuals are quite rare among the inverse problems.

As it was shown, the IWD inverse methods cannot be used with the information criteria model selection. The Section 3.3 presents an alternative to the information criteria: a cross-validation technique. This technique is adapted for the IWD inverse technique. Some practical aspects of the implementation are exposed. Especially, the use of F-statistics is presented. This statistics permits to tell which model has statistically higher residuals. The application of the cross-validation is shown on several experimental examples. Two typical situations are presented, the first is when one model is clearly better then the others, the second example is when several models give comparable results. The applicability of the model selection is discussed in both cases.

4 Case studies

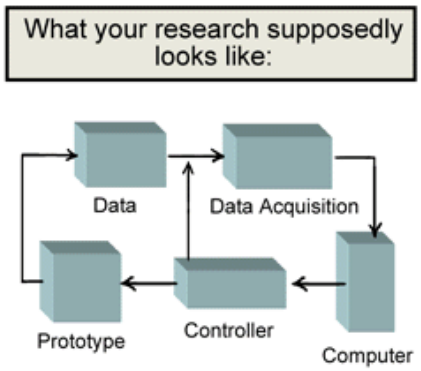

Figure 1. Experimental Diagram

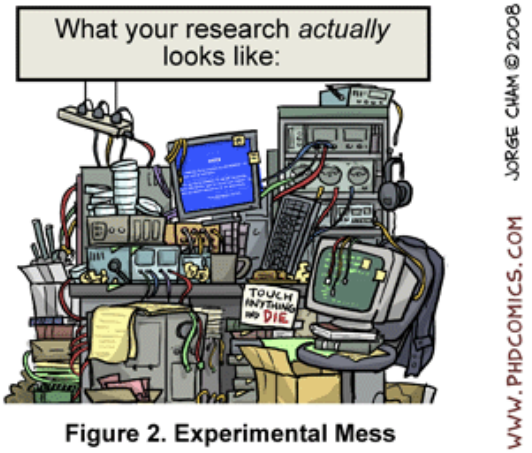

Figure 2. Experimental Mess

"All models are wrong but some models are useful." (George Box)

4.1 Introduction

In this section we shall look at three experimental applications of the model selection technique treated in this thesis.

The first case study deals with determination of axial forces in membranes and beams (for details see Section 4.2). The goal of this study is to show if the axial force is important for the description of the vibration of the structure. In this section three separate cases are tested: aluminium beam under tensile force, silicon microbeams under unknown axial force and a paper membrane under unknown tensile tension.

The second case study consists of determination of the in-plane symmetry of the measured plates (for details see Section 4.3). The question is whether a plate should be considered isotropic or orthotropic. A model selection technique is applied to three experimental cases: an aluminium plate, a composite plate and a wooden plate. The importance of this study is particularly shown in the case of the composite plate, where the symmetry is a priori unknown.

The third case study deals with the determination of the most appropriate model for a "complicated" structure. It is represented by a thick sandwich plate with steel faces and tissue core. The discussion of this study is in the section 4.4.

All the estimated model parameters are calculated together with their standard deviances which are shown by the "±" sign in Tab.4.1 - 4.10. The standard deviance of the parameters identified by the IWC method is calculated using the log-likelihood function as described in Section 2.3.1.1. The standard deviance of the parameters using the IWD method is calculated using the Jacknife method as described in Section 2.4.2.1.

The standard deviance of the identified parameters (some kind of scattering of the inverse method) is not directly linked to the model selection criteria. However, an excessive scattering (standard deviance) is a sign of ill-posedness of the inverse problem and therefore a bad prediction capabilities of the identified model. So, we can expect that a model with large parameter scatter would perform badly on the validation set of data (see Section 1.4.2.3 for details).

The meaning of confidence interval figures like Fig.4.3 is explained in Section 3.3.3.2.

4.2 Determination of in-plane static forces in beams and membranes

4.2.1 Aluminium beam under axial tension

Thin aluminium-based alloy beam of dimensions 400×20×2mm was mounted on a Delta experimental device which permits to pre-stress a beam to a given and controlled axial force (see Fig.4.1). This force can be approximately determined by means of measuring the deformation of the frame of Delta device with a micrometer. Consequently, five levels of axial force were applied: 0, 500, 1000, 2000 and 3000N. For each level of force vibration response of the beam was measured at 43 points by scanning laser vibrometer. The excitation was a pseudo-random signal covering the frequency range from 0 to 10kHz. A phase reference signal was measured by an accelerometer mounted on the end of the beam. The average vibration spectrum is shown in Fig.4.2. The model selection analysis was applied to the 25 vibration shapes for frequencies between 2100 and 7000Hz (Fig.4.2).

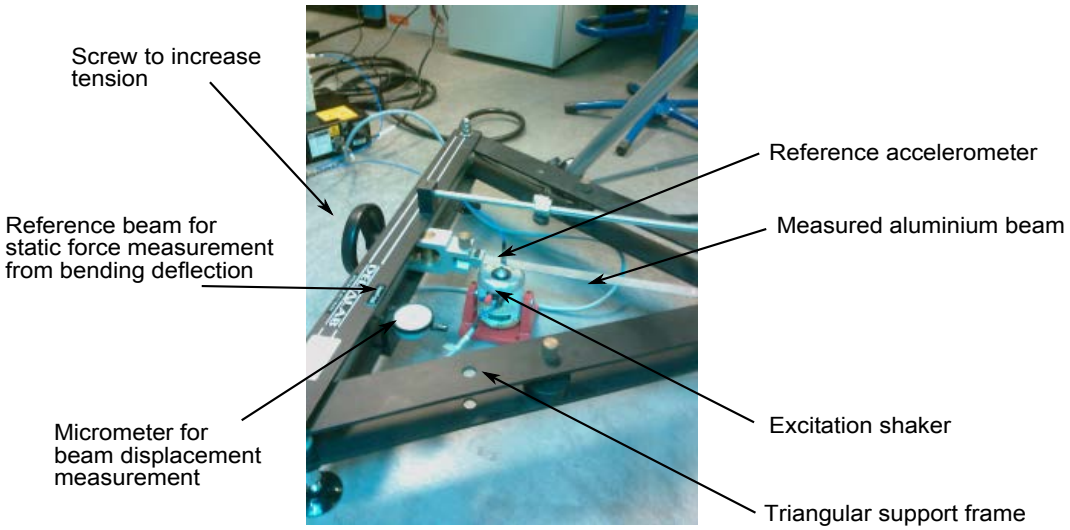

Figure 4.1: Experimental mounting of the aluminium beam on a Delta device.

4.2.1.1 Using AIC and BIC for model selection

Two models were considered for the model selection problem: *A2-Euler* and *A3-Euler+Force*. The idea behind this selection was to see when the axial force becomes important for the description of the vibration of the beam. The results obtained by the IWC method are summarized in Tab.4.1. We can see that both the AIC and BIC criteria favour the mixed A3 model if the applied force is 500N and higher. At zero applied force, however, the A2 model (Euler) is correctly chosen as being the optimal. From the results in Tab.4.1, we can see that the force is determined with lower precision than the rigidity coefficient EI.

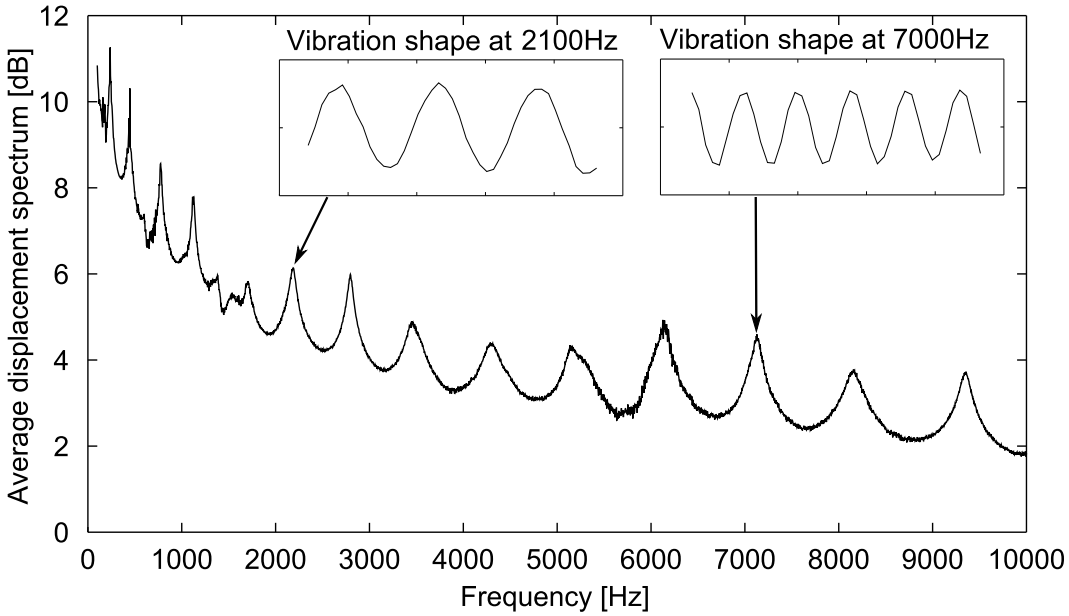

Figure 4.2: Spectrum of the aluminium beam without axial tension. The analysis was done on vibration shapes corresponding to frequencies from 2100Hz to 7000Hz.

Appl. force	0N	500N	1000N	2000N	3000N
Euler	EI=1.01±0.03 ΔAIC=0 ΔBIC=0	EI=1.006±0.01 ΔAIC=14.4 ΔBIC=13.6	EI=1.128±0.02 ΔAIC=22.4 ΔBIC=21.6	EI=1.23±0.02 ΔAIC=53.7 ΔBIC=52.8	EI=1.34±0.03 ΔAIC=79.5 ΔBIC=78.7
Euler+Force	T=-98±114 EI=1.03±0.02 ΔAIC=1.33 ΔBIC=2.18	T=469±129 EI=1.01±0.01 ΔAIC=0 ΔBIC=0	T=1114±204 EI=1.00±0.03 ΔAIC=0 ΔBIC=0	T=2066±125 EI=0.997±0.02 ΔAIC=0 ΔBIC=0	T=2869±87 EI=1.02±0.01 ΔAIC=0 ΔBIC=0

Table 4.1: Optimal results for Euler and Euler-Force models identified by IWC method. The units of bending stiffness EI are [kgm^3/s^2] and units of axial tensile force T are [N].

4.2.1.2 Using Cross-validation for model selection

The Cross-validation technique was used together with IWD method as described in section 3.3. There were the same 25 training vibration shapes that were used for the IWC analysis and there were additional 25 vibration shapes used for validation of obtained results. The A3 model (Euler+Force) was considered as reference for the F-test because it had a lesser fit residuals than the A2 model (Euler). The testing statistics is then $F = s_1^2/s_2^2$ where s^2 are the estimators of the variances corresponding to the fit of the validation vibration shape. Index 1 corresponds to the Euler model and index 2 corresponds to the Euler+Force model. We test hypothesis F=1 which means that a particular validation vibration shape was fitted with statistically equal precision.

The resulting optimal solution obtained by fitting the training set of measurements is shown in Tab.4.2. We can see that both methods, IWC and IWD, lead to similar optimal results. The

validation zone fit shows for how many validation (test) vibration fields is F statistically higher than 1 (That means that model A3 is *better* than A2). We can see, for example, that for a zero applied axial force, F is never statistically higher than 1, which means that model A2 can be used with equal precision and because this model is more parsimonious it should be chosen. However, for higher applied axial forces, there are more and more validation data sets which are better fitted by A3 model (F>1). This phenomenon can be seen in Fig.4.3 for applied forces 1000 and 3000N. In this figure we see the 95% interval of confidence for the F function for different testing data sets. For example, for the applied force 3000N we see that there are about an half of the testing data sets which are under-fitted by the Euler model.

Appl. force	0N	500N	1000N	2000N	3000N
Euler	EI=1.02±0.006	EI=1.06±0.01	EI=1.12±0.01	EI=1.23±0.01	EI=1.34±0.02
Valid.zone fit	0% misfit	8% misfit	24% misfit	32% misfit	52% misfit
Euler+Force	T-95±125	T=527±78	T=1083±106	T=2001±178	T=2825±180
	EI=1.03±0.01	EI=1.01±0.03	EI=1.00±0.02	EI=1.01±0.02	EI=1.03±0.02

Table 4.2: Optimal results for Euler and Euler-Force models identified by IWD method. The units of bending stiffness EI are [kgm^3/s^2] and units of axial tensile force T are [N]

.

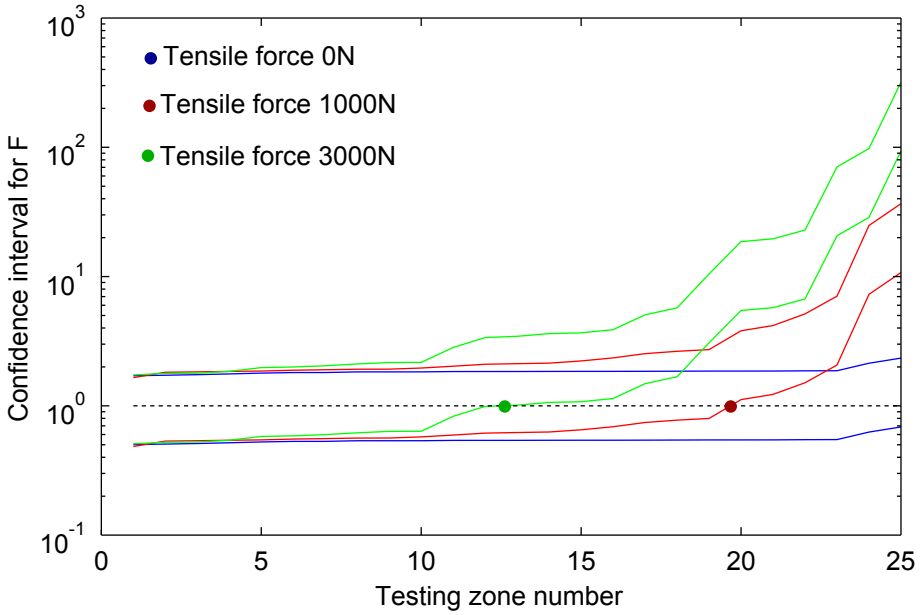

Figure 4.3: Confidence intervals for F-statistics comparing the equivalence of fit obtained by Euler model to the fit obtained by Euler-Force model.

4.2.1.3 Conclusion

In Fig.4.4 we can see the comparison of the optimal results obtained for the Euler+Force model by IWC and IWD methods. These results are also compared to the static estimates

of the same variables. The coefficient c_4 was statically estimated by a three-point method to be 1.02±0.07kgm^3/s^2 (see Appendix B for details on this method). The static axial force was determined by a calibrated micrometer which measures the deformation of the mounting frame. In Fig.4.4 the markers represent the optimal values and boxes the scattering.

We see quite a good correlation of the three independent inverse methods. The model selection problem addressed by the information criteria and Cross-validation technique showed that the axial force should be included in the modelling for all forces superior to 500N. For the case of zero axial force, both model selection methods showed that added force term is unnecessary.

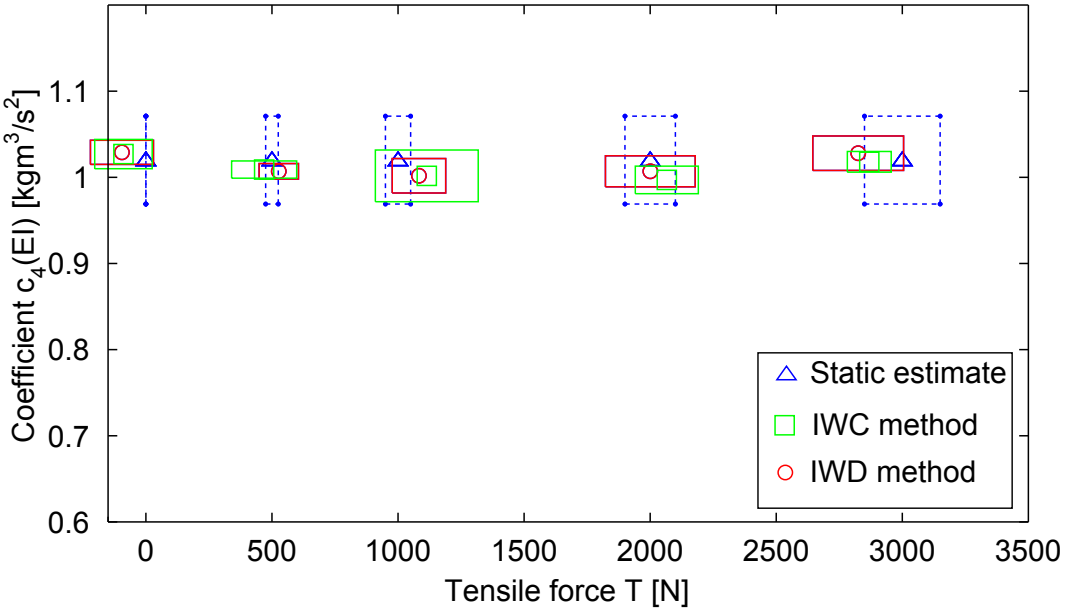

Figure 4.4: Determination of the parameters of the equation of motion of the aluminium beam under static tension. We can see the comparison of the results obtained by the IWC (green), IWD (red) methods and the static estimates (blue). The rectangles represent standard deviance estimates.

4.2.2 Silicon microbeams

Silicon microbeams were fabricated by the laboratory LAUM in Le Mans. They represent part of the research in the MEMS technology domain. The beams are cut within a much larger silicon wafer (see Fig.4.5). The length of the beams is 3mm. Their width is 65μm (microbeam A) and 153μm (microbeam B). The thickness of the beams is known precisely, from the geometry considerations we only know that it is inferior to 36μm. The direction of beam axis corresponds to the (100) crystallographic orientation. The measurement was realized by a Polytec scanning laser microscope in the frequency bandwidth 1MHz. The excitation was done by a piezoelectric elements glued to the silicon wafer. The phase reference signal comes from a second laser measuring fixed point on a wafer.

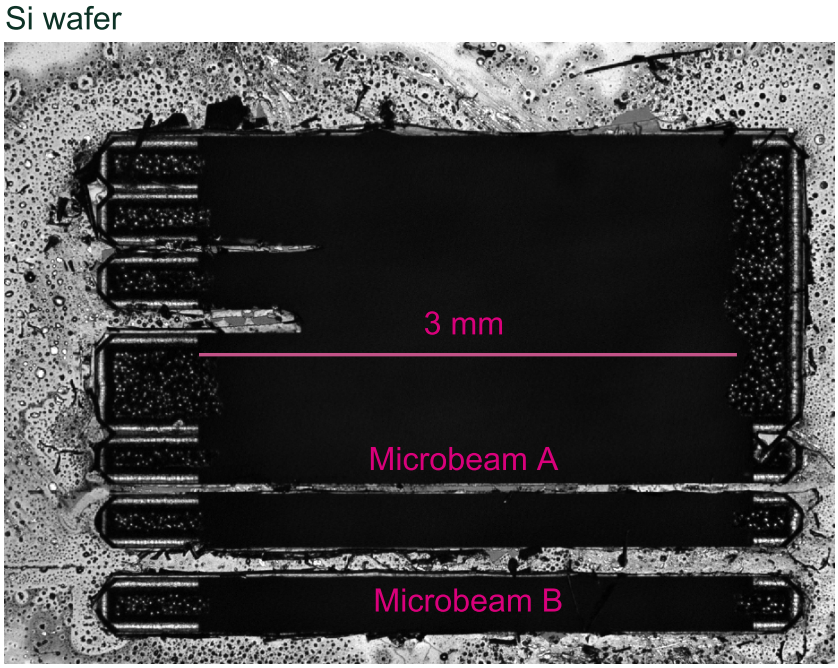

Figure 4.5: Silicon wafer with two microbeams designed A and B.

During the fabrication process of these microbeams, there are number of undesired phenomena which can occur. Among them, there is, for example, buckling under the presence of axial compressive force. Such a buckling would be manifested by a change in the equation of motion. If we consider the Euler beam equation as correct description of the model, then the (small) buckling would be manifested by a change of vibration in lower frequencies, while the vibration at higher frequencies would follow the Euler model. Such a behaviour can be approximately described by Euler+Force model (model A3 in Section Ref.2.2). Such a model is like the Euler model in high frequencies but the low frequency response is influenced by the axial force. Therefore, these two models were candidates in the model selection.

4.2.2.1 Using AIC and BIC for model selection

As mentioned earlier, two models were chosen as candidates for a model selection problem: Euler (A2 model) and Euler+Force (A3 model). The IWC method was applied to 12 vibration shapes for the microbeam A and 20 vibration shapes for microbeam B. The dispersion curves obtained by IWC method were fitted by the two models and the optimal parameters of these models were determined. Both AIC and BIC analysis show that the Euler+Force model is unnecessary.

4.2.2.2 Using Cross-validation for model selection

The cross-validation technique was employed together with IWD method on 12 training and 12 testing zones. The Euler+Force model was taken as reference for F-statistics defined by

	Model	Parameters	ΔAIC	ΔBIC
Microbeam A	Euler	$EI/\rho_L = (3.7\pm0.06)10^{-3}m^4/s^2$	0	0
	Euler+Force	$EI/\rho_L = (3.7\pm0.09)10^{-3}m^4/s^2$	2.1	2.6
		$T/\rho_L = (1.8\pm3)10^{3}m^2/s^2$		
Microbeam B	Euler	$EI/\rho_L = (3.4\pm0.07)10^{-3}m^4/s^2$	0	0
	Euler+Force	$EI/\rho_L = (3.3\pm0.01)10^{-3}m^4/s^2$	2.0	2.5
		$T/\rho_L = (4.6\pm7)10^{3}m^2/s^2$		

Table 4.3: Optimal parameter and model selection criteria obtained by IWC method.

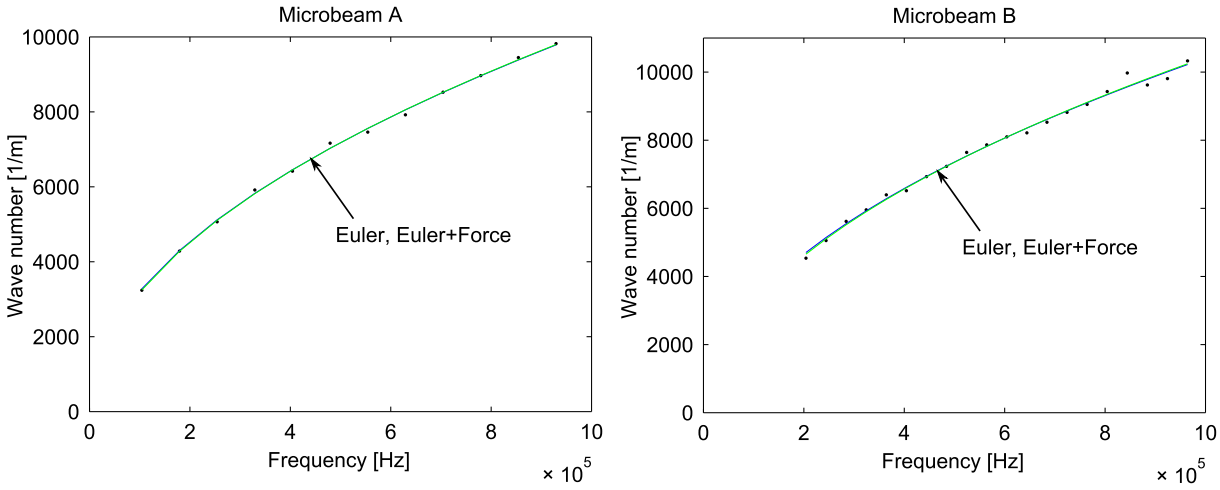

Figure 4.6: Dispersion curves obtained by IWC method on two microbeam examples. We see the fit with two competing models is almost identical.

Eq.3.24. We can see in Fig.4.7 that in neither testing zone the value of F is different from unity. That means that both models are statistically equivalent from the point of view of IWD method. Considering the application of model selection criteria in Section 3.3, the Euler model is preferred instead of the Euler+Force model.

In Tab.4.4 we can see the optimal parameters of the IWD inversion applied to both beams and both models. It should be noted that in this case both inverse methods IWC and IWD yield the same results.

	Model	Parameters	Valid.zone fit
Microbeam A	Euler	$EI/\rho_L = (3.7\pm0.04)10^{-3}m^4/s^2$	100%
	Euler+Force	$EI/\rho_L = (3.8\pm0.07)10^{-3}m^4/s^2$	-
		$T/\rho_L = (5.48\pm4)10^{3}m^2/s^2$	
Microbeam B	Euler	$EI/\rho_L = (3.3\pm0.05)10^{-3}m^4/s^2$	100%
	Euler+Force	$EI/\rho_L = (3.3\pm0.015)10^{-3}m^4/s^2$	-
		$T/\rho_L = (1.47\pm1)10^{3}m^2/s^2$	

Table 4.4: Optimal parameter and model selection criteria obtained by IWD method.

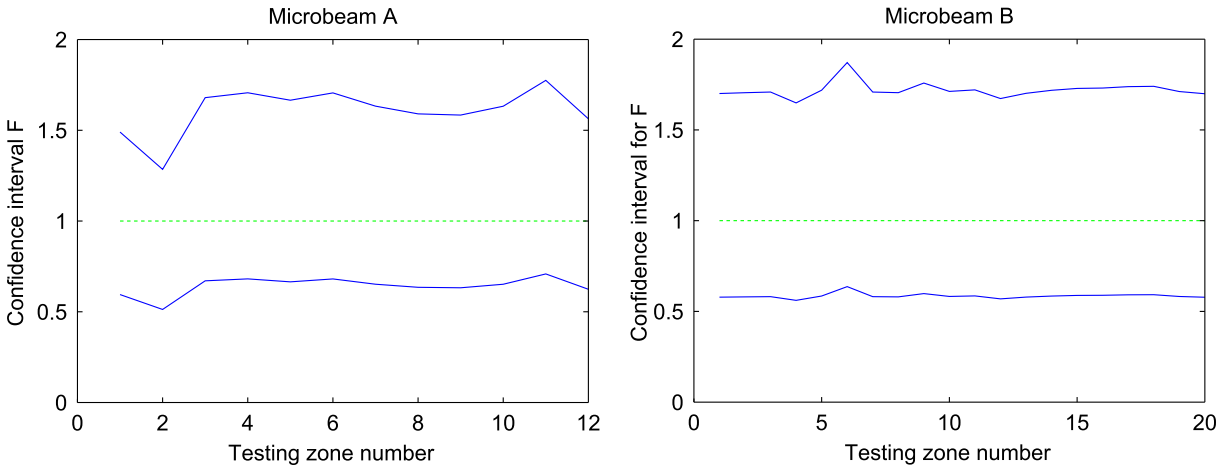

Figure 4.7: Confidence interval for F statistics applied on 12 (microbeam A) and 20 (microbeam B) testing zones.

4.2.2.3 Conclusion

Both model selection criteria showed that the hypothesis of the presence of axial force cannot be affirmed. Taking into account the hypothesis about possible buckling of the microbeams and its effect on the vibration behaviour, we can conclude that the buckling does not take place, or its effect is negligible.

4.2.3 Paper membrane

The paper membrane was made of thick wallpaper cut in the circular form of 0.15m in diameter. Its thickness was approximately 0.2mm and its surface density was 0.17kg/m^2. It was mounted on a plastic cylinder as shown in Fig.4.8 on left. There were sixteen holes along the perimeter of the paper. There was a string passing through each of the holes. These strings were stretched by eight identical tension springs placed along the cylinder perimeter. Its was assumed that approximately homogeneous tension plane-stress conditions can be achieved if all the deformed springs have the same length. This tension is, however, difficult to estimate from the static deformation of the springs because the tension string passes a right angle and there are unknown losses in force due to this passage. Only the upper limit of this tension can be estimated from the static measurements. There were two levels of tensile force which were applied to the paper membrane.

The excitation of the whole structure was effected by a shaker as shown in Fig.4.8 back side. The phase reference accelerometer was also mounted on the back side of the cylinder. The excitation was a pure sine function. The response was measured at 671 points for 15 frequencies between 400 and 2500Hz. The vibration shapes for the lowest and the highest frequencies are shown in Fig.4.9.

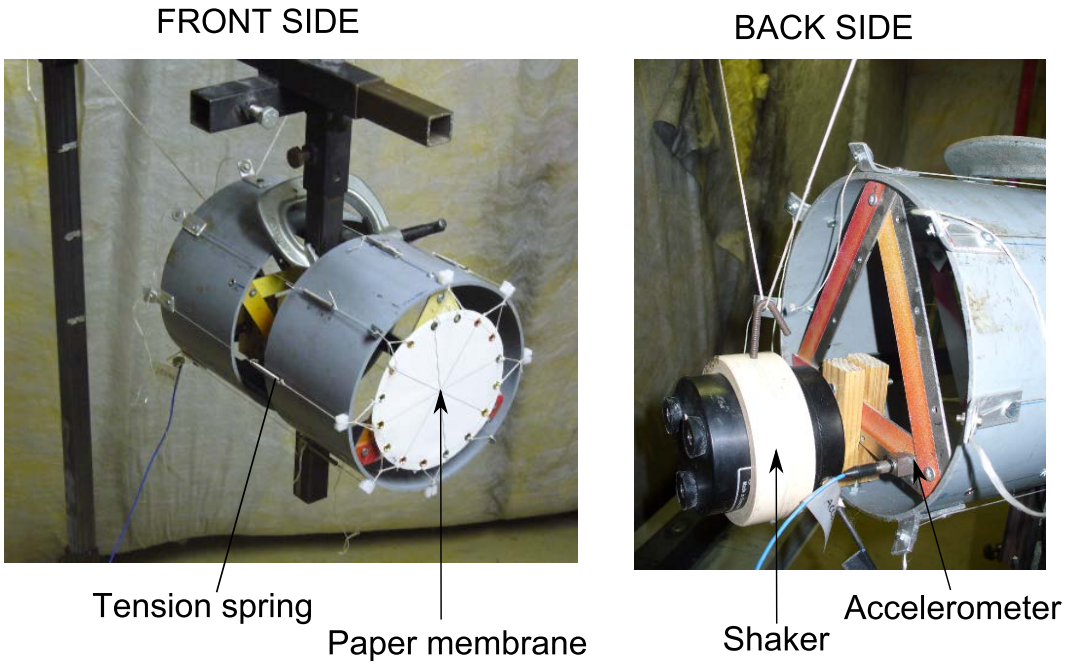

Figure 4.8: Experimental mounting of the paper membrane and excitation of the support frame.

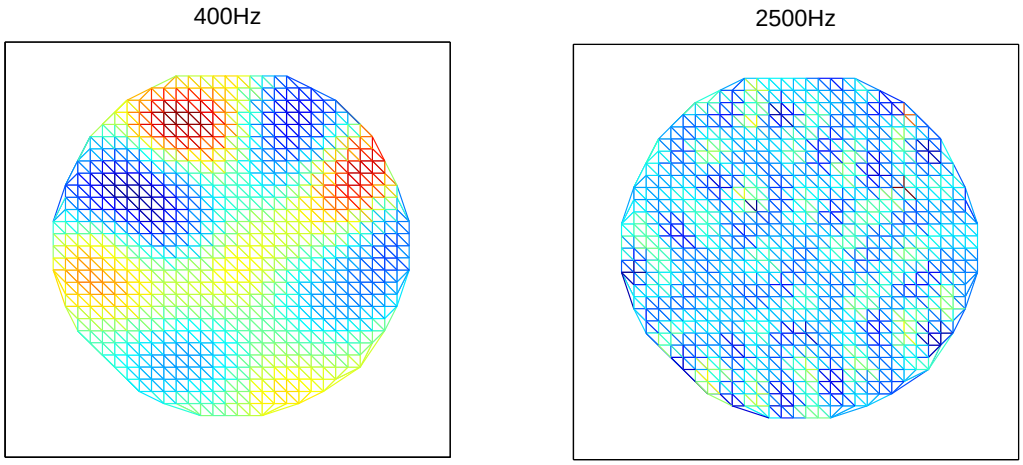

Figure 4.9: Vibration shapes of the paper membrane for the lowest and highest measured frequencies.

4.2.3.1 Using AIC and BIC for model selection

The model selection problem consisted in determining the appropriate equation of motion of the paper membrane. This time, the operator of the structure was unknown, its physical properties could be estimated with only very rough approximation. Three candidate models were considered: B1 - Membrane, B2 - Kirchhoff and B3 - Kirchhoff/membrane. Although, the membrane model seems to be the natural choice, the resulting IWC analysis shows that this model is actually the least adapted to describe the behaviour of the structure. In Fig.4.10 and

Fig.4.11, we can see the dispersion curves of the optimal models B1, B2 and B3 compared to the wave-numbers obtained by IWC. It is clearly visible that in the case of both tension forces, the membrane model is not adapted. Surprisingly, in the case of the tension level 1, the Kirchhoff model seems to be better than the membrane model. In other words, the paper behaves more like a thin plate. The model most adapted in both cases of the tension force is the mixed Kirch./membrane model. The identified parameters of all the models are shown in Tab.4.5.

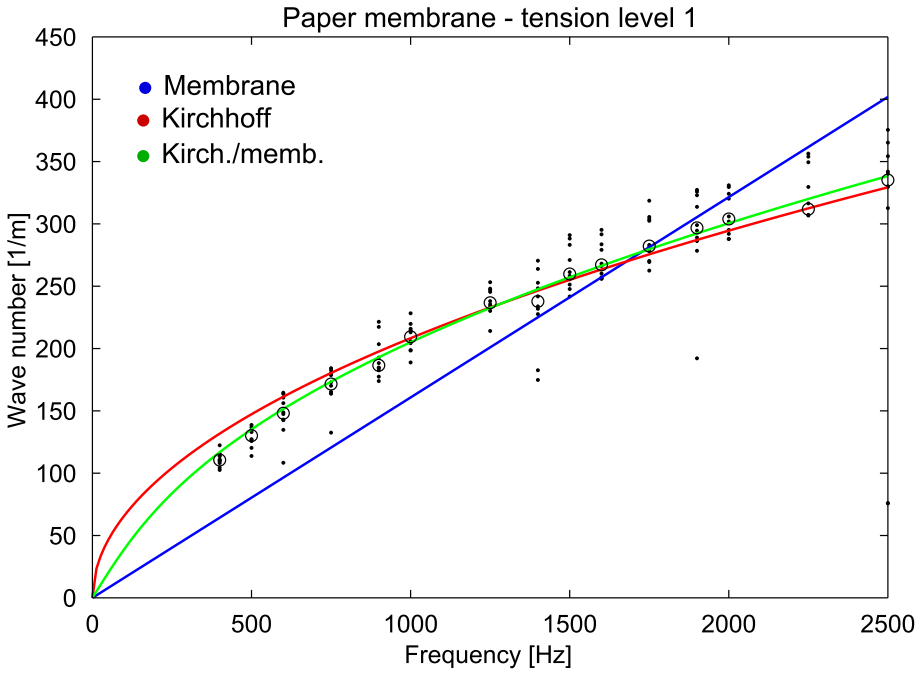

Figure 4.10: Tension level 1: Optimal dispersion curves predicted by Membrane, Kirchhoff and Kirch./membrane models with wave vector estimated obtained by IWC.

	Opt.param.	ΔAIC	ΔBIC
Tension level 1			
B1:Membrane	T=195±18	125	130
B2:Kirchhoff	D=(3.5±0.4).10^{-3}	4.9	1.5
B3:Kirch./membrane	T=39±11 D=(2.8±0.3).10^{-3}	0	0
Tension level 2			
B1:Membrane	T=233±5	292	290
B2:Kirchhoff	D=(4.1±0.2).10^{-3}	143	140
B3:Kirch./membrane	T=81±9 D=(2.4 ± 0.2).10^{-3}	0	0

Table 4.5: Overview of the results obtained by the IWC method and the information criteria. The units of tension T are N/m and the units of the plate bending stiffness D are kgm^2/s^2.

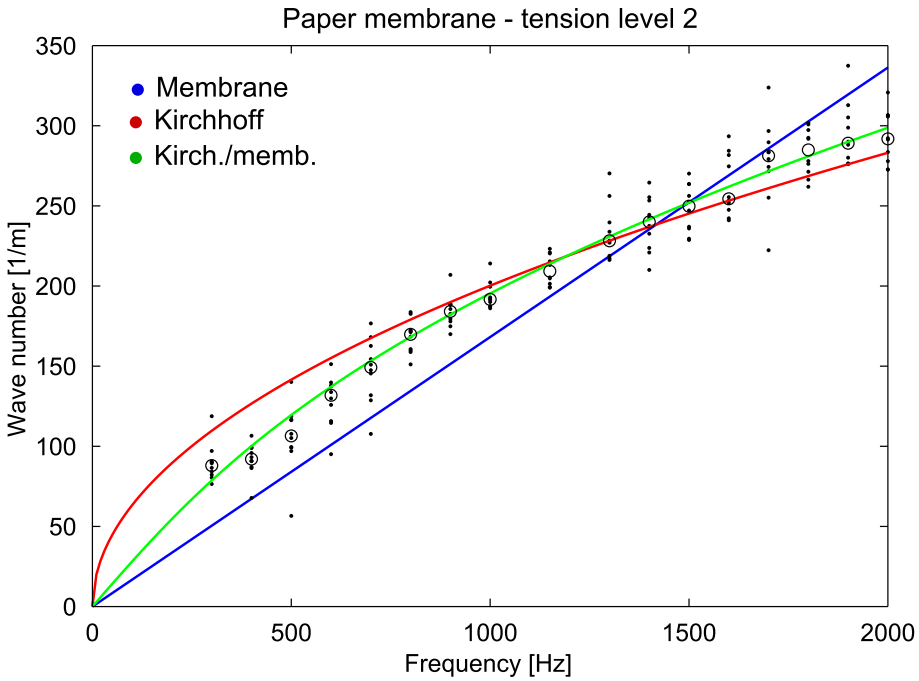

Figure 4.11: Tension level 2: Optimal dispersion curves predicted by Membrane, Kirchhoff and Kirch./membrane models with wave vector estimated obtained by IWC.

4.2.3.2 Using Cross-validation for model selection

In the case of the first level of tension, fifteen vibration shapes were used for identification of operators by IWD and 30 shapes were used for validation. In the second level of tension, there were 17 shapes for identification and 34 for validation. The resulting parameters for the identified operators by the IWD method are shown in the Tab.4.6. The best fit of the data in the validation set was achieved by the Kirch./membrane model. The fit of the other two models was compared to this fit by the means of F statistics as shown in Section 3.3. It can be seen in Fig.4.12 that the F statistics is very far away from 1 for almost all the validation zones for the membrane model while the F statistics for the Kirchhoff model is much closer to 1 for a number of validation zones. This is a similar result to the one obtained by model selection AIC and BIC in the preceding Section 4.2.3.1 where the Kirchhoff model was closer to the best model (Kirch./membrane). For the second tension level, the performance of the Kirchhoff model drops and the membrane models slightly increases. However, in both cases, the mixed Kirchhoff/membrane model is the optimal choice. The ”patch misfit” term in Tab.4.6 shows how many validation data sets (patches) are under-fitted (which means that statistically F>1).

4.2.3.3 Conclusions

Both model selection methods chose the mixed Kirchhoff/membrane model as being the optimal model in the among the three candidate models. This result is not surprising, however, the

	Opt.param.	Patch misfit
Tension level 1		
B1:Membrane	T=141±69	96%
B2:Kirchhoff	D=(3.9±0.3).10^{-3}	37%
B3:Kirch./membrane	T=30.6±3 D=(2.8±0.1).10^{-3}	-
Tension level 2		
B1:Membrane	T=170±22	91%
B2:Kirchhoff	D=(5.5±0.6).10^{-3}	64%
B3:Kirch./membrane	T=62±10 D=(2.8 ± 0.3).10^{-3}	-

Table 4.6: Overview of results obtained by IWD method and the Cross-validation method. The units of tension T are N/m and the units of the plate bending stiffness D are kgm^2/s^2.

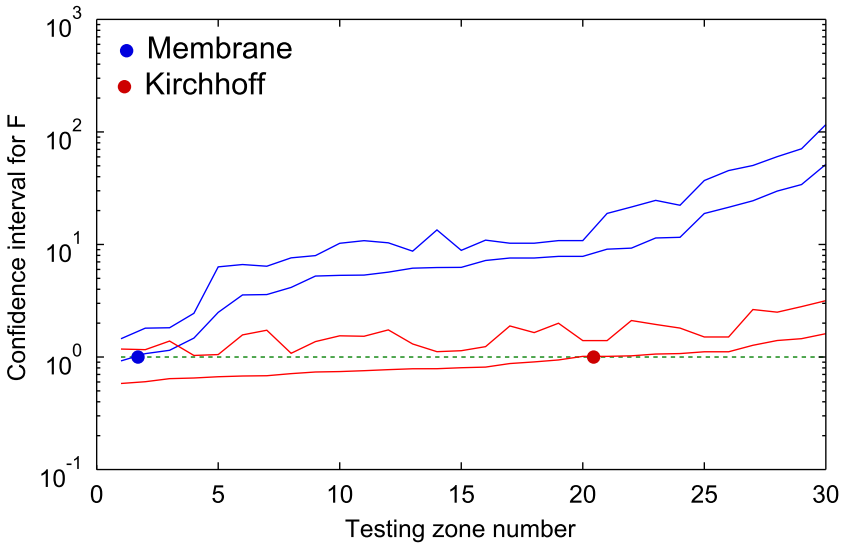

Figure 4.12: Tension level 1: Confidence interval of F statistics applied on validation data set for Membrane and Kirchhoff models. The reference model is supposed to be the Kirch./membrane model.

surprising fact is that the membrane model which seems to be a natural choice ended up as the last choice behind the Kirchhoff model. This means that although the rigidity of the paper may seem negligible, it must be considered at higher frequencies.

The parameters of the identified Kirch./membrane model are difficult to be verified from other independent methods. Concerning the rigidity of the paper, if we consider the paper equal to very thin isotropic plate with Young modulus close to a wood (1-10GPa) we get the static estimate of ranging from 0.73.10^{-3}kg.m^2/s^2 to 7.3.10^{-3}kg.m^2/s^2 as shown in Fig.4.14. The estimate of the static membrane tension T is quite tricky. Although we know approximately the total force applied by the deformed springs, we do not know the real force at the points where

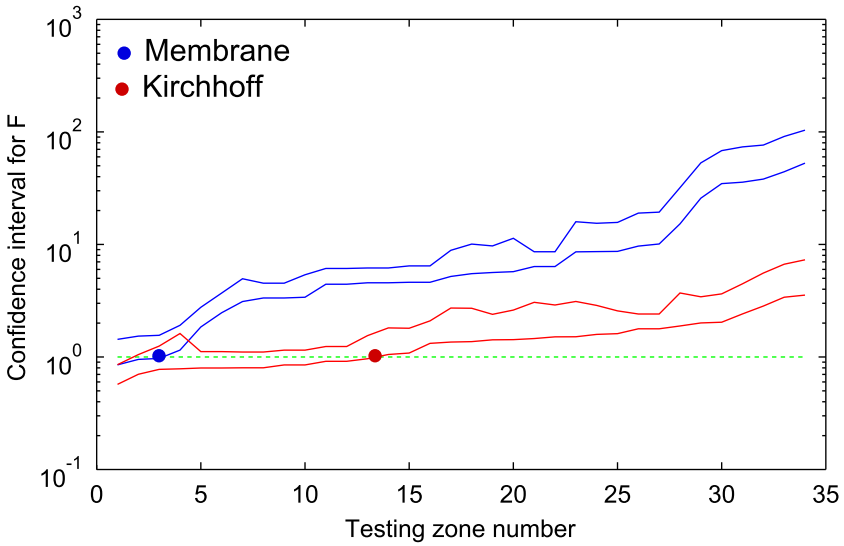

Figure 4.13: Tension level 2: Confidence interval of F statistics applied on validation data set for Membrane and Kirchhoff models. The reference model is supposed to be the Kirch./membrane model.

the strings are attached to the membrane. This force is surely diminished by the passage of the string through the right angle at the perimeter of the cylinder[1]. In Fig.4.14, there is only the estimate of the static tension considering that there is no friction at the perimeter of the cylinder. This estimate is indeed superior to the values obtained by the inverse methods. Although, both static estimates cannot verify directly the results obtained by the inverse methods, they are not in the contradiction to the obtained results and show the utility of the inverse methods.

It should be noted that if we used the ”natural” choice - membrane model, its parameters would be false. For example, the IWC method predicts the tension in the first case T=190N/m while the maximum tension from the static estimates is 78N/m. A wrong model gives wrong physical parameters.

[1]This could be overcome if we knew the friction coefficient, but its determination is beyond the scope of this thesis.

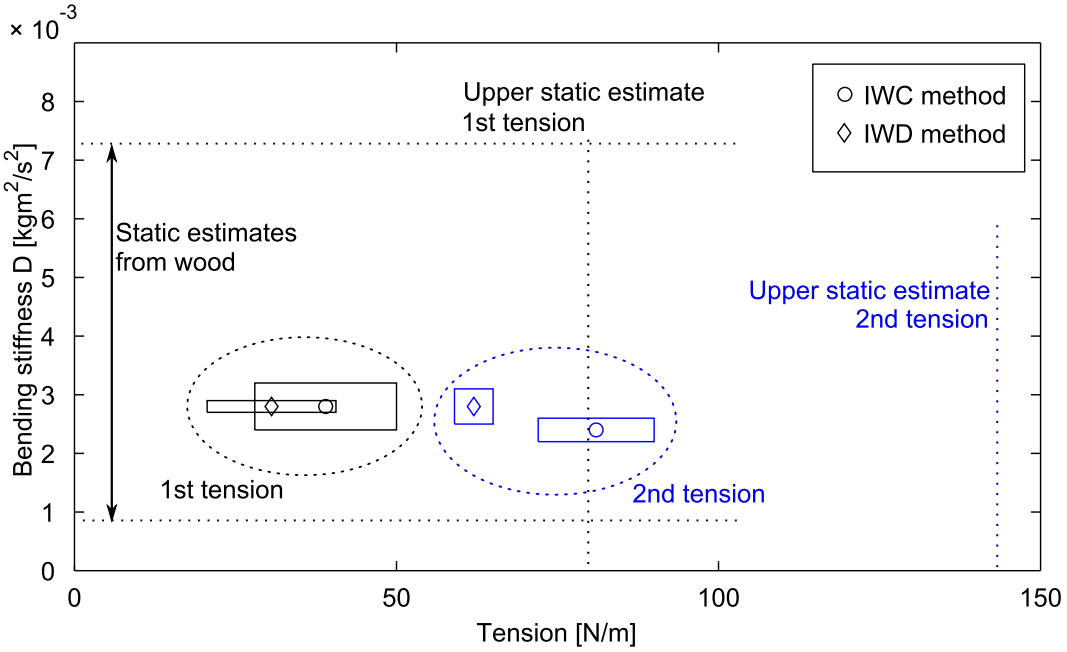

Figure 4.14: Overview of the optimal results for the Kirchhoff/membrane model obtained by two inverse methods. Static estimates of the "plate rigidity" of the paper and the upper estimate of the membrane tension are also shown.

4.3 Question of orthotropy

In this study case, the question of orthotropy is treated. The statement of the problem is as follows: If we have some unknown plate-like structure with known axes of symmetry, how can we determine if the orthotropic model is needed for its description? The situation is illustrated on three different examples: Cedar wooden back-board plate of an acoustic guitar, aluminium 2mm plate (already mentioned in Section 3.2.1 and 3.3) and Epoxy glass composite plate[2]. All of these three plates are described in Appendix A. From the common knowledge, we would naturally consider the wooden plate as orthotropic and the aluminium plate as isotropic, but how is the case of the composite plate? It is surely made of anisotropic layers of fibres so the mechanical behaviour is likely to be anisotropic as well. However, manufacturers try to put different layers in such a way that the mechanical properties are homogeneous and isotropic. So the question we could pose is: Is such a plate isotropic *enough* that the isotropic equation of motion is chosen by the model selection criteria?

In this section we consider only two competing candidate models: B2-isotropic Kirchhoff plate and B6-orthotropic Kirchhoff plate.

4.3.1 Using information criteria for model selection

Fifteen vibration fields were used for the identification of the Aluminium plate, 24 for the Guitar back-board plate and 25 for the Epoxy-glass composite plate. In Fig.4.15, we can see a representative example of a cartography of IWC functions in the k-space for the three considered plates. According to this figure, it is evident that the Guitar back-board plate has an anisotropic behaviour (Fig.4.15 right). However, the other two cartographies are inconclusive. Both aluminium and epoxy-glass seem fairly isotropic. Further analysis, however, shows that while the aluminium plate is isotropic according to the information criteria AIC and BIC (see Tab.4.7), the epoxy-glass composite is definitely not. The factor ΔAIC=16.1 shows that the isotropic model is far less adapted for this composite plate (see Tab.3.1 for the rule of thumb concerning the values of ΔAIC). This result looks surprising because the isotropic model does not seem too bad when we look at the cartography in Fig.4.15 middle. To understand why information criteria exclude the isotropic model, we must take into account that these criteria do not look at the goodness of fit of models in an absolute value. They merely compare this fit to the fit obtained by other models. In this case, the isotropic model is not bad in the sense of the absolute value but it is definitely *not the best model* [3].

[2]This composite panel was made by CETIM under the project AMORTI which included CETIM, LAUM, LRCCP, GeM, OPERO and Région des Pays de la Loire.

[3]Of course, the best model is meant in the sense of choice between the two candidate models - isotropic and orthotropic Kirchhoff model.

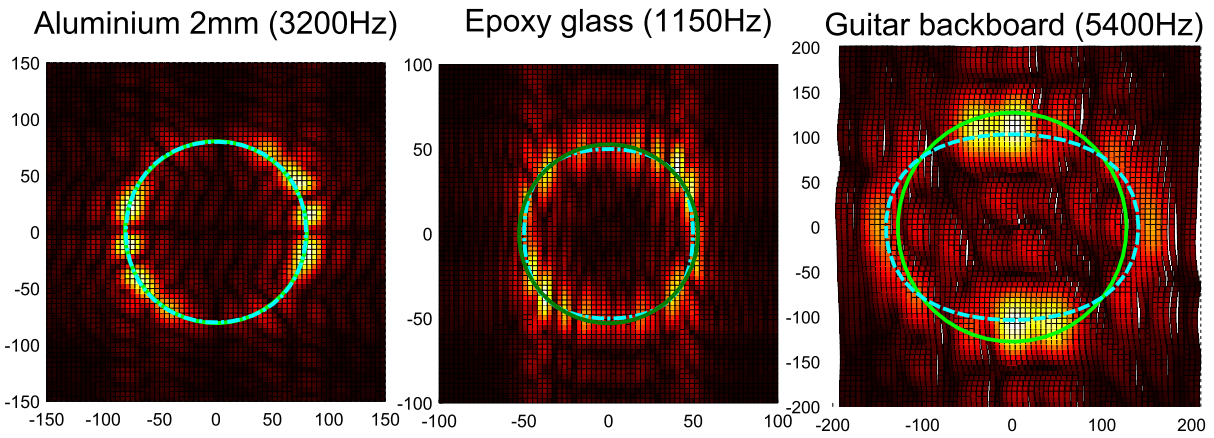

Figure 4.15: IWC cartography for the three vibration fields taken from the measurement of three different plates. The green line corresponds to the isotropic model fit, the cyan dash-dot line shows the orthotropic fit.

	Opt.param.	ΔAIC	ΔBIC
Aluminium 2mm			
B2:Kirchhoff	D=53±0.2	0	0
B6:Kirch. orth.	D_1=55.3±2 D_{24}=95±8 D_3=55±2	2.3	8.2
Epoxy-glass			
B2:Kirchhoff	D=7.2±0.3	16.1	9.2
B6:Kirch. orth.	D_1=9.2±0.3 D_{24}=7.5±2.4 D_3=7.7±1.2	0	0
Guitar back-side			
B2:Kirchhoff	D/ρ_S=4.49±0.37	35	30
B6:Kirch. orth.	D_1/ρ_S=3.02±0.37 D_{24}/ρ_S=7.85±2.8 D_3/ρ_S=10.4±2.2	0	0

Table 4.7: Overview of the results obtained by the IWC method and the information criteria. The units of the plate bending stiffness D are kgm^2/s^2.

4.3.2 Using cross-validation for model selection

The same vibration shapes were used fot the IWD analysis and the cross-validation scheme. There were 15 training and 30 zones for the aluminium plate, 24 training and testing zones for the Guitar back-board plate, 25 training and 100 testing zones for the epoxy-glass composite. We can see the resulting optimal parameters obtained by the IWD method in Tab.4.8. The test Fischer statistics F is shown in Fig.4.16 for the three plates. The B6 model (Kirchhoff orthotropic) was considered as reference for the F-test because it had a lesser fit residuals than

the B2 model (Kirchhoff isotropic). The testing statistics is then $F = s_1^2/s_2^2$ where s^2 are the estimators of the variances corresponding to the fit of the vibration shape in the testing zones. Index 1 corresponds to the Kirchhoff isotropic model and index 2 corresponds to the Kirchhoff orthotropic model. We test hypothesis F=1 which means that a particular validation vibration shape was fitted with statistically equal precision. We can see that while this hypothesis can never be rejected in the case of the aluminium plate, it is always rejected for the guitar back-board and epoxy-glass plates. This bring us to the same conclusion that the information criteria in the preceding section: epoxy-glass plate is not fitted sufficiently well by the isotropic model. It is therefore statistically less adapted than the orthotropic model.

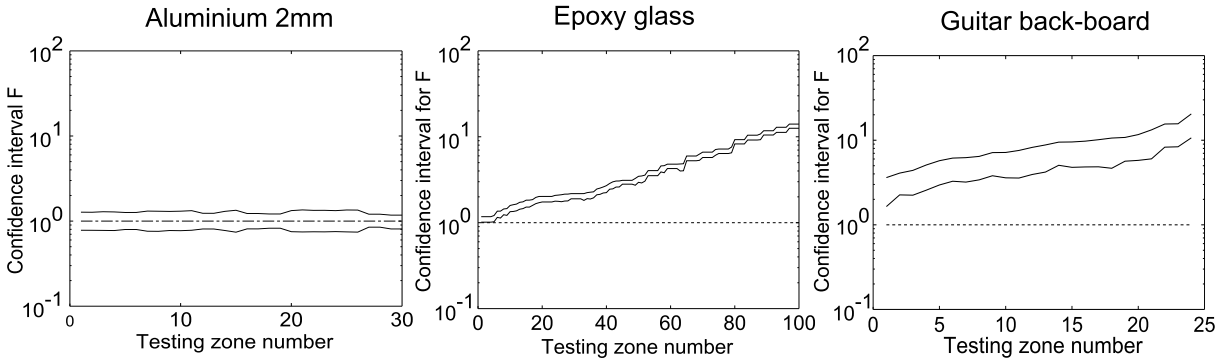

Figure 4.16: Confidence interval for F statistics comparing the Kirchhoff isotropic and orthotropic models.

	Opt.param.	Patch misfit
Aluminium 2mm		
B2:Kirchhoff	D=51±0.2	0%
B6:Kirch. orth.	D_1=51.1±3 D_{24}=100.9±12 D_3=51.2±3	-
Epoxy-glass		
B2:Kirchhoff	D=7.7±0.8	100%
B6:Kirch. orth.	D_1=9.09±1 D_{24}=9.7±1.2 D_3=8.9±1.5	-
Guitar back-board		
B2:Kirchhoff	D/ρ_S=3.48±0.14	100%
B6:Kirch. orth.	D_1/ρ_S=2.42±0.04 D_{24}/ρ_S=5.36±0.35 D_3/ρ_S=9.51±0.24	-

Table 4.8: Overview of the results obtained by the IWD method and the cross-validation. The units of the plate bending stiffness D are kgm^2/s^2.

4.3.3 Conclusions

In this case study, we have seen how both model selection tools can be employed to determine whether an unknown structure is orthotropic or not. We have seen especially the case of the epoxy-glass composite which is an example of unknown structure. It might be isotropic as well as anisotropic. Everything depends on the fabrication process which is often unpredictable. In this particular case of the composite plate, we have seen that although the dispersion curve represented by the IWC cartography in Fig.4.15 middle seems rather isotropic, ortotropic model is much more adapted as shown by both model selection tools.

Otherwise, we have seen that the aluminium plate was confirmed as being isotropic and the Guitar back-board confirmed as orthotropic.

4.4 Double-face thick composite plate

A double-face composite panel is constituted of two steel plates joined together by a solidified tissue. The geometry of this core is quite complicated. It can be seen in detail in Fig.4.17 right. The steel plates and the core are glued together. The dimensions of the plate were $150 \times 90 \times 5$ cm. The thickness of the steel faces was 0.8mm. Its density was supposed 7850kg/m^3. The average density of the core was estimated to 150kg/m^3. The surface density of the composite plate was 12.9kg/m^2. The plate was suspended as shown in Fig.4.17 left and it was excited by a shaker at the lower part of the plate. Excitation was a pure sine signal. The response was measured by a scanning laser vibrometer and an accelerometer which served for the phase reference signal. There were 17 excitation frequencies from 200 to 1000Hz.

Figure 4.17: Double-faced thick composite panel represents a structure with complex behaviour at higher frequencies.

Unlike the other experimental examples mentioned in this work, this plate is considerably thick. Its vibrational behaviour is more complicated and probably there are more than one variable needed to describe the vibration of the plate. Especially, we can imagine that the two steel faces do not necessarily vibrate in phase with each other as it is the case for thin plates. However, in the low-frequency domain there may exist some thin-plate approximation. Indeed, the complicated behaviour at higher frequencies can be seen on the dispersion curve obtained by IWC in Fig.4.18. According to this figure there seem to be a multitude of different wave-numbers for frequencies higher than 550Hz. This phenomenon can also be observed on the map of the IWC function over the k-space in Fig.4.19. At 300Hz, we can see clearly maxima distributed along a circle, however, at 600Hz this circle disappears and there are multiple local minima inside the circle. These minima correspond to the waves with longer wavelength.

This change in behaviour around 550Hz makes us believe that thin plate approximation reaches its limit around this frequency. For higher frequencies, it seems that the two steel faces

vibrate more independently of each other and there may be a multitude of modes of vibration possible. This hypothesis was truly shown when a measurement was taken at *both* faces of the plate.

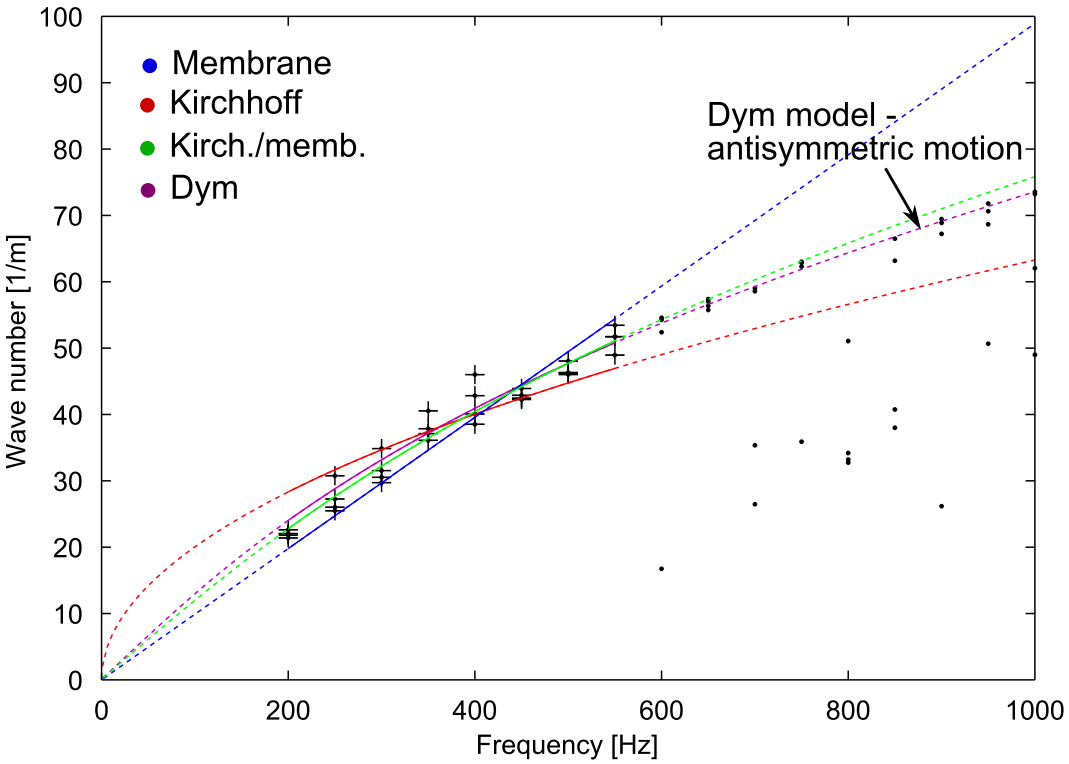

Figure 4.18: Dispersion curves obtained by IWC method. Cross points show which data were used for the inversion.

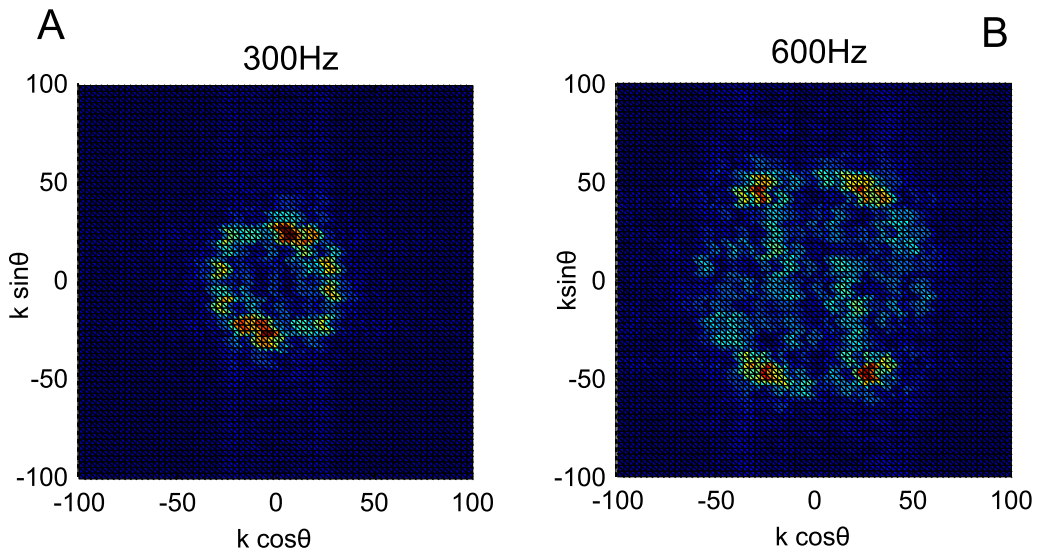

Figure 4.19: Cartography of an IWC as a function of the wave vector of the correlating wave. Example corresponds to the displacement field measured at 300Hz and 600Hz.

Measurement of both faces were done for six frequencies. At first, one face was measured and the position of the measurement points was noted. Then, the laser vibrometer was placed on the other side of the plate and the set-up was done in a way that the measurement points were approximately the same. This procedure is quite difficult to be done precisely and there are numerous possible errors. However, in Fig.4.21 we can compare the two measured vibration fields. It can be seen that until 500Hz, there are similar patterns in both measurements and there is important correlation between the two fields. However, from 650Hz, the correlation between both fields drops quickly and we are witnessing growing independence of these fields. This means that the vibration at higher frequencies than 600Hz cannot be described by means of a unique variable describing the transverse displacement of one face. This conclusion confirms the hypothesis of multiple mode of vibration present in higher frequencies. This hypothesis can also be confirmed in Fig.4.20 where the IWC is shown as a function of frequency and wave number. There is an abrupt change in this cartography between 600 and 700Hz which roughly corresponds to one of the dispersion curves associated with symmetric motion of the Dym model (see Appendix D). However, the measurement is not good enough to make further conclusions.

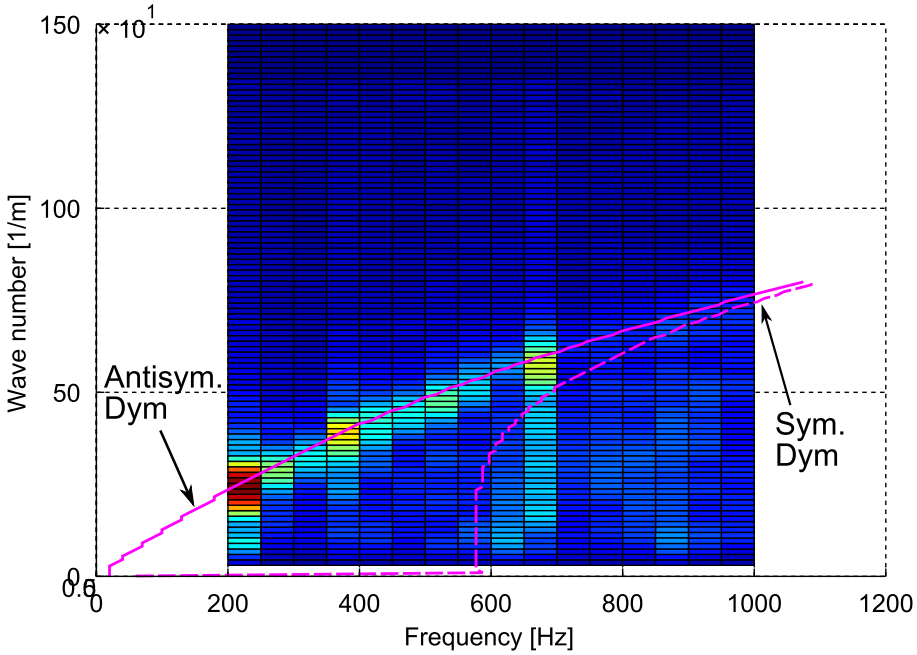

Figure 4.20: Cartography of an mean value of IWC as a function of the wave vector and frequency. In purple we see the dispersion curves obtained by Dym model.

4.4.1 Using AIC and BIC for model selection

In the preceding section, we have seen the limit frequency of a ”thin plate” approximation of our panel. In the following analysis only the measurements up to 600Hz are considered.

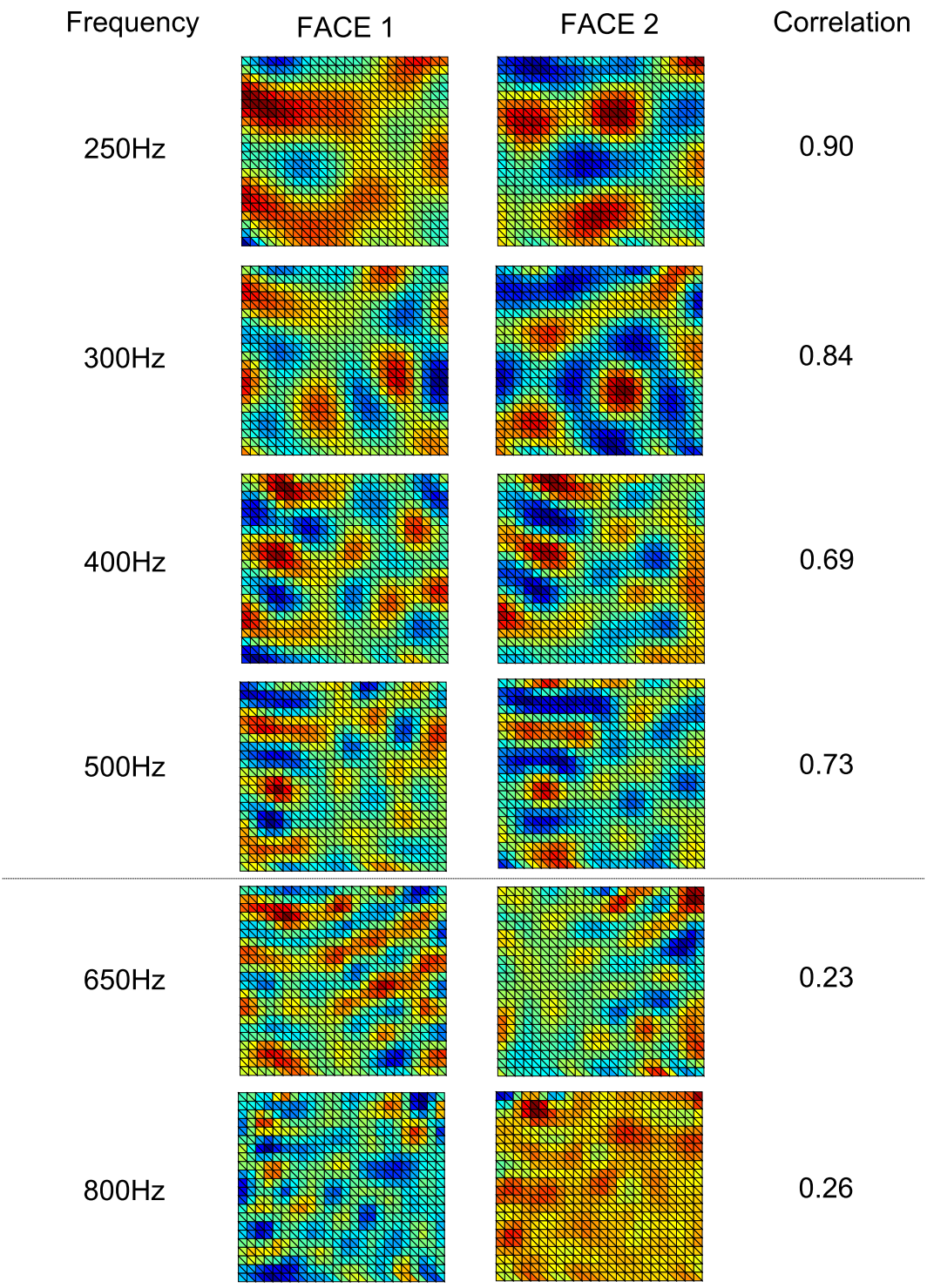

Figure 4.21: Cartography of an IWC as a function of the wave vector of the correlating wave. Example corresponds to the displacement field measured at 300Hz and 600Hz.

Four isotropic models are considered for models selection: B1-Membrane, B2-Kirchhoff, B3-Kirch./membrane and B5-Dym sandwich. The Dym sandwich model is considered only in its antisymmetric form given by Eq.D.8. Its symmetric solution is not taken into account in

the inverse problem. However, the prediction of the anti-symmetric dispersion curve is shown in Fig.4.18. This prediction is obtained using Eq.D.7 and the inversion results from the anti-symmetric dispersion curve. The resulting fit of the dispersion curve obtained by IWC method are shown in Fig.4.18. The parameters of the best models are show in Tab.4.9. Both AIC and BIC criteria show that the mixed Kirch./membrane model is the best model. However, the Dym sandwich model is quite close behind. The ΔAIC value for a Dym model is 2.4 which means that this model has a substantial level of confidence with respect to the other candidate models. Its drawback is that it contains three parameters while the Kirch./membrane model contains only two. It can be seen from the results in Tab.4.9 that the value of the Poisson ratio [4] of the core is badly determined. The inversion values of the Young modulus of the sandwich faces yield 100GPa which is inconsistent with values for steel (which is around 200GPa). This is a sign that the description by the Dym model is good enough from the performance point of view but the model parameters do not represent physical quantities.

Model	Ident.param.	ΔAIC	ΔBIC
Membrane (B1)	T=52069±1735	25.6	24.5
Kirchhoff (B2)	D=31.9±3	40.6	39.4
Kirch./memb. (B3)	T=34700±750 D=9.4±0.3	0	0
Dym (B6)	E_f=(100.2±16)GPa E_c=(2.08±0.4)MPa μ_c=0.04±0.24	2.4	3.5

Table 4.9: Optimal parameters for the three considered models using the IWC method.

4.4.2 Using Cross-validation for model selection

The IWD method was applied with a cross-validation technique. There were eight vibration fields corresponding to eight frequencies and on each field, there were two training zones and two testing zones. In total, there were 16 training and 16 testing zones. The four models described in the preceding section were identified by IWD method on the training set of data. The resulting optimal parameters are shown in Tab.4.10. These parameters are different from the results obtained in Tab.4.9. This is normal because the objective error function is not the same in both cases, so the ”wrong” models are adjusted to measurement in non-equal way. Moreover, if the model is correct (full representation of reality), then the optimal parameters obtained by both method should be the same. It seems that the Kirch./membrane model is not far from the reality because both methods predict similar optimal values.

The validation of models was done on 16 testing zones and the technique described in Section 3.3 was used. In Fig.4.22, we can see confidence intervals for the F-statistics defined by

[4] Actually the Poisson's ratio does not have a physical sense as in the case of isotropic materials, because the core of the sandwich is not a homogeneous isotropic material (see Fig.4.17).

Eq.3.24. This statistics shows how different are the fits of the four models in the considered testing zones. The reference model for the F-statistics is the Dym model which gives the best fit on the training data. As we can see from Fig.4.22 that the Kirch./membrane model is statistically equivalent to the Dym model on all the testing zones. Other two models are less performant: there are 4 testing zones fitted equally (with respect to the Dym model) by the Kirchhoff model (25%) and 10 fitted equally by Membrane model (62.5%).

Model	Ident.param.
Membrane (B1)	T=47400±3770
Kirchhoff (B2)	D=54±11
Kirch./memb. (B3)	T=33455±204 D=12±0.5
Dym (B6)	E_f=(130±19)GPa E_c=(2.23±0.8)MPa μ_c=0.16±0.3

Table 4.10: Optimal parameters for the three considered models using the IWD method.

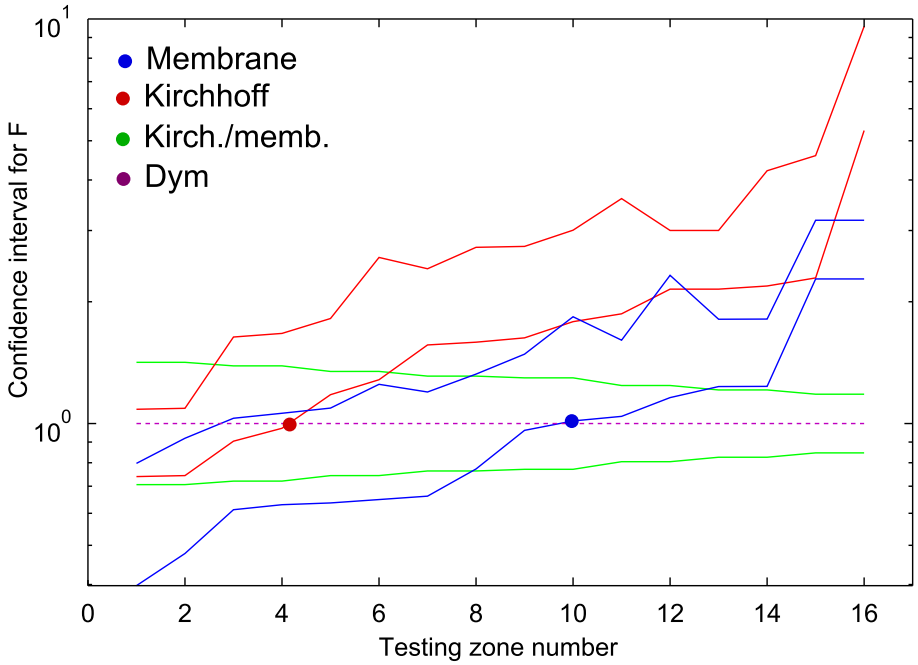

Figure 4.22: Confidence intervals of the F-statistics defined for the fit of the testing zones on the double plate measurements.

4.4.3 Conclusions

This thick composite plate was investigated in the frequency range 200-550Hz. Above this range it has been shown that the motion of the two faces becomes independent. There are probably different modes of vibration kinematics taking place simultaneously at higher frequencies

as is shown in Fig.4.19. However, the dispersion curves corresponding to these modes were not identified. Therefore, only the (anti-symmetric) bending vibration was considered. Four models (Membrane, Kirchhoff, Kirch./membrane and Dym) were investigated by IWC and IWD techniques. Model selection criteria associated with IWC showed the Kirch./membrane model as the most adapted with Dym model close behind. Similar conclusion was found using the IWD and a model selection criterion. Both Kirchhoff and Membrane models were substantially lacking behind. However, the Membrane model is better then the Kirchhoff model according to both model selection criteria.

5

Conclusion and perspectives

Conclusion In this thesis the possibility of identification of the equation of motion from experimental vibration response was studied. A so-called *model selection* approach was chosen. This general approach consists of a number of different mathematical techniques. It has been shown, however, that these techniques cannot be used blindly, but some preliminary hypothesis must be respected.

This work was divided into two big parts. The first part, Section 2, describes the inverse techniques which can be used for identification of parameters of some model (equation of motion). A special attention was given to two inverse techniques judged adapted for our purpose: IWC and IWD. The second part, Section 3, describes more in detail some model selection techniques and shown how they can be used together with the inverse techniques described earlier. It is shown that the crucial question is the mathematical nature of the estimators obtained from the measurement. By estimators we mean any numerical value obtained from the measurement and which can be deterministically calculated from a model. It was shown that these estimators are rarely statistically independent. Their dependence hampers the use of many model selection techniques as it is shown in Sections 3.2.4-3.2.6. However, it was shown that the estimators of the natural wavenumbers by the IWC method can be considered independent under some constraints. In this case, traditional methods AIC and BIC can be used for selection of models. The advantage of these model selection techniques is the simplicity and easy evaluation of the results. However, it was shown that it is more difficult or impossible to obtain independent estimators when using the IWD, FAT(RIFF) or asymptotic methods. Therefore, a special version of cross-validation technique was developed for the IWD inverse method to overcome this problem. Although the use of the cross-validation technique is less restrained than the other methods of model selection, its disadvantage is the need for large measurement samples. The problem with the cross-validation is how to evaluate its results. To overcome this, a test based on Fisher statistics was employed with the cross-validation technique.

The proposed methodology was employed on a number of experimental measurements. Three main problems were treated: the presence of axial force, the question of plate orthotropy and identification of complex composite structures.

Perspectives Even tough this thesis reaches its end, there are still open questions and possibly a new work can be done in the years to come.

The author believes that more inverse methods dealing with 2D vibration field are still to be discovered. Especially, there is a potential to use a Galerkin approach proposed in other scientific problems (see Section 1.3.2.5). Another new inverse problem would be to use the method of fundamental solutions (see Section 1.3.2.3) in its inverse sense (similar to IWD). Both of these new inverse problems could also have model selection post-processing.

The proposed methodology can be further applied in other physical problems. So far, the model selection criteria were used in statistics but their use in concrete physical (mechanical)

problems was limited. The author would like to point out several possible ways to exploit this mathematical tool. In the **fields of dynamics** there is a possibility to apply the model selection for a choice of models for composite plates. Especially, when a number of competing models is at hand. It would be probably necessary to measure the vibration field at both sides of the composite panels, especially if these panels are thick, as it was shown in Section 4.4. Another application would be in the experimentally-based model reduction techniques. These techniques (see for example Nowakowski [66]) are often based on direct calculations. But the inverse identification or validation of reduced models from experiments would also be possible. A modal-based inverse problem of determination of elasticity symmetry of processed polycristaline copper as shown by Seiner [71] might be further developed by adding the model selection techniques. A very interesting seems an application to the domain of porous materials. There exists a substantial number of models describing the acoustic behaviour of these materials. A review paper by Sagartzazu [80] mentions six different models, he also shows the comparison of these models with some measured quantities. A number of possible applications are in the domain of **material science**. This need is especially true for the physical phenomena which are described by a number of competing models. Let us consider, for example, the long-lasting question of metal plasticity. The plastic behaviour of metals is rather complicated and a very large number of analytical and empirical models including different phenomena like hardening, softening, cycle-loading, strain-rate, relaxation etc. were developed (see Chaboche [73]). Another problem consists of a choice of an appropriate model for a contact fatigue life prediction (Tallian [79] mentions 11 physical and empirical models). Also the problem of ultimate strength of materials is under question. There exist a number of criteria for composites (see Dharan [65]) and there are 12 criteria for brittle failure of rocks (see Lakirouhani [64]).

A

Measurements overview

A.1 General remarks

In this appendix there are some issues believed useful to describe the experimental conditions of measurements done in this research work. All the measurements were done with Polytec scanning laser vibrometer with mobile head. The experimental scheme was more or less changed in function of different structures measured but it follows the same connection logic as shown in Fig.A.1. Apart from the signal from the laser vibrometer there are also two reference signals from the force sensor and the accelerometer. The force sensor is located between the shaker head and the structure. The location of the accelerometer can be versatile. Most often it is advantageous to place it at the corners of the structure where the signal is maximal regardless the frequency of excitation [1]. The measurement was taken at a number of points (200-1000) inside the borders of the structure. Nevertheless, the excitation force was always outside of this zone in order to comply with the conditions imposed by the inverse methods used in this work.

The excitation signal was of three types:

- **Pure sine signal**. This excitation gives the best results, however, the measurement needs to be repeated for every frequency separately and therefore it takes a lot of manipulation when more excitation frequencies are to be measured.

- **White random noise.** This excitation permits to recover the vibration response at a very large number of frequencies at one time. Unlike the preceding excitation, this measurement can be automated but as more averages are needed, it takes a lot of time.

- **Pseudo-random noise.** Pseudo-random noise behaves similarly like the white noise, but its advantage is that it excited the structure not at *all* frequencies equally but only on the frequencies that are later used for the FFT transform. In this way less vibration energy

[1] Actually, the problem occurs when the reference signal is close to zero, because we use transfer function and in the transfer function the reference function is in the denominator. The reference signal can become zero for example on nodes of vibration for the accelerometer and on the modal frequencies for the force sensor.

is ”lost” on frequencies which are not present in the FFT decomposition. This excitation yields generally better coherence between the reference signal and the vibration signal measured by laser. The advantage of pseudo-random excitation is discussed by Jacobsen in [69].

If broadband excitation was used, broadband transfer functions were recovered. As the information present in these transfer functions is often redundant, we choose only several best vibration shapes. The judgement is based upon the coherence function. The shapes with highest coherence function are chosen.

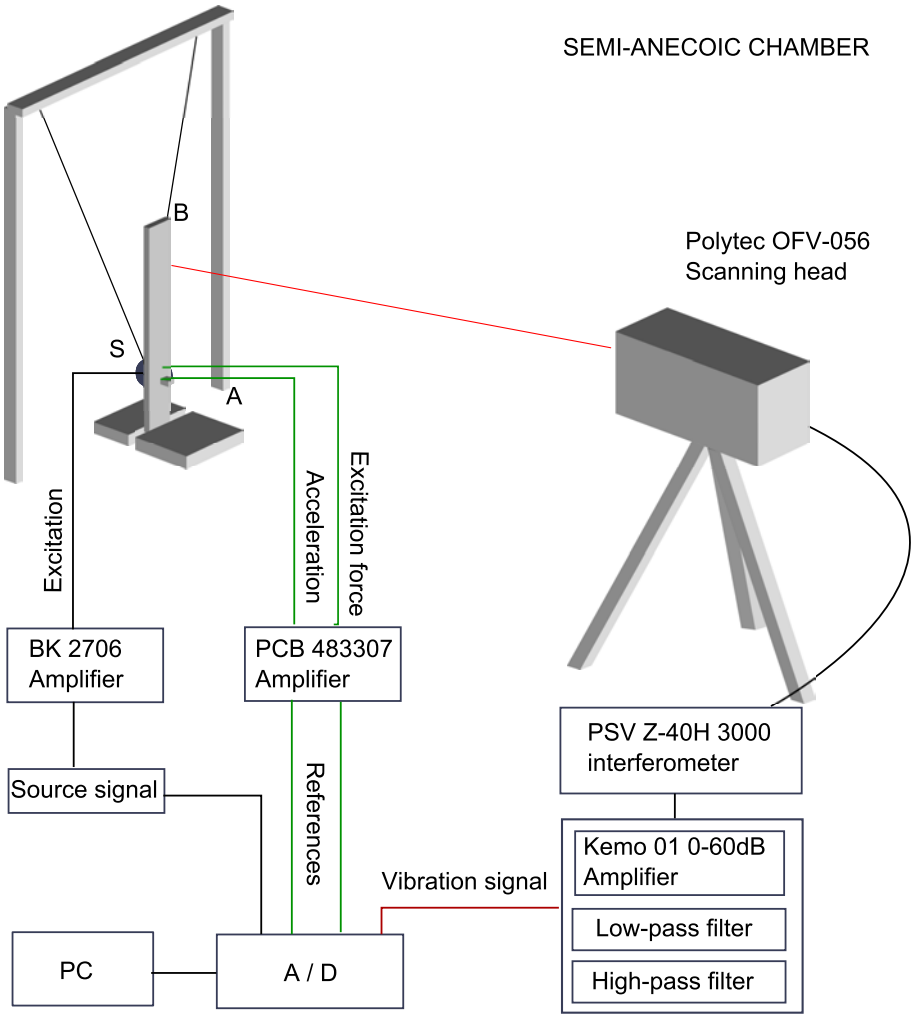

Figure A.1: Schematic signal routing of the measurement set-up.

Many different mountings of the beams, plates and membranes were used. In Fig.A.2 we see a measurement set-up for the aluminium 4mm plate. The boundary conditions are not of importance for the inverse methods used in this work, so different boundary conditions were used.

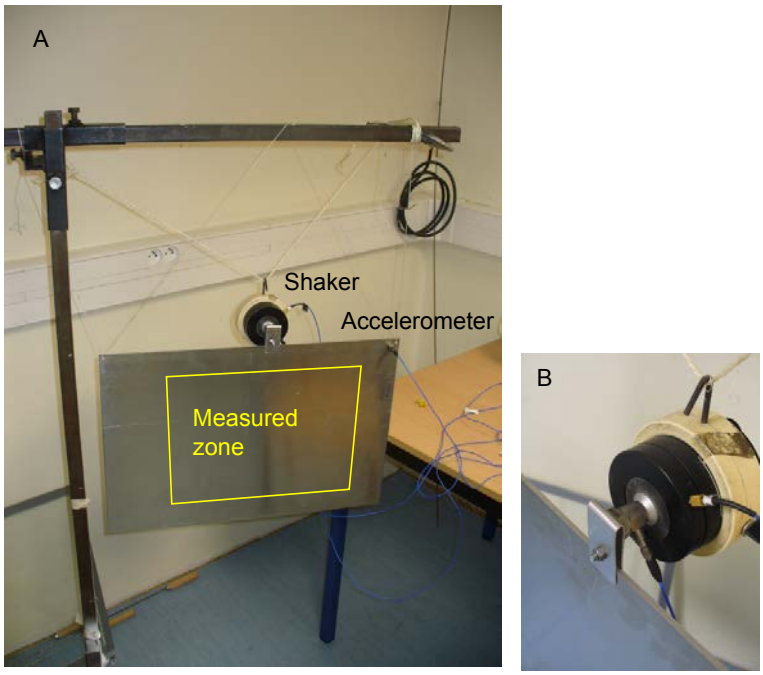

Figure A.2: An example of the measurement set-up for the aluminium 4mm plate. In detail we see a mounting of the excitation shaker.

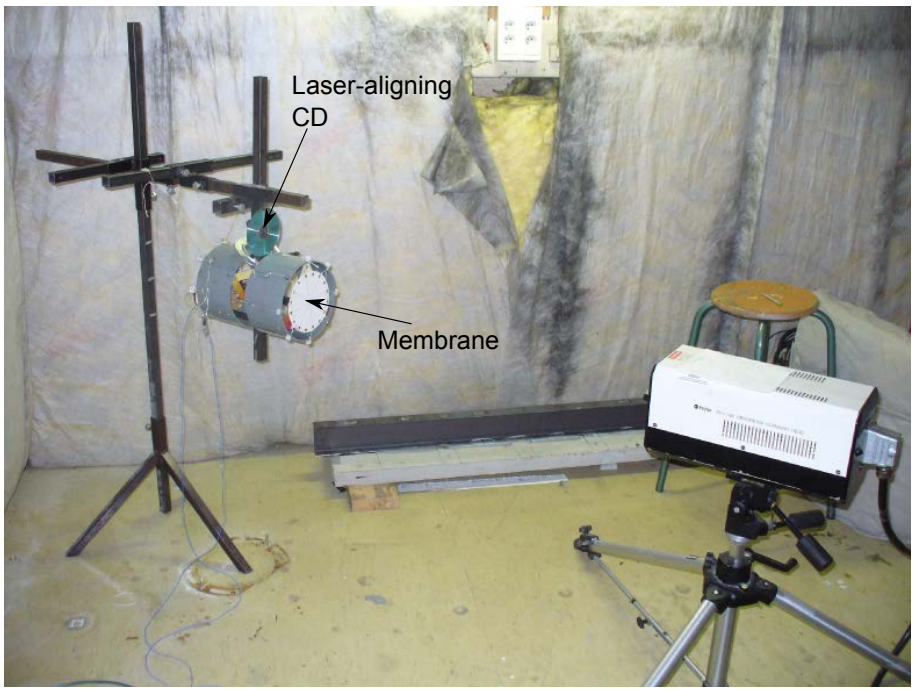

Figure A.3: Illustrative example of aligning the measurement plane to the coordinate system of the scanning laser vibrometer. Paper membrane measurement.

A simple method was used for aligning the coordinate system of the laser vibrometer to the coordinate system of the measured structure. The reason is that the internal system of Polytec assumes that all the measurement points are on a plane surface normal to the axis of the laser. With a help of a CD this alignment can be done five steps:

- Point the laser beam straight ahead (zero degrees in x and y-axes)
- Place the plate to suitable distance with the laser beam in the middle.
- Place the mirror CD onto the plate to reflect the laser spot.
- Rotate with the plate until the reflected and incident beams are common.
- Remove the reflective CD (if possible).

One illustrative example is shown in Fig.A.3. The difficulty of the presented approach is that we must be sure that the plane of the CD is *parallel* to the plane the measured structure. This is easy if the structure is solid and well-attached. Then the CD can be glued onto it. If the structure is more subtle this can be a bit tricky.

A.2 Aluminium 2mm plate

A rectangular plate made of aluminium-based alloy had dimensions 420×620 mm. Its nominal thickness was (2±0.05)mm. The surface density of the plate was 5.55kg/m^2. Vibration measurement was effected at 571 points defined over 300×300 mm domain. The reference signal was taken from the accelerometer situated in the corner of the plate. Boundary conditions were free except for one side of the plate whose one part was clamped. The excitation signal was pseudo-random in the bandwidth 0-3200Hz.

If a standard Young modulus E=70GPa is considered and μ=0.33, than we can we obtain the plate stiffness after Eq.2.7 D=(52±4)kg.m^2/s^2.

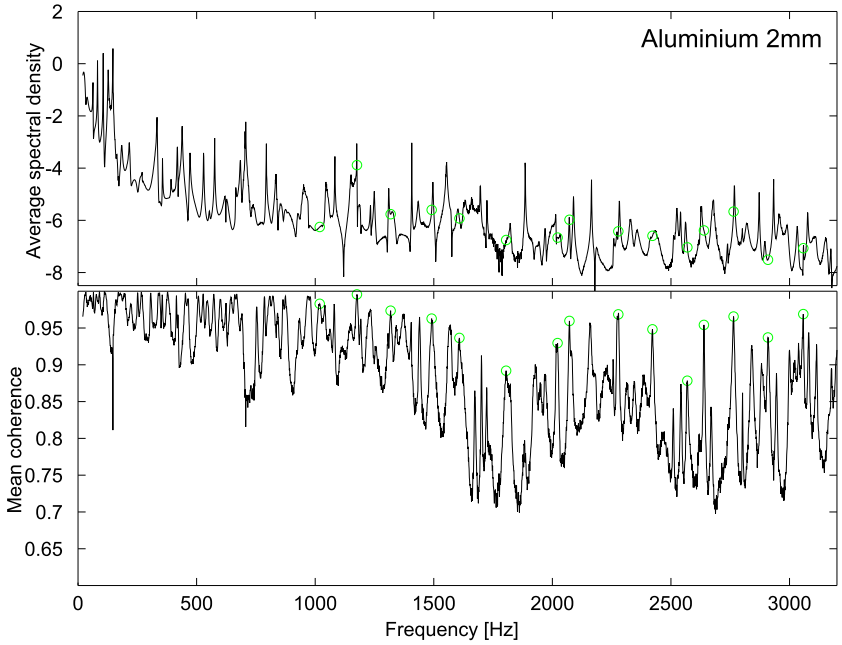

Figure A.4: Above: average spectral density of measured displacement. Below: Average coherence function as function of frequency. The green circles represent vibration shapes chosen for further analysis.

In total there were 3200 vibration shapes measured. From these fifteen shapes for frequencies from 1000 to 3200Hz were selected for the identification of equation of motion. These measurements had locally a maximum of coherence function as shown by green circles in Fig.A.4. These maximum do not correspond necessarily to the modal frequencies as it is shown in the above figure.

A.3 Acoustic guitar backboard

The measurement were effected on the backside of the acoustic guitar. The zone is situated between two stiffeners placed on the inner side of the guitar. The excitation is done by shaker placed on the front-side of the guitar as shown in Fig.A.5C.

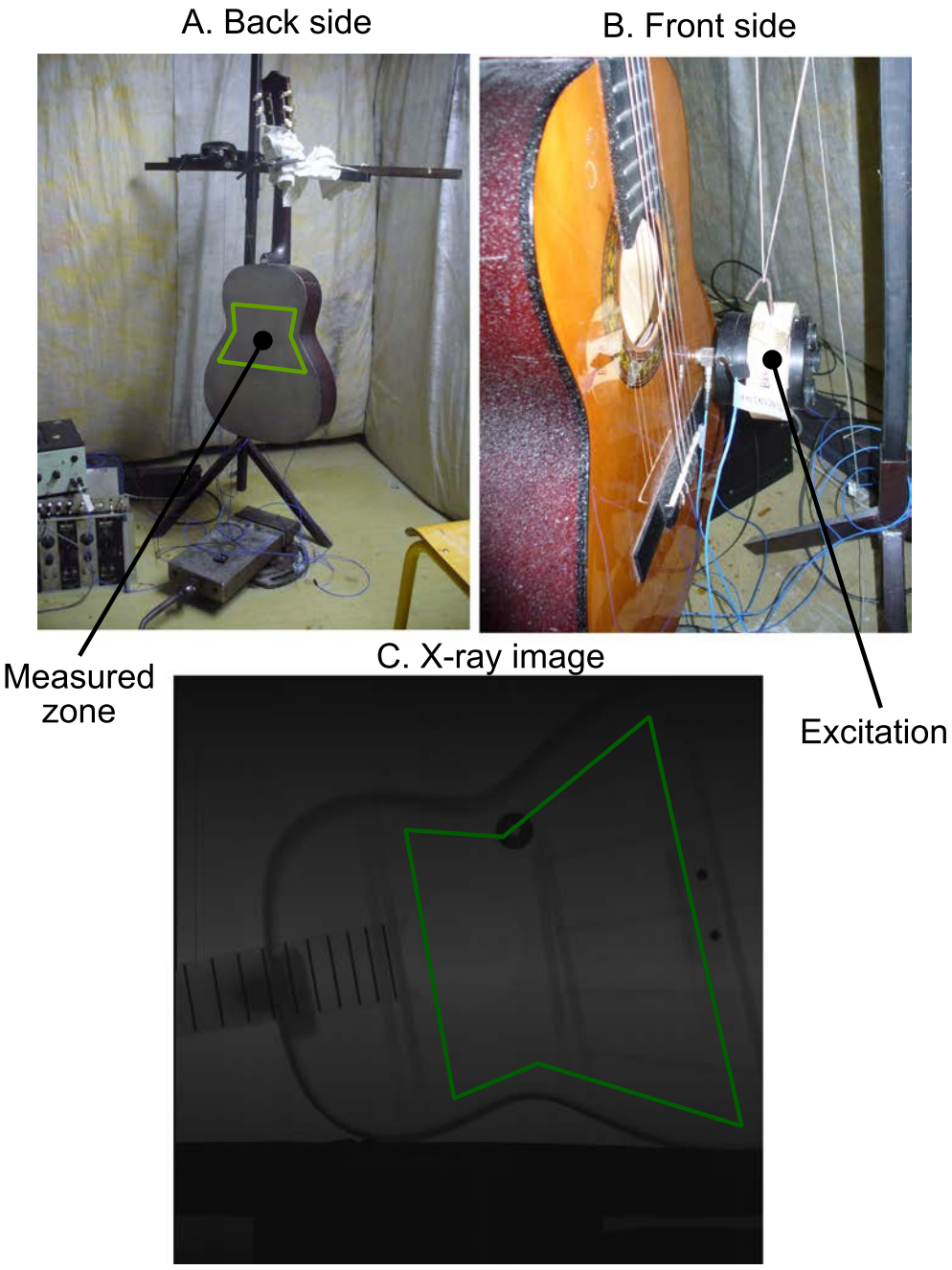

Figure A.5: A: Back-side of the guitar with the zone of measurement (green). B: Front-side of the acoustic guitar with the excitation shaker. C: X-ray image of the guitar, we can see the wooden stiffeners inside the guitar. The green measured zone is without transverse stiffeners.

Pseudo-random signal of 6400Hz bandwidth was used for excitation. Response was measured at 214 points by scanning laser vibrometer. The thickness and surface mass density are unknown. The direction of the fibers corresponds to the y-direction of the Cartesian coordinate system.

A.4 Epoxy-glass composite plate

Epoxy glass composite plate was measured at LAUM laboratory in LeMans (courtesy of F.Ablitzer). This panel was fabricated by CETIM as a part of the project AMORTI [72] which studied the damping of composite plates. This project was done in partnership between CETIM, LAUM, LRCCP, GeM, OPERP and Région Pays de la Loire. The panel of 0.88×0.3m was suspended at two ends. The excitation shaker was placed at the border of the plate. Excitation was sweep sinus signal from 200 to 2000Hz. The excitation response was measured at 10797 points by scanning laser vibrometer. These points were placed inside a rectangle of 0.85×0.28m dimensions. The reference signal for the transfer function was taken from the force sensor B&K 8001 mounted on the excitation impedance head. The surface mass density is 5.2kg/m^2.

A.5 Red cedar plate

A plate cut from red cedar wood (Fig.A.6) had dimensions 500×190×2mm. Its long dimensions was parallel to wood fibres (x-direction). Its surface density was 0.855kg/m^2. This wooden plate is used for manufacture of the soundboard of musical instruments like guitars. The particularity of this wood is its homogeneity and relatively low damping.

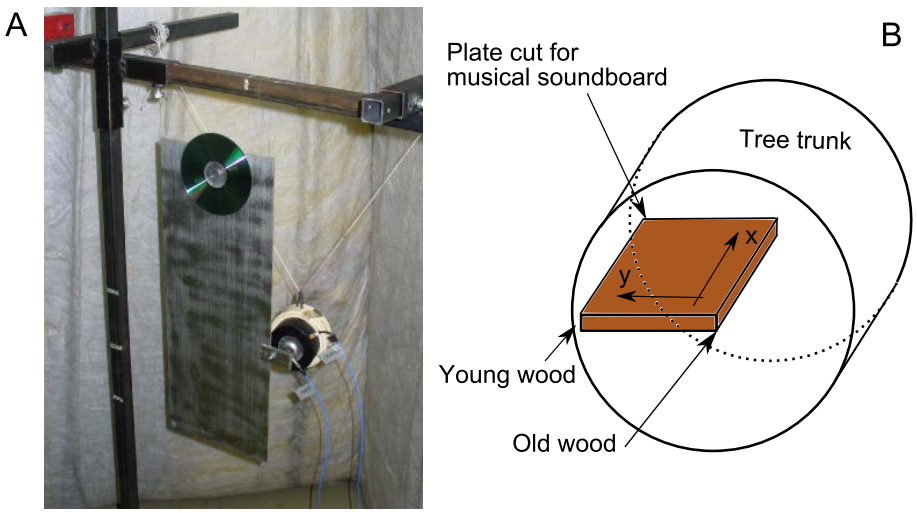

Figure A.6: A: Mounting of the red cedar plate during vibration measurement. B: Position of the wooden plate in a tree trunk.

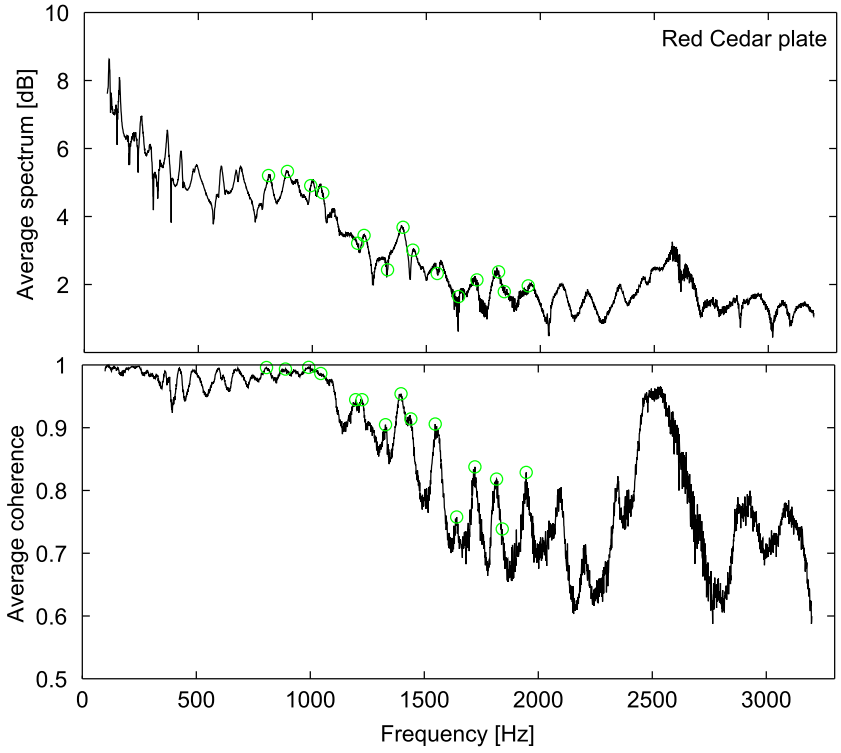

Figure A.7: Above: average spectral density of measured displacement. Below: Average coherence function as function of frequency. The green circles represent vibration shapes chosen for further analysis.

The vibration measurement was effected at 377 points. The driving force was measured and served as a reference for the transfer function. Excitation was a pseudo-random in the bandwidth 0-3200Hz. Fifteen vibration fields between 800 and 2000Hz were selected for model selection analysis. Chosen frequencies can be seen in Fig.A.7. The chosen vibration fields had locally the best coherence function (the best signal).

B

Three-point bending test

The traditional 3-point bending test were performed on numerous samples to verify the results obtained from dynamical inverse problem. For practical experimental reasons it was sometimes necessary to change the symmetrical geometry of the test to a non-symmetrical (see Fig.B.1. According to the theory of thin beams in bending the acceptance of the beam at the point of displacement measurement is

$$\begin{aligned} \frac{y}{F}|_{x=L_m} &= \frac{1}{EI}\left(1-\frac{L_f}{L}\right)\left(\frac{L_m^3}{6}+C_1 L_m\right) \quad \text{if} \quad L_f > L_m \\ &= \frac{1}{EI}\left(\frac{L_f L_m^2}{2}-\frac{L_f L_m^3}{6L}+C_3 L_m + C_4\right) \quad \text{if} \quad L_f < L_m \end{aligned} \tag{B.1}$$

where y is the displacement measured by micrometer, F is the force of mass, EI is the beam rigidity, L is the length of the beam,L_m is the position of the measurement, L_f is the position of the applied force, coefficienst C are defined as follows

$$\begin{aligned} C_1 &= \frac{L}{L-L_m}\left(\frac{L_m^2}{2}-\frac{L_m L}{3}-\frac{L_m^3}{6L}\right) \\ C_3 &= -\frac{L_m^3}{6L}-\frac{L_m L}{3} \\ C_4 &= \frac{L_m^3}{6} \end{aligned} \tag{B.2}$$

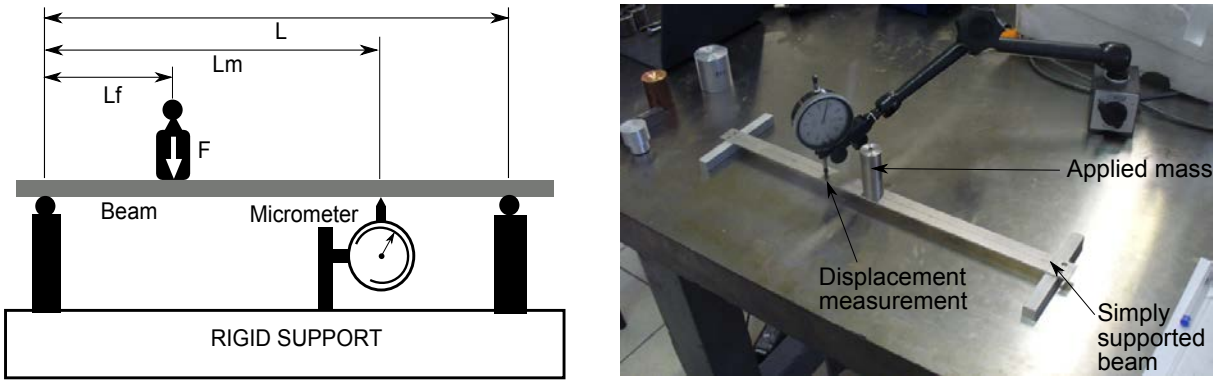

Figure B.1: Schematical setup for modified 3-point bending test on left and a realisation on right.

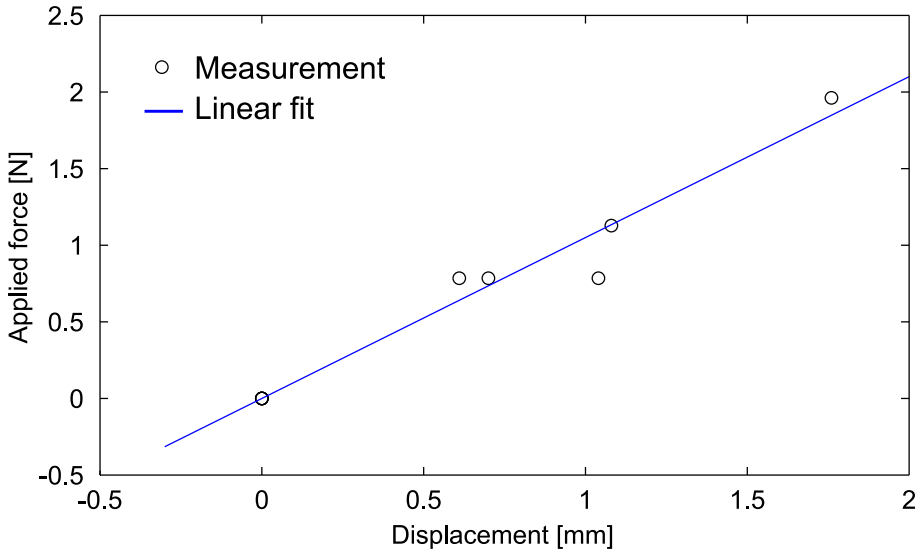

Figure B.2: Experimental setup for 3-point bending test. Micrometer was used for displacement measurement. On lower figure we can see typical force-displacement data set and the linear fit of the data.

C

Question of plate coupling with air

So far we neglected the influence of surrounding media upon the vibration of the plate. Mathematically, it means that the acoustic pressure p=f on RHS of the Eq.2.6 is equal to zero. This approach is true for most plate-like structures which are relatively heavy with respect to the mass of surrounding air. However, for some light membranes the level of acoustic presure might influence the vibration of the structure. To estimate the influence of the pressure p we do several assumptions.

- We consider the plate (or membrane) infinite
- We neglect all the external sources of acoustic pressure
- We consider the perfect anechoic conditions of the testing room with no reflections

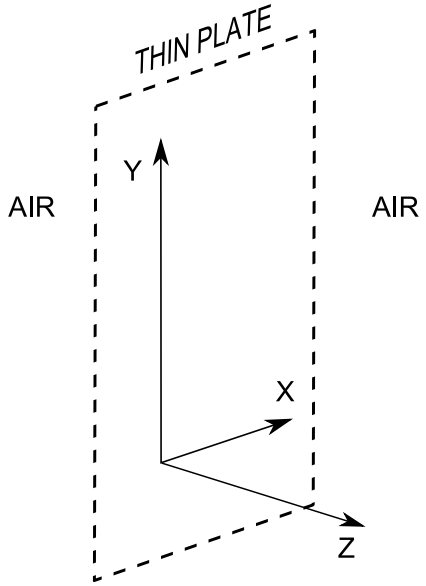

Figure C.1: Coordinate system of the thin plate coupled with surrounding air.

Under these assumptions it can be shown that the acoustic pressure is proportional to the displacement field of the plate corresponding to the plane wave with wave vector k_{plate}. The plate lies in the plane XY, its displacement $u(x, y)$ is normal to the plane positive in the positive z-direction, the air is the both sides of the plate (see Fig.C.1. According to Maxit [74]

$$p(x, y, z = 0) = \frac{i\omega^2 \rho_{air}}{2\pi \left(||k_{air}||^2 - ||k_{plate}||^2 \right)^{1/2}} u(x, y) \tag{C.1}$$

where k_{air} is the wave vector of the plane waves in the air and ρ_{air} is the density of the air. In the domain of our frequency range we have always $||k_{air}|| \ll ||k_{plate}||$ so we can simplify the Eq.C.1

$$p(x, y, z = 0+) \approx \frac{\omega^2 \rho_{air}}{2\pi ||k_{plate}||} u(x, y) \tag{C.2}$$

The wave vector k_{plate} can be approximately estimated from the measured vibrational field. Because of the symmetry of the problem we have $p(x, y, z = 0-) = -p(x, y, z = 0+)$ and the difference between the pressure on the two sides of the plate is $\Delta p(x, y) = p(x, y, z = 0+) - p(x, y, z = 0-) = 2p(x, y, z = 0+)$. To see the influence of the air upon the equation of motion let's consider the equation of the Kirchhoff plate

$$D\Delta^2 u - \omega^2 \rho_S u = \Delta p = \omega^2 \frac{\rho_{air}}{2\pi ||k_{plate}||} u \tag{C.3}$$

The pressure term on th RHS can be seen as mass added to the surface mass density of the plate ρ_S

$$D\Delta^2 u - \omega^2 (\rho_S + \frac{\rho_{air}}{2\pi ||k_{plate}||}) u = 0 \tag{C.4}$$

If we define following quantities $plate\ mass = \rho_S$ and $air\ mass = \rho_{air}/(2\pi ||k_{plate}||)$ we can plot the ratio of these two mass components (air mass)/(plate mass) on Fig.C.2. It can be seen that the influence of the air coupling is not important for metallic plates but it can become important for lightweight structures at low frequencies.

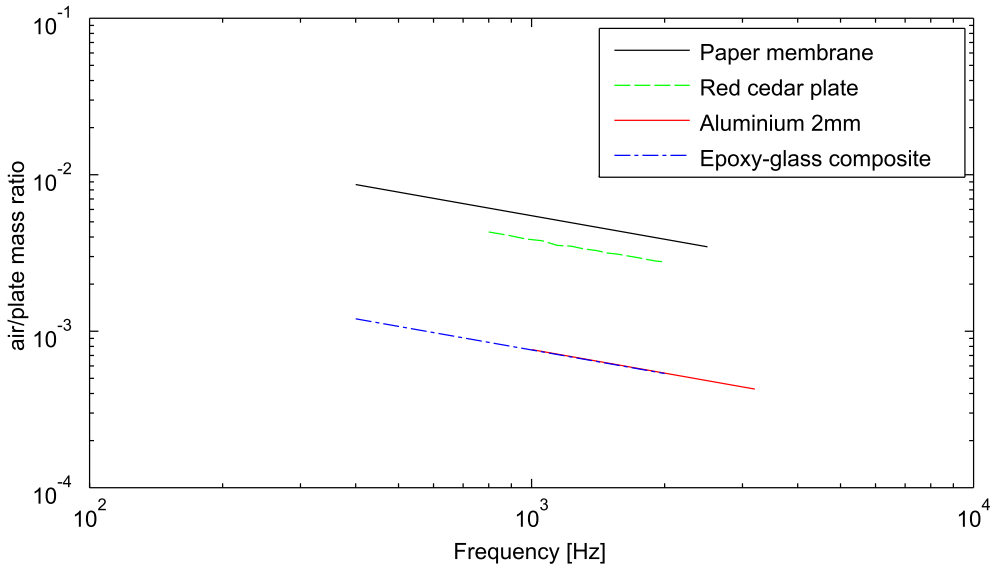

Figure C.2: Ratio of the air and plate mass in function of the frequency for various tested plates and membranes. We can see, that the most importance of the air is at the low frequencies for light structures like paper membrane.

D

Dym sandwich model

Under some simplifying hypothesis described in [68] the kinematics of the section of the Dym sandwich plate can be entirely described by five independent variables u_1, u_2, w_1, w_2 and g. Variables $u_{1,2}$ describe the in-plane displacement of the skins and variables $w_{1,2}$ describe the transverse displacements of the skins. Then the transverse and in-plane displacements in the core can be expressed as

$$u_c(x,z) = \frac{u_1(x)+u_2(x)}{2} + g(x) \tag{D.1}$$

$$w_c(x,z) = \frac{w_1(x)+w_2(x)}{2} + \frac{z}{h}(w_2(x)-w_1(x)) \tag{D.2}$$

As it is shown in [68], if we define the symmetric displacements as

$$\overline{u} = \frac{u_1+u_2}{2} \tag{D.3}$$

$$\overline{w} = \frac{w_2-w_1}{2} \tag{D.4}$$

and the anti-symmetric displacements as

$$\tilde{u} = \frac{u_2-u_1}{2} \tag{D.5}$$

$$\tilde{w} = \frac{w_1+w_2}{2} \tag{D.6}$$

then the differential equation of the Dym plate can be uncoupled into two systems of independent equations:

$$\left[D_{symm}\right]\begin{pmatrix}\overline{u}\\ \overline{w}\\ g\end{pmatrix}=\begin{pmatrix}0\\0\\0\end{pmatrix} \tag{D.7}$$

$$\left[D_{anti}\right]\begin{pmatrix}\tilde{u}\\ \tilde{w}\end{pmatrix}=\begin{pmatrix}0\\0\end{pmatrix} \tag{D.8}$$

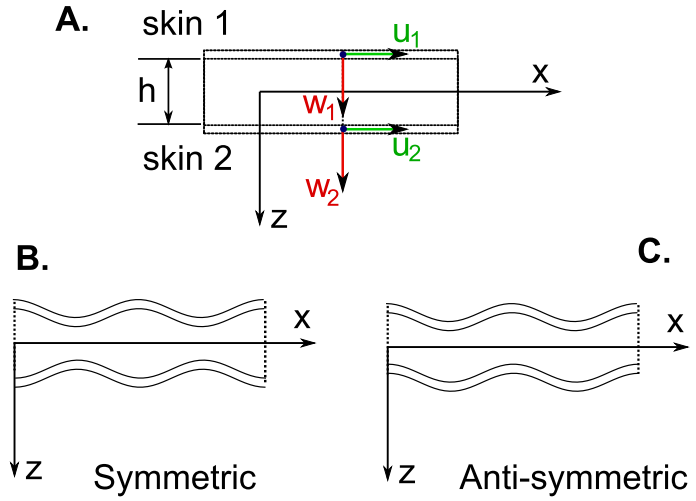

Figure D.1: Model of symmetric sandwich proposed by Dym and Lang.

The matrix for anti-symmetric motion (classic bending) is a two-by-two symmetric matrix constructed of a partial differential operator

$$D_{anti}^{(11)} = 2\overline{C}_1\frac{\partial^2}{\partial x^2}-\frac{4}{h}\kappa^2 G-2\tilde{m}^*\frac{\partial^2}{\partial t^2} \tag{D.9}$$

$$D_{anti}^{(12)} = -2\tilde{F}_1\frac{\partial^3}{\partial x^3}+\tilde{m}^* h\frac{\partial^3}{\partial x\partial t^2} \tag{D.10}$$

$$D_{anti}^{(22)} = 2\tilde{D}_1\frac{\partial^4}{\partial x^4}+2\tilde{m}\frac{\partial^2}{\partial t^2}-\frac{1}{2}h^2\tilde{m}^*\frac{\partial^4}{\partial x^2\partial t^2} \tag{D.11}$$

the constants used above are defined by following relations

$$\tilde{C}_1 = C_1+\tfrac{1}{6}C \qquad C=(\lambda+2G)h$$
$$\tilde{F}_1 = F_1+\tfrac{1}{12}Ch \qquad \tilde{D}_1 = D_1+\tfrac{1}{24}Ch^2$$
$$\tilde{m} = \rho_1 t_1+\tfrac{1}{2}\rho h \qquad \tilde{m}^* = \rho_1 t_1+\tfrac{1}{6}\rho h$$
$$C_1 = \tfrac{E_1 t_1}{1-\mu_1^2} \qquad F_1 = \tfrac{C_1}{2t_1}\left[(\tfrac{h}{2}+t_1)^2-(\tfrac{h}{2})^2\right]$$
$$D_1 = \tfrac{C_1}{3t_1}\left[(\tfrac{h}{2}+t_1)^3-(\tfrac{h}{2})^3\right]$$

where ρ, G, λ, h are the density of the core, shear modulus, Lame constant and thickness

of the core respectively. E_1, t_1, μ_1 are the Young modulus, thickness and Poisson ratio of the face respectively. It should be noted that if we know the geometry and mass properties of the sandwich, then the term of the operator D_{anti} depend on three independent parameters: E_1, G, μ_c [1].

Similarly, the terms of a symmetric three-by-three D_{sym} can be developed

$$D_{sym}^{(11)} = 2\overline{C}_1\frac{\partial^2}{\partial x^2} - 2\overline{m}\frac{\partial^2}{\partial t^2} \tag{D.12}$$

$$D_{sym}^{(12)} = 2\overline{F}_1\frac{\partial^3}{\partial x^3} + 2\lambda\frac{\partial}{\partial x} + h\overline{m}\frac{\partial^3}{\partial x\partial t^2} \tag{D.13}$$

$$D_{sym}^{(13)} = \frac{2}{\pi}C\frac{\partial^2}{\partial x^2} - \frac{2}{\pi}\rho h\frac{\partial^2}{\partial t^2} \tag{D.14}$$

$$D_{sym}^{(22)} = 2\overline{D}_1\frac{\partial^4}{\partial x^4} + \frac{4}{h^2}C - (2\lambda h + \kappa^2 Gh/3)\frac{\partial^2}{\partial x^2} + 2\overline{m}^*\frac{\partial^2}{\partial t^2} - \frac{1}{2}h^2\overline{m}\frac{\partial^4}{\partial x^2\partial t^2} \tag{D.15}$$

$$D_{sym}^{(23)} = -\frac{h}{\pi}C\frac{\partial^3}{\partial x^3} + \frac{4}{\pi}(\lambda + \kappa^2 G)\frac{\partial}{\partial x} + \frac{1}{\pi}\rho h^2\frac{\partial^3}{\partial x\partial t^2} \tag{D.16}$$

$$D_{sym}^{(33)} = \frac{1}{2}C\frac{\partial^2}{\partial x^2} - \frac{\pi^2}{2}\frac{\kappa^2 G}{h} - \frac{1}{2}\rho h\frac{\partial^2}{\partial t^2} \tag{D.17}$$

The constants used in the above expressions are defined as

$$\begin{array}{ll} \overline{C}_1 = C_1 + \frac{1}{2}C & C = (\lambda + 2G)h \\ \overline{F}_1 = F_1 + \frac{1}{4}Ch & \overline{D}_1 = D_1 + \frac{1}{8}Ch^2 \\ \overline{m} = \tilde{m} & \overline{m}^* = \tilde{m}^* \end{array}$$

A numerical example of dispersion curves is presented below. One considers a sandwich panel with two equal 1mm thick aluminium faces and 80mm thick polystyrene core. The following values of sandwich parameters are employed: E_1 = 70GPa, μ_1=0.3, t_1=1mm, ρ_1=2700kg/m^3, G=0.7MPa, μ_c=0.4, ρ=40kg/m^3, t_c=80mm. The analysis of dispersion curves determined by the two systems of equations D.7 and D.8 are shown in Fig.D.2. Dispersion cuves represent points where the determinant of these systems is zero.

In Fig.D.2 there are two branches of antisymmetric motion. One represents antisymmetric shear motion (motion in plane of the sandwich). The other represents antisymmetric bending. However, this bending is coupled to the in-plane motion as well (shear). Symmetric motion has three branches of dispersion curves. Typically, these motions have a very low wave-number fro frequencies below some cut-off frequency (around 700Hz in this case). Then we see apparition of these dispersion curves. The symmetric branch with highest wave-number is asymptotically approaching the antisymmetric bending dispersion curve.

[1] Evidently, this choice is arbitrary, other combinations of *three* independent elastic parameters are possible.

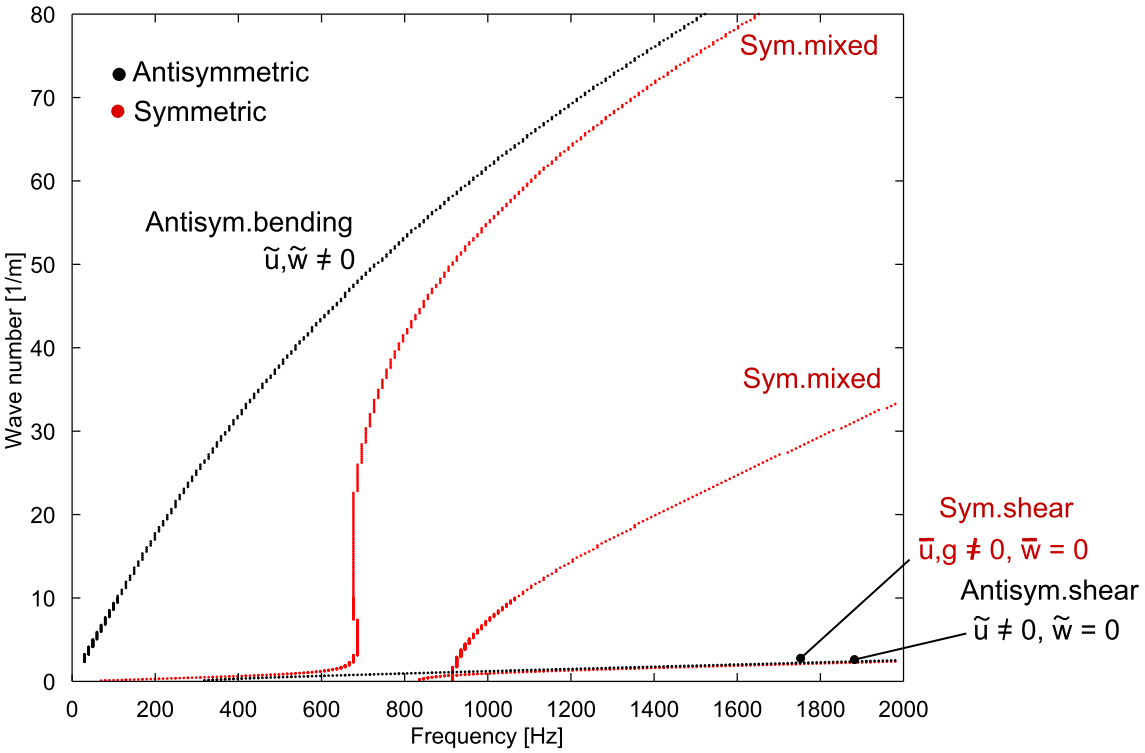

Figure D.2: Symmetric and antisymmetrix motion dispersion curves of sandwich model proposed by Dym and Lang.

Indirect methods for identification of equation of motion

[1] A.Moiola, R.Hiptmair, and I.Perugia. Vekua theory for the helmholtz operator. *Zeitschrift fur Angewandte Mathematik und Phusik (ZAMP)*, 62:779–807, 2011.

[2] A.Shidfar and A Babaei. The sinc-galerkin method for solving an inverse parabolic problem with unknown source term. *Numerical methods for partial differential equations*, 10, 2011.

[3] J. Berthaut. *Contribution à l'identification large bande des structures anisotropes*. PhD thesis, Ecole centrale Lyon, 2004.

[4] B.Pluymers, B.Van Hal, D.Vandepitte, and W.Desmet. Trefftz-based methods for time-harmonic acoustics. *Arch. of Comp.Meth. in Eng.*, 14:343–381, 2007.

[5] G. Chardon and L. Daudet. *Computational Mechanics: Low-complexity computation of plate eigenmodes with Vekua approximations and the method of particular solutions*. Springer, 2013.

[6] G. Chardon, A. Leblanc, and L. Daudet. Plate impulse response spatial interpolation with sub-nyquist sampling. *Journal of sound and vibration*, 330:5678–5689, 2011.

[7] C.J.S.Alves and P.R.S.Antunes. The method of fundamental solutions applied to the calculation of eigensolutions for 2d plates. *International Journal for Numerical Methods in Engineering*, 77:177–194, 2009.

[8] D. Colton and R. Kress. On the denseness of herglotz wave functions and electromagnetic herglotz pairs in sobolev spaces. *Mathematical methods in the applied sciences*, 24:1289–1303, 2001.

[9] C.Vanmaele, D.Vandepitte, and W.Desmet. An efficient wave based prediction technique for dynamic plate bending problems with corner stress singularities. *Comp.Meth.in App.Mech and Eng.*, 198:2227–2245, 2009.

[10] E.Barkanov, E.Skukis, and B.Petitjean. Characterisation of viscoelastic layers in sandwich panels via an inverse technique. *Journal of sound and vibration*, 327:402–412, 2008.

[11] B. Elie, F. Gautier, and B. David. Macro parameters describing the mechanical behavior of classical guitars. *J.Acoust.Soc.Am*, 132:4013–4024, 2012.

[12] E.Perray-Debain. Plane wave decomposition in the unit disc: Convergence estimates and computational aspects. *Journal of Computational and Applied Mathematics*, 193:140–156, 2006.

[13] E.Perray-Debain, O.Laghrouche, P.Bettess, and J.Trevelyan. Plane-wave basis finite elements and boundary elements for three dimensional wave scattering. *Philos.Trans.Roy.Soc.London*, A 362:629–645, 2004.

[14] E.Skudrzyk. The mean value method of predicting the dynamic response of complex vibrators. *J.Acoust.Soc.Am.*, 67:1105–1135, 1980.

[15] G.Fairweather and A.Karageorghis. The method of fundamental solutions for elliptic boundary value problems. *Advances in Computational Mathematics*, 9:69–95, 1998.

[16] G.Xie, D.J.Thompson, and C.J.C.Jones. Mode count and modal density of structural systems. *Journal of sound and vibration*, 274:621–651, 2004.

[17] P.Ladevèze H.Riou, L. Kovalevsky. A multiscale computational approach for medium frequency vibrations of composite structures. DYNACOMP, 2012.

[18] J.Cunha and J.Piranda. Application of model updating techniques in dynamics for the identification of elastic constants of composite materials. *Composites B*, 30:79–85, 1998.

[19] K.Ege. *La table d'harmonie du piano - Etudes modales en basses et moyennes fréquences (Piano soundboard - Study at low and mid-frequecies)*. PhD thesis, École polytechnique, 2009.

[20] K.Ege, D.Boutillon, and B.David. High-resolution modal analysis. *Journal of sound and vibration*, 325:852–869, 2009.

[21] L.Fox, P.Henrici, and P.Moller. Approximations and bounds for eigenvalues of elliptic operators. *SIAM J.Num.Anal.*, 4:89–102, 1967.

[22] L.Kovalevsky, P.Ladevèze, and H.Riou. The fourier version of the variational theory of complex rays for medium-frequency acoustics. *Comp.Methods Appl.Mech.Eng.*, 225:142–153, 2012.

[23] J.G. McDaniel, P. Dupont, and L.Salvino. A wave approach to estimate frequency-dependent damping under transient loading. *Journal of Sound and Vibration*, 231:433–449, 2000.

[24] M.Katsurama and H.Okamoto. A mathematical study of the charge simulation method. *J. Fac. Sci., Univ. of Tokyo*, 35:507–18, 1988.

[25] N.S.Ferguson, C.R.Halkyard, B.R.Mace, and K.H.Heron. The estimation of wavenumbers in two-dimensional structures. ISMA 2002, 2002.

[26] O.Laghrouche, P.Betess, and R.J.Astley. Modelling of short wave diffraction problems using approximating systems of plane waves. *International Journal of Numerical Methods in Engineering*, 54:1501–1533, 2002.

[27] P.Ortiz and E.Sanchez. An improved partition of unity finite element model for diffraction problems. *International Journal of Numerical Methods in Engineering*, 50:2727–2740, 2001.

[28] R.Badeau, B.David, and G.Richard. A new perturbation analysis for signal enumeration in rotational invariance techniques. *IEEE Transactions on signal processing*, 54, 2006.

[29] R.Roy and T.Kailath. Esprit estimation of sisgnal paramaters via roational invariance techniques. *IEEE Transactions on Acoustics Speech and Signal Processing*, 37:984–995, 1989.

[30] R.S.Langley. Some perspectives on wave-mode duality in sea. IUTAM Symposium on Statistical Energy Analysis, 1997.

[31] S.R.Arridge and J.C.Hebden. Optical tomography in medical imaging: Topical review. *Inverse problems*, 15:41–93, 1999.

[32] S.W.Kang. Free vibration analysis of arbitrarily shaped plates with clamped edges using wave-type functions. *Journal of sound and vibraiton*, 242:9–26, 2001.

[33] S.Y.Reutskiy. The method of fundamental solutions for problems of free vibration of plates. *Engineering analysis with boundary elements*, 31:10–27, 2007.

[34] T.Betcke and L.Trefethen. Reviving the method of particular solutions. *SIAM Review*, 47:469–491, 2005.

[35] T.Saito, R.D.Parbery, S.Okuno, and S.Kawano. Parameter indentification for aluminium honeycomb sandwich panels based on orthotropic timoshenko beam theory. *Journal of sound and vibration*, 208:271–287, 1997.

[36] Y.Epshteyn, T.Khan, and B. Riviere. Inverse problem in optical tomography using discontinuous galerkin method. *Mathematics and Computers in Simulation*, 79:1989–2000, 2009.

[37] Y.Liao and V.Wells. Estimation of complex modulus using wave coefficients. *Journal of Sound and Vibration*, 295:165–193, 2006.

[38] Y.Shi, H.Sol, and H.Hua. Material parameter identification of sandwich beams by an inverse method. *Journal of sound and vibration*, 290:1234–1255, 2006.

Direct methods for identification of equation of motion

[39] C.Chochol, S.Chesne, and D.Remond. An original differentiation tool for identification on continuous structures. *Journal of sound and vibration*, in press, 2013.

[40] C.Chohol, S.Chesne, and D.Remond. Identification à temps continue sur structure continue, 2011.

[41] C.Pézerat. *Mèthode d'identification des efforts appliqués sur une structure vibrante, par résolution et régularisation du problème inverse (Identification of Force Applied to a Vibrating Structure by the Resolution of The Inverse Problem)*. PhD thesis, INSA-Lyon, 1996.

[42] C.Pézerat and J.-L.Guyader. Force analysis technique: reconstruction of force distribution on plates. *Acustica united with Acta Acustica*, 86:322–332, 2000.

[43] C.Pézerat, Q.Leclère, N.Totaro, and M.Pachebat. Identification of vibration excitation from acoustic measurements using near field acoustic holography and the force analysis technique. *Journal of sound and vibration*, 326:540–556, 2009.

[44] C.Renzi. *Identification expérimentale de sources vibratoires par résolution du probléme inverse modélisé par un opérateur éléments finis local*. PhD thesis, INSA-Lyon, 2011.

[45] C.Rouby, D.Rémond, and P.Argoul. Orthogonal polynomials or wavelet analysis for mechanical system direct identification. *Ann.Solid Struct.Mech.*, 1:41–58, 2010.

[46] F.Ablitzer, C.Pézerat, and J.-M.Génevaux. Identification of the damping ratio of multilayered composite panels from the verification of their local equation of motion. *18th symposium VISHNO*, Clamart, 2012.

[47] H.Xu, L.Cheng, Z.Su, and J.-L.Guyader. Identification of structural damage based on locally perturbed dynamic equilibrum with an application to beam component. *Journal of sound and vibration*, 330:5963–5981, 2011.

[48] M.-C.Djamaa, N.Ouelaa, C.Pézerat, and J.-L.Guyader. Reconstruction of a distributed force applied to a thin cylindrical shell by an inverse method and spatial filtering. *Journal of sound and vibration*, 301:560–575, 2007.

Model selection

[49] A.Barron, J.Rissanen, and B.Yu. The minimum description length principle in coding and modelling. *IEEE transactions on information theory*, 44, 1998.

[50] S. Arlot. A survey of cross-validation procedures for model selection. *Statistics Surveys*, 4:40–79, 2010.

[51] C.L.Mallows. Some comments on cp. *Technometrics*, 15, 1973.

[52] E.Lebarbier and T.Mary-Huard. Le critère bic: fondements théoriques et interprétation. Technical report, INRIA, 2004. Rapport de recherche no.5315.

[53] G.Schwarz. Estimating the dimension of a model. *Annals of Statistics*, 6:461–464, 1978.

[54] H.Akaike. Information theory as an extension of the maximum likelihood principle. Second International Symposium on Information Theory in Budapest, 1973.

[55] J.L.Beck and K.V.Yuen. Model selection using response measurements: Bayesian probabilistic approach. *Journal of Enginnering Mechnaics*, 130:192–203, 2004.

[56] K.P.Burnham and D.R.Anderson. *Model selection and multimodel inference*. Springer, 2002.

[57] K.Takeuchi. Distribution of information statistics and criteria for adequacy of models. *Mathematical Science*, 153, 1976.

[58] S. Kullback and R. A. Leibler. On information and sufficiency. *Ann. Math. Statist.*, 22, 1951.

[59] M.H.Hansen and B.Yu. Model selection and the principle of minimum description length. *Journal of the American Statistical Association*, 96:746–774, 1998.

[60] M.Stone. Cross-validatory choice and assessment of statistical predictions. *Journal of Royal Statistical Society B*, 36:111–147, 1974.

[61] M.Sugiyama and H.Ogawa. Subspace information criterion for model selection.

[62] V.K.Hombal and S.Mahadevan. Model selection among physics-based models. *Journal of mechanical design*, 135, 2013.

[63] W.Zucchini. An introduction to model selection. *Journal of Mathematical Psychology*, 44:41–61, 2000.

Other bibliography

[64] A.Lakirouhani and H.Hasanzadehshooiili. Review of rock strength criteria. 22nd world mining congress in Istanbul, 2011.

[65] C.K.H.Dharan. Fracture mechanics of composite materials. *J.Eng.Mater.Technol.*, 100:233–247, 1978.

[66] C.Nowakowski, J.Fehr, M.Fischer, and P.Eberhard. Model order reduction in elastic multibody systems using the floating frame of reference formulation. 7th Vienna international conference on mathematical modelling, 2012.

[67] D.Tong. *Classical Dynamics*. University of Cambridge, 2005.

[68] C.L. Dym and M.A.Lang. Transmission of sound though sandwich panels. *J.Acoust.Soc.Am*, 56:1523–1532, 1974.

[69] F.Jacobsen. An elementary introduction to applied signal analysis. Technical report, Technical university of Denmark, 2006.

[70] G.Bontempi. Resampling techniques for statistical modelling. http://www.ulb.ac.be/di/map/gbonte/ecares/boot1.pdf, 2002. Université libre de Bruxelles.

[71] H.Seiner, L.Bodnárová, P.Sedlák, M.Janeček, O.Srba, R.Kral, and M.Land. Application of ultrasonic methods to determine elastic anisotropy of polycristalline copper processed by equal-channel angular pressing. *Acta Materialia*, 58:235–247, 2012.

[72] J.Bégué, N.Le Maout, A.Frikha, and F.Ablitzer. Amorti project: damping function for composite materials to reduce the vibration. *Dynacomp*, Arcachon, 2012.

[73] J.L.Chaboche. A review of some plasticity and viscoplasticity constitutive theories. *Int.Journal of Plasticity*, 24:1642–1693, 2008.

[74] L.Maxit. Wavenumber space and physical space responses of a periodically ribbed plate to a point drive: A discrete approach. *Applied Acoustics*, 70:563–578, 2009.

[75] M.Gérardin and D.Rixen. *Théorie des vibrations. Applications à la dynamique des structures.* Masson, Paris, 1992.

[76] M.Klesnil and P.Lukáš. Influence of strength and stress history on growth and stabilisation of fatique cracks. *Eng.Fract.Mech.*, 4:77–92, 1972.

[77] E. Nilsson and A. C. Nilsson. Prediction and measurement of some dynamic properties of sandwich structures with honeycomb and foam cores. *Journal of Sound and Vibration*, 251:409–430, 2002.

[78] P.C.Paris and F.Erdogan. A critical analysis of crack propagation laws. *Journal of Basic Engineering*, 85:528–534, 1963.

[79] T.E.Tallian. Simplified contact fatigue life prediction model-part i: Review of published models. *Journal of tribology*, 114, 1992.

[80] X.Sagartzazu, L.Hervella-Nieto, and J.M.Pagalday. Review in sound absorbing materials. *Comp.Meth. in Eng.*, 15:311–342, 2008.

FOLIO ADMINISTRATIF

THESE SOUTENUE DEVANT L'INSTITUT NATIONAL DES SCIENCES APPLIQUEES DE LYON

NOM: RUZEK DATE DE SOUTENANCE:17/12/2013
(avec précision du nom de jeune fille, le cas échéant)
Prénoms: MICHAL

TITRE: Identification expérimentale de l'équation du mouvement de milieux vibroacoustiques

NATURE: Doctorant Numéro d'ordre:

Ecole doctorale: MEGA

Specialité: Vibrations Acoustique

RESUME: Ce travail répond à la question de l'identifiquation de l'équation du mouvement à partir des mesures expérimentales. Les structures considérées ont soit une soit deux dimensions. La méthode presentée utilise les méthodes inverses locales qui se basent sur les mesures du champs vibratoire stationaire. Ces méthodes sont indépendentes des conditions aux limites qui sont inconnues pour l'observateur. Deux méthodes de sélection des modeles sont utilisées pour choisir l'équation du mouvement la plus adaptée parmi un ensemble des modeles a priori. La méthode est appliquée a des nombreux cas expérimentaux. Trois problématiques sont traités: identification de la force axiale dans les poutres et membranes, identification de l'orthotropie de la plaque et identification d'un panel sandwich épais.

MOTS-CLES: mèthodes inverses vibratoires,inverse wave correlation, inverse wave decomposition, séléction des modèles, Akaike information criterion, Baysian information criterion.

Laboratoire de recherche: LVA, INSA-Lyon

Directeur de thèse: Jean-Louis Guyader

Président de jury: Jerôme Antoni

Composition du jury: Jean-Louis Guyader, Charles Pézerat, Alain Berry, Robin Langley, Emmanuel Foltète, Gilles Chardon, Jerôme Antoni